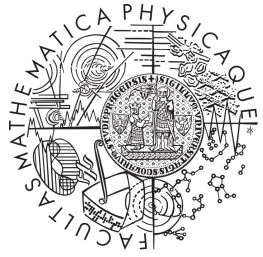

FACULTY
OF MATHEMATICS
AND PHYSICS
Charles University

**MASTER THESIS**

Michal Ptáček

# Theory of ultrafast relaxation and internal conversion in chlorophyll molecules

Institute of Physics

Supervisor of the master thesis: doc. Mgr. Tomáš Mančal, Ph.D.

Study programme: Biophysics and chemical physics

Study branch: Theoretical biophysics and chemical physics

Prague 2023

I declare that I carried out this master thesis independently, and only with the cited sources, literature and other professional sources. It has not been used to obtain another or the same degree.

I understand that my work relates to the rights and obligations under the Act No. 121/2000 Sb., the Copyright Act, as amended, in particular the fact that the Charles University has the right to conclude a license agreement on the use of this work as a school work pursuant to Section 60 subsection 1 of the Copyright Act.

In ..... date .....  .....

Author's signature

I'd like to thank my supervisor, Dr Tomáš Mančal, for all the time he dedicated to me over the many years and to my parents, who provided me with great support.

Title: Theory of ultrafast relaxation and internal conversion in chlorophyll molecules

Author: Michal Ptáček

Institute: Institute of Physics

Supervisor: doc. Mgr. Tomáš Mančal, Ph.D., Institute of Physics

Abstract: Extremely fast relaxation processes in photosynthetic molecular complexes and in chlorophyll molecules have been observed for decades. The emergence of multidimensional spectroscopic techniques with femtosecond temporal resolution resulted in the discovery of many new, previously unseen physical phenomena in these systems. These ultrafast phenomena occurring on the timescale of tens of femtoseconds ($10^{-15}$ s) have been the subject of intense discussions and experimental measurements, but theoretical models of these processes are sparse. In this thesis, a new spectroscopic theoretical model for chlorophyll-like molecules is formulated and tested. The physical parameters of the model were optimised on experimental linear absorption spectra obtained from the literature. The parameterised model was then used to reproduce the experimental data with great precision and also to simulate excited state population dynamics using the Redfield equations, which were derived, implemented and computationally optimised. The relaxation times of the $Q_x - Q_y$ transition in chlorophyll *a* molecule were roughly estimated from the dynamics and compared with the literature. The limitations of the new model were studied and discussed as well.

Keywords: excitation energy transport, ultrafast processes, chlorophyll a, internal conversion

# Contents

# Preface

Photosynthesis is quite possibly the most important process that has developed in living organisms since their origin billions of years ago (Blankenship, 2014). It had an important role in the development of Earth's atmosphere, the formation of oceans, and—with a pinch of salt—it even indirectly provided humanity with the resources to enter the iron age, followed by the industrial age thousands of years later, as it contributed to the oxidation of iron in long past history and the creation of iron-rich sediments humankind is steadily mining for millennia (Thompson et al., 2019; Heard et al., 2022).

On top of that, photosynthetic molecular complexes have a cherished place as a physical model for a plethora of physical phenomena. Because of the general complexity of the molecular aggregates, and their overall variability across all three domains of living organisms, there is basically always something even a specialist can be interested in. Besides, the ongoing technological advancements are enabling us to observe and detect processes that are weaker and faster than ever before. And at the same time, the ever-increasing power and—most importantly—availability of computational resources are enabling the theorists to simulate larger systems in greater detail and precision.

Photosynthetic molecular complexes have gone through a long path of biophysical and chemical research that successfully uncovered most of their structure, chemical and physical properties and provided insight into quantum mechanical effects that play a role behind the curtain of classical statistical physics. Despite the intensive and decades-long research, there is still much to explore and understand, as some experiments keep pointing out new physical phenomena.

An exceptional uprise of interest in the study of photosynthesis and the energy transfer processes that are occurring there happened at the beginning of our millennia as new spectroscopic techniques of high-temporal resolution came into popularity—and existence (see Maiuri et al. (2020); Croce et al. (2018) for reviews). The most influential was the emergence of two-dimensional electronic spectroscopy with femtosecond resolution (Brixner et al., 2004), which enabled us to quantitatively measure molecular dynamics occurring on the timescale of light travelling micrometres long distances. Processes taking place on the femtosecond timescale ($10^{-15}$ s) are usually referred to as *ultrafast*[1].

As the temporal resolution and achievable signal-to-noise ratio keep improving, new ultrafast processes in molecules and molecular complexes are getting identified. One such experiment was performed a couple of years ago on a purple-bacterial photosynthetic molecular complex (Niedringhaus et al., 2018). They identified intermolecular excitation energy transfer on the timescale of tens of femtoseconds, which represents exceptionally (ultra)fast dynamics. Several factors are expected to contribute to and facilitate such fast relaxation between pigment molecules noncovalently bound to protein scaffold (Policht et al., 2022).

[1] As a side note, the term *fast* is frequently used for the picosecond range ($10^{-12}$ s), and the term *hyperfast* for the attosecond range ($10^{-18}$ s).

One relaxation process that had been long neglected or classified as of insignificant importance (Zakutauskaite et al., 2022) is the relaxation between the second $S_2$ (also denoted as $Q_x$) and the first $S_1$ ($Q_y$) excited electronic states of chlorophyll molecules. Such relaxations are usually called by the term *internal conversion*. This transition has been observed for many decades, and by means of the spectroscopic techniques and equipment available at those times, it was considered almost instantaneous. Modern spectroscopic methods provided us with better estimates of the timescale, which was found to be tens to mere hundreds of femtoseconds (Meneghin et al., 2017; Shi et al., 2005). The mechanism of this relaxation is generally known since the active vibrational modes of the chlorophyll molecules are roughly resonant in energy with the electronic $S_2 \rightarrow S_1$ transition (Meneghin et al., 2017).

The question that arises is if the fast relaxation observed by Niedringhaus et al. (2018) originates in the vibrational modes as well, and, eventually, to what extent. To shine some light onto this question in terms of theoretical approaches, a robust theoretical model of the relaxation (internal conversion) between the first two excited states of chlorophyll molecules has to be formulated first.

After summarising the aims of this thesis and its content, the following Chapter 1 will introduce the reader to the prior research made on this and related topics. The Chapter 2 is focused on the theoretical apparatus necessary for constructing the model and performing the simulations. The Chapter 3 contains the results of the performed simulations with regard to the developed model, followed by discussion at Chapter 4.

## Aims of the thesis

The aim of my ongoing work is to formulate a robust theoretical model of a chlorophyll-like molecule that would explain the ultra-fast relaxation dynamics between its first and second excited states ($S_2 \rightarrow S_1$) observed in experiments (Meneghin et al., 2017; Shi et al., 2005). Since the master plan is to use this model later—in my following research—on much larger systems than just a single molecule (or a solution of molecules, to be precise), and on nonlinear spectroscopic simulations, the model should be reasonably scalable and dependence-free on other—presumably computationally very expensive—simulations like the fields of quantum chemistry (QCh) and molecular dynamics (MD) offer (Segatta et al., 2019; Cignoni et al., 2022; Curutchet and Mennucci, 2017).

The last and quite possibly the most important demand on the model is to be generally compatible with the "language" and already existing techniques of theoretical spectroscopy. It's desirable that the model will be easily adoptable by other researchers for use in simulations of advanced spectroscopic experiments as they are formulated and implemented.

To parameterise the model and validate its expected properties, linear absorption spectra were chosen to be simulated and fitted to selected experimental data.

# 1. Introduction

Photosynthetic molecular complexes are very popular models for the study of excitation energy transfer. The same applies to their integral parts—the pigment molecules—as well. Since they are pigments, they generally interact with light in the visible region of light spectra. The evolution of photosynthetic pigments was governed by the organisms that were synthesising them. Considering the natural sources of light on Earth—or radiation in general—are rather limited to only one of any greater significance—the Sun—a competition for its availability produced myriads of chemical structures that are used by photosynthetic organisms. Each such pigment has its own spectral properties.

However, the chemical structure of the pigments isn't the only feature that affects their spectroscopic properties. The influence of their surroundings and of neighbouring molecules is as much important (see e.g. Mennucci and Curutchet, 2011). Therefore, the information about the experimental setup, the solvent, the structure and the size of the molecular system are all uttermost important pieces of information for a theorist reproducing the experimental data.

## 1.1 Pigments

Photosynthetic molecular complexes have two essential constituents: the protein and the ligands. The ligands can be of various chemical natures, and they can play different roles in the photosynthetic machinery. The class of ligands pertinent to our interests are the pigments. By and large, there are three major groups of photosynthetic pigments: carotenoids, bilins, and chlorophyll. Chlorophylls usually have the most prominent function, and hence they are by far the most abundant pigments on Earth. To be more specific, this prominent title is given to chlorophyll *a* (Chl*a*) as it is used by almost every photosynthetic organism in existence, throughout all domains of life (Scheer, 2003).

### 1.1.1 Chlorophyll *a*

Many different types of chlorophyll were found in nature—and some more were synthesised artificially—but they all have a common chemical structure and two distinctly distinguishable parts: the planar core derived from chlorine and a phytyl chain that freely wobbles around (if the molecule is in solvent) (Blankenship, 2014). The chemical structure of Chl*a* can be seen in in Figure 1.1.

Only the planar part, the tetrapyrrole ring, interacts with the visible region of light and hence is relevant for spectroscopy. An efficient spectroscopic model of chlorophyll-like molecules was proposed by Goutermann (Gouterman, 1961; Gouterman et al., 1963). His model, usually called the (*Gouterman's*) *four-orbital model*, assumed only four electronic states, as the name suggests. Namely, the two lowest unoccupied molecular orbitals (LUMO) and the two highest occupied molecular orbitals (HOMO). In total, four electronic transitions can be described in such a system. Two of such transitions are lower in energy, and they have lower oscillator strength (denoted by $Q$) than the other two (denoted by $B$). Besides, he also noticed from experiments of his time that the transitions are

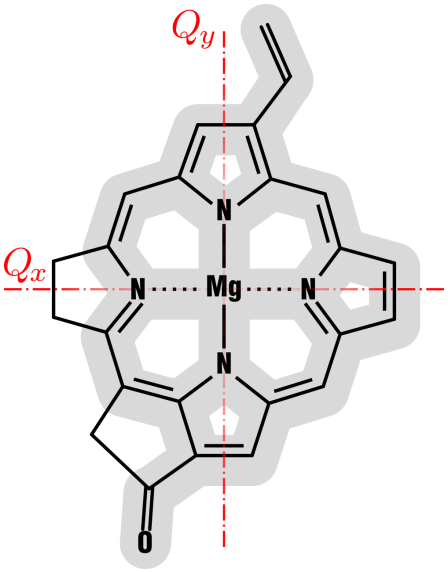


**Figure 1.1:** A simplified chemical structure of Chl*a* where the phytyl chain was omitted and only the main backbone is depicted. The grey shading highlights the extent of conjugated double bonds, which contribute significantly to the spectroscopic properties of the molecule. The red axis denotes the orientation of the $Q_x$ and $Q_y$ transitions as originally considered by Gouterman (1961); Gouterman et al. (1963). The image was taken and edited from Björn and Ghiradella (2014).

perpendicularly polarised. Hence, he introduced the following notation for the four electronic transitions that are visible in absorption spectra as four more-or-less distinct absorption bands: $Q_y$, $Q_x$, $B_x$, $B_y$, sorted in energetic order from the lowest to the highest. Even though his model has been mostly overcome and replaced by more exact approaches stemming from higher-resolution experiments and quantum chemical calculations, his notation is still in active use in the scientific community, and it will also be used in this thesis.

## 1.2 Overview of the prior research

The Chl*a* molecule was studied quite intensively in the last decade from both the experimental and theoretical points of view. Numerous techniques of time-resolved spectroscopy with femtosecond temporal resolution were used to measure molecular solutions of chlorophyll molecules in order to study the $Q_x - Q_y$ transition relaxation (internal conversion).

Bricker et al. (2015) performed ultrafast transient absorption spectroscopy measuremnts accompanied by nonadiabatic excited-state molecular dynamics (NA-ESMD) simulation of Chl*a* in ethanol and the $Q_x - Q_y$ relaxation time was identified as $128 \pm 2$ fs.

Meneghin et al. (2017) used two-dimensional electronic spectroscopy (2DES) to study internal conversion of Chl*a* soluted in methanol. They identified the overall $Q_x - Q_y$ relaxation time to be 170 fs with an intermediate step of 40 fs that involves a redistribution of energy among vibronic states of $Q_y$ prior to relaxation to the zeroth vibronic level.

Also, femtosecond time-resolved stimulated emission pumping fluorescence depletion (FS-TR-SEP-FD) spectroscopy (Shi et al., 2005) and femtosecond transient absorption spectroscopy (Shi et al., 2006) were used to measure the relaxation times of the $Q_x - Q_y$ transition. Chl*a* in pyridine was studied by polarisation-resolved femtosecond Vis-pump – IR-probe anisotropy spectroscopy (Zahn et al., 2022).

Linear absorption spectra of molecular samples in different solvents, namely in diethyl ether (Rätsep et al., 2009; Umetsu et al., 1999; Nonomura et al., 1997), propan-1-ol, propan-2-ol (Reimers et al., 2013; Rätsep et al., 2009), tetrahydrofuran (THF) (Rätsep et al., 2009), pyridine (Rätsep et al., 2009; Umetsu et al., 1999), triethylamine (TEA) (Rätsep et al., 2019). methanol/ethanol mixture (Reimers et al., 2013), ethyl acetate (Shi et al., 2005), were later used to parameterize the model formulated in the following chapters.

The structure of vibrational modes of Chl*a* was studied by 2DES–Raman spectroscopy (Meneghin et al., 2018), or by fluorescence line-narrowing spectroscopy (FLN) and difference FLN (ΔFLN) (Rätsep et al., 2009).

Regarding the theoretical research, the most notable contribution to the theoretical description of $Q_x - Q_y$ relaxation is considered to be the article of Reimers et al. (2013). Especially due to the amount of calculations and thoroughness in the experimental data evaluation. They proposed a model chlorophyll-like molecule that included a single vibrational mode of $\Omega = 1500$ $\mathrm{cm}^{-1}$ in the system Hamiltonian and a linear diabatic coupling with a coupling constant $\alpha = 750\,\mathrm{cm}^{-1}$ that resulted in a mixing of the electronic/vibronic states and fast $Q_x - Q_y$ relaxation (for Chl*a* in ethylether) of 99 fs. For comparison, the experimentally obtained value reads $100 \pm 12$ fs (Shi et al., 2005).

Another important contribution, which is, however, rather overlooked and only sparsely cited by other authors, are the works of Dong et al. (2006, 2007a,b); Niu et al. (2008). They adopted number of different approaches to simulate various experiments. The most relevant to us (Niu et al., 2008) introduced a theoretical model similar to the one proposed by Reimers et al. (2013). The main difference was the form of diabatic coupling they considered. Instead of the linear one, they used a Gaussian profile centred at the minima of excited states' potential energy surfaces gap. Using this approach, they calculated the $Q_x - Q_y$ internal conversion relaxation times of Chl*a* for a triad of solvents (ethyl acetate, THF, dimethylformamide (DMF)), attempting to reproduce the corresponding constants obtained from experiments (Shi et al., 2005), which they successfully did. The relaxation times they calculated were 141 fs, 147 fs, and 241 fs, in corresponding order with regard to the solvents. The experimental data read 132 fs, 138 fs, and 226 fs (the error estimates were omitted here; Shi et al., 2005).

Methods of QCh were also numerously used. A review of quantum chemical methods used within the context of assigning $Q_x$ and $Q_y$ bands was published by Reimers et al. (2014). The excited states properties of Chl*a* were calculated using the domain-based local pair natural orbital similarity transformed equations of motion with coupled cluster singles and doubles (DLPNO–STEOM–CCSD) (Sirohiwal et al., 2020) or numerous density functional theory (DFT) methods (Cai et al., 2006)

Other chlorophylls are studied as well. For example, chlorophyll *b* (Chl*b*) in methanol/ethanol mixture was measured by 2DES (Fresch and Collini, 2020).

Theoretical insight into the role of $Q_y$ and $Q_x$ states when a 2DES experiment would be performed on a dimer of chlorophyll molecule was provided by Zakutauskaite et al. (2022). A last notable piece of work that touches our topic rather tangentially looked into the solvent-dependence of Chl*a* *Q*-band as observed by 2DES (Moca et al., 2015).

# 2. Theoretical background

There are numerous theoretical techniques to describe and simulate the physical and chemical properties of molecules and molecular aggregates observed in experiments. These techniques can be roughly categorised into the following three categories: quantum chemistry, molecular dynamics, and theoretical spectroscopy. Even though all these approaches are in practice usually combined, this thesis is restricted particularly to the latter one – theoretical spectroscopy.

This chapter provides insight into the origin of theoretical methods that were used during my work. Firstly, the theory of open quantum systems is introduced, and the method of the quantum master equations is derived. The essential physical objects and terminology are introduced on the way. The specific quantum master equation I used—the Redfield equation—is derived, and the limits of its validity are outlined.

The second part introduces the physical model of a chlorophyll-like molecule that was developed. The adopted model of the environment is also introduced and explained. The section is wrapped up by an overview of the parameters that enter the simulations. Their physical meaning is described, and their theoretical importance, i.e. the influence they are expected to have on the linear absorption spectra, is estimated.

The third section focuses on theoretical spectroscopy. In particular, on building up the tools necessary for simulating linear absorption spectra of open quantum systems.

The fourth and final part of this chapter sheds some light on the methods and computational optimisations I've implemented during my work. The computational limits of the current state of my code are mentioned as well, and possible improvements are outlined.

## 2.1 Isolated quantum systems

Before making our life difficult, let's first focus on isolated quantum systems that don't interact with their surroundings. The archetypal feature of quantum systems is the concept of discrete quantum states. A quantum system is limited to these discrete states only or to their linear combination – superposition. The first postulate of quantum mechanics says the state and dynamics of an isolated quantum system are in their entirety described by a wavefunction $|\psi(t)\rangle$ which solves the time-dependent Schrödinger equation:

$$\frac{\partial}{\partial t}|\psi(t)\rangle = -i\hat{H}|\psi(t)\rangle \ , \tag{2.1}$$

where $\hat{H}$ is the system Hamiltonian. Finding of a wavefunction is usually done by an expansion into an already-known complete basis set:

$$|\psi(t)\rangle = \sum_n |n\rangle \underbrace{\langle n|\psi(t)\rangle}_{c_n(t)} , \tag{2.2}$$

where $\{c_n(t)\}$ is now a set of time-dependent expansion coefficients that can be organised into a vector. This is the reason wavefunctions are also called state vectors.

Wavefunctions can be useful for describing small, well-defined and isolated systems whose quantum nature is well preserved, for example, a particle scattering on a potential, atomic gases, or in quantum chemistry.

However, the applicability of wavefunctions on large systems consisting of multiple molecules (let alone interacting with each other as well as with their surroundings, as will be mentioned further in this chapter) is very limited and, most importantly, rather inconvenient. The problem stems from the fact that, in our case, we are not dealing with a clearly defined quantum system but rather a statistical ensemble. A probability weighting factor can be assigned to each available quantum microstate. Since we are interested in the overall behaviour and macroscopic measurable variables of the whole statistical mixture, a better formalism than the wavefunction-oriented would be preferred.

### 2.1.1 Density matrix

The mathematical object that is better suited for our use case is called a *density matrix*[1] $\hat{W}$ and it's defined as:

$$\hat{W} = \sum_i w_i \, |\psi_i\rangle\langle\psi_i| \ , \tag{2.3}$$

where $w_i$ is a probability of a normalized state $|\psi_i\rangle$. Density matrix has the following properties (May and Kühn, 2011):

1. hermiticity: $\hat{W}^\dagger = \hat{W}$, where † denotes Hermite conjugate,
2. normalization: $\mathrm{Tr}\{\hat{W}\} = 1$ ,
3. positive semi-definite form: $\forall\, |n\rangle : \langle n|\hat{W}|n\rangle = \sum_i w_i |\langle n|\psi_i\rangle|^2 \geq 0$ ,
4. Schwarz inequality (implied by property 3): $\forall\, |n\rangle$ forming orthonormal basis:
   $\hat{W} = \underbrace{\sum_n |n\rangle\langle n|}_{\mathbb{1}} \hat{W} \underbrace{\sum_{n'} |n'\rangle\langle n'|}_{\mathbb{1}} = \sum_{n,n'} W_{nn'} \, |n\rangle\langle n'| : W_{nn} W_{n'n'} \geq |W_{nn'}|^2$ .
5. non-negative eigenvalues: $p_i \geq 0$, $\sum_i p_i = 1$ (implied by property 3)

Properties 3 and 4 will be used later to evaluate the correctness of time propagation methods.The normalization of $\hat{W}$ implies the proper interpretation of weighing factors $w_i$ as probabilities since the relation $\sum_i w_i = 1$ has to hold. In case $\exists w_i : w_i = 1$, the density matrix is classified as *pure* since it reduces to a single projector to state $|\psi_i\rangle$. In every other case, i.e. $\forall w_i : 0 \leq w_i < 1$, the density matrix is called *mixed*.

[1] In fact, the object is known by many names besides just the *density matrix*. The other frequently used names are the *statistical operator* and the *density operator*. However, strictly speaking, there is a difference in the meaning between the former and the latter two names. The term *operator* should refer to a general object. In contrast, the term matrix should be understood as a representation of the operator in some basis. Nevertheless, for the sake of simplicity, I'll use the terms interchangeably and, most of the time, stick with the term *density matrix*.

An expectation value for some macroscopic quantity $\hat{A}$ measured on a statistical ensemble of quantum systems in a wavefunction formalism can be expressed as:

$$\left\langle \hat{A} \right\rangle = \sum_i w_i \left\langle \psi_i | \hat{A} | \psi_i \right\rangle = \tag{2.4}$$

$$= \mathrm{Tr}\{\hat{W}\hat{A}\} \, . \tag{2.5}$$

The expression (2.5) represents an equivalent of (2.4) but is expressed using the density matrix $\hat{W}$.

A specific nomenclature is associated with density matrices, which introduces two important terms. The diagonal elements of a density matrix are referred to as *populations* since, if properly normed, they represent the probabilities of individual states. The rest of the matrix elements are called *coherences*[2]. The physical meaning of coherences is a little more perplexing than that of the populations since they are related to the expectation values of noncommuting operators that don't share their eigenbases. This brings up an important piece of information that is always necessary to carry in mind—the coherences are entirely basis-dependent.

### 2.1.2 Isolated Quantum system dynamics

The general solution of the first-order differential equation (2.1) leads to an evolution operator $\hat{U}(t - t_0)$ in the form of a complex exponential:

$$|\psi(t)\rangle = \underbrace{e^{-i\hat{H}(t-t_0)}}_{\hat{U}(t-t_0)} |\psi(t_0)\rangle \, . \tag{2.6}$$

The evolution operator $\hat{U}(t - t_0)$ is Hermitian and unitary. Thus, the evolution it describes is usually called *unitary* as well as it preserves the norm of the wavefunction in time:

$$\langle \psi(t)|\psi(t)\rangle = e^{i\hat{H}(t-t_0)} \langle \psi(t_0)|\psi(t_0)\rangle \, e^{-i\hat{H}(t-t_0)} = \langle \psi(t_0)|\psi(t_0)\rangle \, . \tag{2.7}$$

If the Hamiltonian is time-dependent, which is commonly the case, the formal solution of (2.1) becomes:

$$|\psi(t)\rangle = \underbrace{\hat{T} \exp\left\{-i \int_{t_0}^{t} \mathrm{d}\tau \, \hat{H}(\tau)\right\}}_{\hat{U}(t-t_0)} |\psi(t_0)\rangle \, , \tag{2.8}$$

where $\hat{T}$ is a time-ordering operator[3] and the object $\hat{T}$ exp is usually called time-ordered exponential.

[2] A mathematical separation of these two parts of a density matrix expressed in an orthonormal basis can be performed using the Kronecker delta symbol as follows: $\hat{W}(t) = \underbrace{\left(\sum_i |i\rangle\langle i|\right)}_{\mathbb{1}} \hat{W}(t) \underbrace{\left(\sum_j |j\rangle\langle j|\right)}_{\mathbb{1}} = \sum_{ij} W_{ij} |i\rangle\langle j| \underbrace{\left(\delta_{ij} + \left(\mathbb{1} - \delta_{ij}\right)\right)}_{=\mathbb{1}} = \underbrace{\sum_i W_{ii} |i\rangle\langle i|}_{\text{populations}} + \underbrace{\sum_{i,j(\neq i)} W_{ij} |i\rangle\langle j|}_{\text{coherences}}$.

[3] The time-ordering operator $\hat{T}$ ensures the causality of integrals occurring in the exponential, which can be expanded into the following infinite series: $\hat{T} \exp\left\{-i \int_{t_0}^{t} \mathrm{d}\tau \, \hat{H}(\tau)\right\} = 1 - i \int_{t_0}^{t} \mathrm{d}\tau \, \hat{H}(\tau) - \int_{t_0}^{t} \mathrm{d}\tau \int_{t_0}^{\tau} \mathrm{d}\tau' \hat{H}(\tau)\hat{H}(\tau') + i \int_{t_0}^{t} \mathrm{d}\tau \int_{t_0}^{\tau} \mathrm{d}\tau' \int_{t_0}^{\tau'} \mathrm{d}\tau'' \hat{H}(\tau)\hat{H}(\tau')\hat{H}(\tau'') + \ldots$

The Schrödinger equation (2.1) can be briskly rewritten into its alternative form describing the time evolution of density matrices. This alternative form is called the *Liouville–von Neumann equation*, or alternatively *quantum Liouville equation* (May and Kühn, 2011):

$$\frac{\partial}{\partial t}\hat{W}(t) = -i\left[\hat{H}, \hat{W}(t)\right], \tag{2.9}$$

where the square brackets denote a commutator defined as:

$$[A, B] = AB - BA\,. \tag{2.10}$$

The solution of (2.9) can be expressed as:

$$\hat{W}(t) = \hat{U}(t - t_0)\hat{W}(t_0)\hat{U}^{\dagger}(t - t_0)\,, \tag{2.11}$$

or alternatively by introducing a rank four tensor constructed as follows. Consider the evolution of a density matrix element $W_{il}$:

$$W_{il}(t) = \sum_{jk} U_{ij}(t - t_0)W_{jk}(t_0)U^{\dagger}_{kl}(t - t_0) \tag{2.12}$$

$$= \underbrace{\left(\sum_{jk} U_{ij}(t - t_0)U^{\dagger}_{kl}(t - t_0)\right)}_{\breve{U}_{ijkl}(t-t_0)} W_{jk}(t_0)\,, \tag{2.13}$$

$$\hat{W}(t) = \breve{U}(t - t_0)\hat{W}(t_0)\,. \tag{2.14}$$

The tensor object $\breve{U}(t - t_0)$ introduced in (2.14) is an example of a so-called *superoperator*—an "operator" that acts on a different operator. Superoperators will be discussed and properly introduced further in the text. From now on, a breve symbol ($\breve{}$) will be used to denote superoperator-like objects.

However, in case the Hamiltonian is time-dependent, there is no elegant way to write the formal solution of (2.9). The culprit is the commutator (which is again an example of a superoperator) since the infinite series cannot be expressed as a time-ordered exponential this time, using our current notation:

$$\begin{aligned}\hat{W}(t) = \hat{W}(t_0) &- (i)^1 \int_{t_0}^{t} \mathrm{d}\tau\big[\hat{H}(\tau), \hat{W}(t_0)\big] \\ &+ (i)^2 \int_{t_0}^{t} \mathrm{d}\tau \int_{t_0}^{\tau} \mathrm{d}\tau'\big[\hat{H}(\tau), \big[\hat{H}(\tau'), \hat{W}(t_0)\big]\big] \\ &- (i)^3 \int_{t_0}^{t} \mathrm{d}\tau \int_{t_0}^{\tau} \mathrm{d}\tau' \int_{t_0}^{\tau'} \mathrm{d}\tau''\big[\hat{H}(\tau), \big[\hat{H}(\tau'), \big[\hat{H}(\tau''), \hat{W}(t_0)\big]\big]\big] \\ &+ \ldots \quad .\end{aligned} \tag{2.15}$$

To overcome this technical difficulty, an alternative formalism can be easily adopted.

### 2.1.3 Liouville space

Elements of density matrices, as well as of operators on Hilbert space, can be reorganised into vectors. This can be done by a re-indexation procedure[4]:

$$W_{ij} \to W_\sigma\,, \quad A_{ij} \to A_\sigma\,. \tag{2.16}$$

By doing so, we are leaving the Hilbert space and entering the so-called *Liouville space*. Liouville space is a linear vector space, very much like the Hilbert space. The differences between both spaces and the formal transitions between them are summarised in the Table 2.1. The most notable advantage of Liouville space is the simplified notation for superoperators. Superoperators (for example, a commutator as defined in (2.10)) can be expressed in Hilbert space either by two separate operands or alternatively by introducing a rank four tensor:

$$A_{ij}B_{jk} - B_{jk}A_{kl} = \left(A_{ij}\mathbb{1}_{kl} - \mathbb{1}_{ij}A_{kl}\right)B_{jk} = \underbrace{\left(A_{ik}\mathbb{1}_{jl} - \mathbb{1}_{ik}A_{lj}\right)}_{\left(\breve{\mathcal{L}}_A\right)_{ijkl}} B_{jk}\,. \tag{2.17}$$

The latter form can be directly translated into the Liouville space by a re-indexation $ij, kl \to \sigma\tau$, transforming the tensor and reducing its rank to two. Using this notation, the Liouville–von Neumann equation can now be simplified to:

$$\frac{\partial}{\partial t}\hat{W}(t) = -i\breve{\mathcal{L}}_H\hat{W}(t)\,, \tag{2.18}$$

where $\breve{\mathcal{L}}_H = \left[\hat{H}, \cdot\right]$ is a so-called *Liouville superoperator*, or *Liouvillian*, representing a commutator with Hamiltonian. The solution of (2.18) with time-independent Liouvillian (i.e. Hamiltonian) can be expressed as:

$$\hat{W}(t) = \underbrace{e^{-i\breve{\mathcal{L}}_H(t-t_0)}}_{\breve{U}(t-t_0)}\hat{W}(t_0)\,. \tag{2.19}$$

As long as the system is isolated and the Hamiltonian $\hat{H}$ is Hermitian, the evolution superoperator $\breve{U}(t-t_0)$ is Hermitian as well:

$$\breve{U}(t)\left(\breve{U}(t)\right)^\dagger = \left(\hat{U}(t)\otimes\hat{U}^\dagger(t)\right)\left(\hat{U}^\dagger(t)\otimes\hat{U}(t)\right) = \underbrace{\hat{U}(t)\hat{U}^\dagger(t)}_{\mathbb{1}}\otimes\underbrace{\hat{U}^\dagger(t)\hat{U}(t)}_{\mathbb{1}} = \mathbb{1}\,. \tag{2.20}$$

The previously troublesome case with time-dependent Liouvillian (Hamiltonian) written in (2.15) can now be expressed in a much simpler and more graspable form:

$$\hat{W}(t) = \hat{T}\exp\left\{-i\int_{t_0}^{t}\mathrm{d}\tau\breve{\mathcal{L}}_H(\tau)\right\}\hat{W}(t_0)\,. \tag{2.21}$$

[4]Technically, it is a bijective mapping acting on indices of object elements: $f : i,j \in \mathbb{N} \to \sigma \in \mathbb{N}$, which results in a transformation of the original object: $\hat{A} \in \mathbb{C}^{n\times n} \to \tilde{\hat{A}} \in \mathbb{C}^{n^2}$

**Table 2.1:** Summary of differences between Hilbert and Liouville linear vector spaces. The vectorised matrices in Liouville space are sometimes called *supervectors*, or *superkets* ($|\psi_\sigma\rangle\!\rangle = |\psi_i\rangle\langle\psi_j|$) and *superbras* ($\langle\!\langle\psi_\sigma| = |\psi_j\rangle\langle\psi_i|$) (Gyamfi, 2020), referring to a much broadly used term of a superoperator.

| | Hilbert space | Liouville space |
|---|---|---|
| wavefunction | vector<br>$\|\psi_i\rangle$ | – |
| density matrix | matrix<br>$\hat{W} = \sum_{ij} W_{ij} \|\psi_i\rangle\langle\psi_j\|$ | vector<br>$\hat{W} = \sum_\sigma W_\sigma \|\psi_\sigma\rangle\!\rangle$ |
| operator | matrix<br>$\hat{A} = \sum_{ij} A_{ij} \|i\rangle\langle j\|$ | vector<br>$\hat{A} = \sum_\sigma A_\sigma \|\sigma\rangle\!\rangle$ |
| superoperator | rank four tensor<br>$\left[\hat{A}, \hat{B}\right] = A_{ij}B_{jk} - B_{jk}A_{kl} =$<br>$= \breve{A}_{ijkl} B_{kl}$ | matrix<br>$\breve{A} = \sum_{\sigma\tau} \|\sigma\rangle\!\rangle\langle\!\langle\tau\|$<br>$\breve{A}\hat{B} = \breve{A}_{\sigma\tau} B_\tau$ |

## 2.2 Open quantum systems

Samples measured by experimental physicists and chemists don't consist of isolated non-interacting molecules very often. The molecules we are interested in, tend to be surrounded by an environment—a thermodynamic bath. It can be, for example, a solvent, a protein scaffold, or just different units of our molecule. Or it can be a combination of all of that. Besides, the electromagnetic vacuum is always present, which enables us to describe effects such as spontaneous emission and fluorescence. Quantum systems embedded and interacting with a much larger bath are referred to as *open quantum systems*.

Even though the previous section 2.1 introduced essential tools for describing quantum dynamics, the tools have their limitations. First and foremost, both Schrödinger and Liouville–von Neumann equations describe unitary, energy-conserving dynamics on Hilbert space. That's due to the hermiticity of Hamilton operators. However, our aim is to describe relaxation processes, energy dissipation and radiative transitions. To achieve that, we need to go beyond the unitary evolution.

### 2.2.1 Introduction to open quantum systems

The simplest open quantum systems can be modelled by splitting the universe into two parts: the quantum system we are interested in (from now on, it'll be referred to as the system) and the rest we are not (the bath[5]). There are, in gen-

[5]Usually called the bath, the environment, or the reservoir. I'll stick to using the former term.

eral, three types of processes and interactions now happening. (1) Processes in which the system evolves on its own, (2) processes in which the environment evolves on its own, and finally, (3) the interaction between both. We can thus postulate a Hamiltonian of the following form:

$$\hat{H} = \hat{H}_S + \hat{H}_B + \hat{H}_{S-B} \,, \tag{2.22}$$

where $H_S$ is the system Hamiltonian (belonging to a Hilbert space $\mathcal{H}_S$), $\hat{H}_B$ is the bath Hamiltonian ($\in \mathcal{H}_B$), and $H_{S-B}$ is the system–bath interaction Hamiltonian ($\in \mathcal{H}_{S-B} = \mathcal{H}_S \otimes \mathcal{H}_B$). The Liouville–von Neumann equation describing the dynamics of the entire universe (represented here by the density matrix $\hat{W}(t) \in \mathcal{H}_S \otimes \mathcal{H}_B$) reads:

$$\frac{\partial}{\partial t}\hat{W}(t) = -i\check{\mathcal{L}}_{\hat{H}}\hat{W}(t) \tag{2.23}$$

$$= -i\left(\check{\mathcal{L}}_{\hat{H}_S} + \check{\mathcal{L}}_{\hat{H}_B} + \check{\mathcal{L}}_{\hat{H}_{S-B}}\right)\hat{W}(t) \,. \tag{2.24}$$

### 2.2.2 Reduced density matrix

If we'd like to find an expectation value of some macroscopic quantity represented by an operator $\hat{C}$, the general approach would be to calculate the trace:

$$\left\langle \hat{C} \right\rangle = \mathrm{Tr}\left\{\hat{C}\hat{W}(t)\right\} \,. \tag{2.25}$$

If this quantity depends on the system degrees of freedom (DOF) only, i.e. $\hat{C} \in \mathcal{H}_S$, we can treat the system and the bath parts of the trace separately:

$$\left\langle \hat{C} \right\rangle = \mathrm{Tr}\left\{\hat{C}\hat{W}(t)\right\} = \mathrm{Tr}_S\left\{\mathrm{Tr}_B\left\{\hat{C}\hat{W}(t)\right\}\right\} = \mathrm{Tr}_S\left\{\hat{C}\mathrm{Tr}_B\left\{\hat{W}(t)\right\}\right\} = \mathrm{Tr}_S\left\{\hat{C}\hat{\rho}(t)\right\} \,. \tag{2.26}$$

Since the trace over bath $\mathrm{Tr}_B\{\}$ has no effect on the operator $\hat{C}$, we can let it act on the total density matrix $\hat{W}(t)$ only. That results in a new object $\hat{\rho}(t)$ called the *reduced density matrix* ($\in \mathcal{H}_S$). It's defined as:

$$\mathrm{Tr}_B\left\{\hat{W}(t)\right\} = \sum_\alpha \langle\alpha|\hat{W}(t)|\alpha\rangle = \hat{\rho}(t) \,, \tag{2.27}$$

where $|\alpha\rangle \in \mathcal{H}_B$.

### 2.2.3 Dynamics of open quantum systems

The concept of space reduction can be applied to Liouville–von Neumann equation (2.24) as well since we are not particularly interested in the dynamics of the universe, only in our system. That is, only in dynamics occurring on the Hilbert space $\mathcal{H}_S$. Without any loss of (for us currently interesting) information, we can trace out the bath DOF:

$$i\frac{\partial}{\partial t}\mathrm{Tr}_B\left\{\hat{W}(t)\right\} = \mathrm{Tr}_B\left\{\check{\mathcal{L}}_{\hat{H}}\hat{W}(t)\right\} \tag{2.28}$$

$$= \mathrm{Tr}_B\left\{\check{\mathcal{L}}_{\hat{H}_S}\hat{W}(t)\right\} + \underbrace{\mathrm{Tr}_B\left\{\check{\mathcal{L}}_{\hat{H}_B}\hat{W}(t)\right\}}_{=0} + \underbrace{\mathrm{Tr}_B\left\{\check{\mathcal{L}}_{\hat{H}_{S-B}}\hat{W}(t)\right\}}_{\equiv\frac{1}{i}\mathcal{R}\left[\hat{W}(t)\right](t)} \tag{2.29}$$

$$= \check{\mathcal{L}}_{\hat{H}_S}\underbrace{\mathrm{Tr}_B\left\{\hat{W}(t)\right\}}_{\hat{\rho}(t)} + \frac{1}{i}\mathcal{R}\left[\hat{W}(t)\right](t) \,. \tag{2.30}$$

The second term in (2.29) equals zero due to the cyclic property of trace[6]:

$$\mathrm{Tr}_B\left\{\breve{\mathcal{L}}_{\hat{H}_B}\hat{W}(t)\right\} = \mathrm{Tr}_B\left\{\left[\hat{H}_B, \hat{W}(t)\right]\right\} = \mathrm{Tr}_B\left\{\hat{H}_B\hat{W}(t)\right\} - \underbrace{\mathrm{Tr}_B\left\{\hat{W}(t)\hat{H}_B\right\}}_{=\mathrm{Tr}_B\left\{\hat{H}_B\hat{W}(t)\right\}} = 0\,, \tag{2.31}$$

and correctly excludes the dynamics of the bath from our equation. To sum it up, the still formally exact Liouville–von Neumann equation describing the dynamics of a quantum subsystem embedded in an environment (bath) reads:

$$\frac{\partial}{\partial t}\hat{\rho}(t) = -i\breve{\mathcal{L}}_{\hat{H}_S} + \mathcal{R}\left[\hat{W}(t)\right](t)\,, \tag{2.32}$$

where $\mathcal{R}\left[\hat{W}(t)\right](t)$ is so far a rather general object, a functional of the total density matrix $\hat{W}(t)$. By comparing the original Liouville–von Neumann eq. (2.18) with (2.32), it's apparent that the transition from a simple unitary evolution to a relaxation process of our system is realised purely by the functional $\mathcal{R}$. Henceforth, it will be referred to as the *relaxation functional*. Since it stems from the system-bath interaction Hamiltonian $\hat{H}_{S-B}$, which can be expected to be time-dependent, the relaxation functional will depend on time as well.

There are many different ways of describing open quantum systems dynamics. To mention some examples, there are the quantum master equations, stochastic approaches, hierarchical equations of motion, path-integral techniques, tensor-network approaches, and even non-hermitian approaches.

All of the theories mentioned have their own drawbacks as well as cases they can truly shine out. In this thesis, the former approach—quantum master equation in a weak system-bath coupling limit—was adopted as it arguably provides the best compromise between accuracy, computational demands, and implementation difficulty. It also provides a decent insight into the physical processes and doesn't lay that many limitations on the actual physical use case.

### 2.2.4 Quantum master equations

The derivation of the quantum master equation in the second order of interaction is rather straightforward. We'll begin with the expression (2.24):

$$\frac{\partial}{\partial t}\hat{W}(t) = -i\left(\breve{\mathcal{L}}_{\hat{H}_S} + \breve{\mathcal{L}}_{\hat{H}_B} + \breve{\mathcal{L}}_{\hat{H}_{S-B}}\right)\hat{W}(t)\,. \tag{2.33}$$

To simplify the equation and get rid of the terms that are sources of the unitary evolution only, an *interaction picture* can be introduced. The interaction picture is basically a form of a rotating frame since we transform the total density matrix $\hat{W}(t)$ with respect to both system and bath Hamiltonians (i.e. with respect to everything else but the system-bath interaction Hamiltonian) by a

[6]The cyclic property of trace reads: $\mathrm{Tr}\{\hat{A}\hat{B}\} = \sum_{i,j}\langle i|\hat{A}|j\rangle\langle j|\hat{B}|i\rangle = \sum_{i,j}\langle j|B|i\rangle\langle i|\hat{A}|j\rangle = \mathrm{Tr}\{\hat{B}\hat{A}\}$. This property is applicable even in our case in which we are dealing with two objects, one spanning a single and the other spanning two Hilbert spaces: $\mathrm{Tr}_B\{\hat{W}(t)\hat{H}_B\} = \sum_{\alpha,\beta}\langle\alpha|\hat{W}(t)|\beta\rangle\underbrace{\langle\beta|\hat{H}_B|\alpha\rangle}_{\in\mathbb{C}} = \sum_{\alpha,\beta}\langle\beta|\hat{H}_B|\alpha\rangle\langle\alpha|\hat{W}(t)|\beta\rangle = \mathrm{Tr}_B\{\hat{H}_B\hat{W}(t)\}$.

negative time. Countering the complex oscillations caused by them. The total density matrix in the interaction picture can be expressed followingly:

$$\hat{W}^{(I)}(t) = \breve{U}_B^\dagger(t)\breve{U}_S^\dagger(t)\hat{W}(t) = \hat{U}_B^\dagger(t)\hat{U}_S^\dagger(t)\hat{W}(t)\hat{U}_S(t)\hat{U}_B(t)\,. \tag{2.34}$$

The interaction Hamiltonian in the interaction picture becomes:

$$\hat{H}_{S-B}^{(I)}(t) = \breve{U}_B^\dagger(t)\breve{U}_S^\dagger(t)\hat{H}_{S-B}(t) = \hat{U}_B^\dagger(t)\hat{U}_S^\dagger(t)\hat{H}_{S-B}(t)\hat{U}_S(t)\hat{U}_B(t)\,. \tag{2.35}$$

The Liouville–von Neumann equation in the interaction picture then reads:

$$\frac{\partial}{\partial t}\hat{W}^{(I)}(t) = -i\breve{\mathcal{L}}_{\hat{H}_{S-B}^{(I)}}(t)\hat{W}^{(I)}(t) \tag{2.36}$$

$$= -i\Big[\hat{H}_{S-B}^{(I)}(t), \hat{W}^{(I)}(t)\Big]\,. \tag{2.37}$$

As previously stated, the system-bath interaction is expected to be weak and can be considered as a source of perturbation to the otherwise unitarily evolving system only. Hence, it might be appropriate to treat the system-bath interaction within the framework of perturbation theory[7]. Equation (2.37) can be formally integrated, leaving only the sought term $\hat{W}^{(I)}(t)$ on the left-hand-side:

$$\hat{W}^{(I)}(t) = \hat{W}^{(I)}(t_0) - i\int_{t_0}^{t} \mathrm{d}\tau\,\Big[\hat{H}_{S-B}^{(I)}(\tau), \hat{W}^{(I)}(\tau)\Big]\,. \tag{2.38}$$

The result of (2.38) can then be plugged back into (2.37). The equation in up-to-second order in system-bath interaction then reads:

$$\frac{\partial}{\partial t}\hat{W}^{(I)}(t) = -i\Big[\hat{H}_{S-B}^{(I)}(t), \hat{W}^{(I)}(t_0)\Big] + (i)^2\int_{t_0}^{t}\mathrm{d}\tau\Big[\hat{H}_{S-B}^{(I)}(t), \Big[\hat{H}_{S-B}^{(I)}(\tau), \hat{W}^{(I)}(\tau)\Big]\Big]\,. \tag{2.39}$$

Now, we reduce the equation of motion to describe the dynamics of our system only:

$$\frac{\partial}{\partial t}\mathrm{Tr}_B\{\hat{W}^{(I)}(t)\} = -i\,\mathrm{Tr}_B\Big\{\Big[\hat{H}_{S-B}^{(I)}(t), \hat{W}^{(I)}(t_0)\Big]\Big\} + (i)^2\int_{t_0}^{t}\mathrm{d}\tau\mathrm{Tr}_B\Big\{\Big[\hat{H}_{S-B}^{(I)}(t), \Big[\hat{H}_{S-B}^{(I)}(\tau), \hat{W}^{(I)}(\tau)\Big]\Big]\Big\}\,. \tag{2.40}$$

Up to this point, the equation (2.40) is still formally exact—no approximations have been made yet. However, since both the system-bath interaction Hamiltonian and the total density matrix spread over the combined Hilbert space $\mathcal{H}_S \otimes \mathcal{H}_B$, the cyclic property described on page 16 can't be applied here. To move forward, one of these objects has to be factorized into a (Kronecker) product of two parts, each spreading only one space.

[7]There are several different understandings of the term perturbation theory. The most widely perceived is the so-called *Rayleigh–Schrödinger perturbation theory* known from the introductory quantum mechanics courses. In our case, though, we are referring to a more general concept of solving differential equations by an iterative expansion of the formal solution up to a certain order.

As mentioned in Chapter 1, an assumption about our model is that the interactions within the system are larger than with the environment. Hence, we can assume a weak system-bath coupling limit and assume that the effect of our system on the environment is minimal. Thus, the environment stays in a state close to its thermal equilibrium throughout the studied dynamics, and we can introduce the following factorization, usually referred to as *Born approximation* (Valkunas et al., 2013):

$$\hat{W}(t) \equiv \hat{W}_{eq} \otimes \hat{\rho}(t) \; . \tag{2.41}$$

The equilibrium bath density matrix $\hat{W}_{eq}$ doesn't evolve in time, as already stated. As a result, it's immune to any changes of representations/pictures:

$$\begin{aligned}
\hat{W}^{(I)}(t) &= \hat{U}_B^\dagger(t)\hat{U}_S^\dagger(t)\left(\hat{W}_{eq}\otimes\hat{\rho}(t)\right)\hat{U}_S(t)\hat{U}_B(t) && (2.42)\\
&= \underbrace{\left(\hat{U}_B^\dagger(t)\hat{W}_{eq}\hat{U}_B(t)\right)}_{=\hat{W}_{eq}} \otimes \left(\hat{U}_S^\dagger(t)\hat{\rho}(t)\hat{U}_S(t)\right) && (2.43)\\
&= \hat{W}_{eq}\otimes\hat{\rho}^{(I)}(t) \; . && (2.44)
\end{aligned}$$

The equation (2.40) then becomes:

$$\begin{aligned}
\frac{\partial}{\partial t}\mathrm{Tr}_B\{\hat{W}^{(I)}(t)\} = &-i\mathrm{Tr}_B\left\{\left[\hat{H}^{(I)}_{S-B}(t), \hat{W}_{eq}\otimes\hat{\rho}^{(I)}(t_0)\right]\right\}\\
&+ (i)^2\int_{t_0}^{t} \mathrm{d}\tau \mathrm{Tr}_B\left\{\left[\hat{H}^{(I)}_{S-B}(t), \left[\hat{H}^{(I)}_{S-B}(\tau), \hat{W}_{eq}\otimes\hat{\rho}^{(I)}(\tau)\right]\right]\right\} \; . . \qquad (2.45)
\end{aligned}$$

The first term of (2.45) can be expressed further as:

$$\begin{aligned}
\mathrm{Tr}_B\left\{\left[\hat{H}^{(I)}_{S-B}(t), \hat{W}_{eq}\otimes\hat{\rho}^{(I)}(t_0)\right]\right\} =&\mathrm{Tr}_B\left\{\hat{H}^{(I)}_{S-B}(t)\hat{W}_{eq}\otimes\hat{\rho}^{(I)}(t_0)\right\}\\
&- \mathrm{Tr}_B\left\{\hat{W}_{eq}\otimes\hat{\rho}^{(I)}(t_0)\hat{H}^{(I)}_{S-B}(t)\right\} && (2.46)\\
=&\mathrm{Tr}_B\left\{\hat{H}^{(I)}_{S-B}(t)\hat{W}_{eq}\right\}\otimes\hat{\rho}^{(I)}(t_0)\\
&- \hat{\rho}^{(I)}(t_0)\otimes\underbrace{\mathrm{Tr}_B\left\{\hat{W}_{eq}\hat{H}^{(I)}_{S-B}(t)\right\}}_{\mathrm{Tr}_B\left\{\hat{H}^{(I)}_{S-B}(t)\hat{W}_{eq}\right\}} && (2.47)\\
=&\left[\mathrm{Tr}_B\left\{\hat{H}^{(I)}_{S-B}(t)\hat{W}_{eq}\right\}, \hat{\rho}^{(I)}(t_0)\right]_\otimes \; , && (2.48)
\end{aligned}$$

where a simplified notation for a commutator on a tensor product operation $A\otimes B - B\otimes A = [A,B]_\otimes$ was used. Since the system-bath interaction Hamiltonian spans over both Hilbert spaces, the commutator is generally non-zero. By comparing equations (2.48) with (2.25), it's apparent that the trace stands for an expectation value—or in better wording, an averaged quantity over the bath degrees of freedom—of the system-bath interaction:

$$\begin{aligned}
\mathrm{Tr}_B\left\{\hat{H}^{(I)}_{S-B}(t)\hat{W}_{eq}\right\} &= \mathrm{Tr}_B\left\{\hat{U}_B^\dagger(t)\hat{U}_S^\dagger(t)\hat{H}_{S-B}(t)\hat{U}_S(t)\hat{U}_B(t)\hat{W}_{eq}\right\} && (2.49)\\
&= \mathrm{Tr}_B\left\{\hat{H}_{S-B}(t)\underbrace{\hat{U}_S(t)\hat{U}_B(t)\hat{W}_{eq}\hat{U}_B^\dagger(t)\hat{U}_S^\dagger(t)}_{\hat{W}_{eq}}\right\} && (2.50)\\
&= \left\langle\hat{H}_{S-B}(t)\right\rangle_B \; , && (2.51)
\end{aligned}$$

where the cyclic property of trace and the equilibrium property (2.43) of the bath density matrix were used in the second line (2.50). We can see that the entire term from the last line (2.48) would vanish if the trace equals zero. That is, however, a reasonable claim that we can take into account in the formulation of the system-bath interaction Hamiltonian later. Henceforth, let's assume:

$$\left\langle \hat{H}_{S-B} \right\rangle_B = \mathrm{Tr}_B\left\{ \hat{H}^{(I)}_{S-B}(t)\hat{W}_{eq} \right\} \equiv 0 \,. \tag{2.52}$$

The equation (2.45) then simplifies to:

$$\frac{\partial}{\partial t}\hat{\rho}^{(I)}(t) = -\int_{t_0}^{t} \mathrm{d}\tau \; \mathrm{Tr}_B\left\{ \left[ \hat{H}^{(I)}_{S-B}(t), \left[ \hat{H}^{(I)}_{S-B}(\tau), \hat{W}_{eq} \otimes \hat{\rho}^{(I)}(\tau) \right] \right] \right\} \,. \tag{2.53}$$

Let's also introduce at this point a formal change of integration variable $t \to t - \tau$ for reasons that will be shown shortly. Besides, we can move the initial time $t_0$ back to $-\infty$ since the system is assumed to be in equilibrium prior to $t_0$ anyway. The result of these changes reads:

$$\frac{\partial}{\partial t}\hat{\rho}^{(I)}(t) = -\int_{0}^{\infty} \mathrm{d}\tau \; \mathrm{Tr}_B\left\{ \left[ \hat{H}^{(I)}_{S-B}(t), \left[ \hat{H}^{(I)}_{S-B}(t-\tau), \hat{W}_{eq} \otimes \hat{\rho}^{(I)}(t-\tau) \right] \right] \right\} \,. \tag{2.54}$$

### 2.2.5 Markov approximation

Equation (2.54) represents a *time-non-local equation*. That is, the dynamics of the reduced density matrix $\hat{\rho}(t-\tau)$ (in either interaction or Schrödinger picture, even though there is an important difference as will be discussed shortly) at time $t$ depend not only on its current state—at time $t$—but also on all states prior to that by a time $\tau$. This effect is usually referred to as a *system memory*, and it represents a direct consequence of the reduction of the system performed in (2.40). The concept of a system memory relates to the Markov property, or Markovianity, known from statistical physics and probabilistic theory in general. The Liouville–von Neumann equation describing the dynamics of an entire system in (2.33) represents an exact equation that is time-local, memoryless, and Markovian. By comparison, the introduction of the reduced density matrix and the equations of motion presented up to this point represented time-non-local, memory-involving, non-Markovian equations.

In order to restore the Markovianity of equation (2.54), an approximation has to be made. We can see there are two terms in the equation that depend on the retarded time $\tau$. As will be discussed in the following section, the temporal dependence of the interaction Hamiltonians reflects the memory of the environment. In case the environment is very fluid and inhomogeneous, the temporal dependence of the object stemming from the interaction Hamiltonians can be expected to be rather short. The characteristic "bath memory" time can be denoted by $\tau_B$. Let's now have a look at the reduced density matrix $\hat{\rho}^{(I)}(t-\tau)$:

$$\hat{\rho}^{(I)}(t-\tau) = \hat{U}_S^{\dagger}(t-\tau)\hat{\rho}(t-\tau)\hat{U}_S(t-\tau) \,. \tag{2.55}$$

As already mentioned, the interaction picture counters the fast oscillations caused by the system Hamiltonian. The equation of motion in the interaction

picture (2.54) thus describes only the dynamics governed by the system-bath interaction Hamiltonian. Since the interaction is assumed to be weak, the induced dynamics will be slow. Therefore, it seems justifiable to expect the reduced density matrix in the interaction picture won't change significantly on the time scale given by $\tau_B$. Hence we can approximate the temporal dependence of $\hat{\rho}^{(I)}(t-\tau)$ by $t$ only. This is called the *Markov approximation* since it recovers the Markov property of the equation of motion.

The resulting time-local equation of motion for the reduced density matrix in the second order of system-bath interaction is by some authors[8] (May and Kühn, 2011; Valkunas et al., 2013) called the *quantum master equation*:

$$\frac{\partial}{\partial t}\hat{\rho}^{(I)}(t) = -\int_0^\infty \mathrm{d}\tau\, \mathrm{Tr}_B\Big\{\Big[\hat{H}^{(I)}_{S-B}(t), \Big[\hat{H}^{(I)}_{S-B}(t-\tau), \hat{W}_{eq}\otimes\hat{\rho}^{(I)}(t)\Big]\Big]\Big\}\ . \tag{2.56}$$

At this point, it's possible to return from the interaction picture back to the Schrödinger picture by using the relations from (2.34) and (2.35):

$$\begin{aligned}\frac{\partial}{\partial t}\hat{\rho}(t) = -i\big[\hat{H}_S, \hat{\rho}(t)\big] - \hat{U}_S(t)\int_0^\infty \mathrm{d}\tau\, \mathrm{Tr}_B\Big\{\big[\hat{U}_B^\dagger(t)\hat{U}_S^\dagger(t)\hat{H}_{S-B}(t)\hat{U}_S(t)\hat{U}_B(t),\\ \big[\hat{U}_B^\dagger(t-\tau)\hat{U}_S^\dagger(t-\tau)\hat{H}_{S-B}(t-\tau)\hat{U}_S(t-\tau)\hat{U}_B(t-\tau),\\ \hat{W}_{eq}\otimes\hat{\rho}^{(I)}(t)\big]\big]\Big\}\hat{U}_S^\dagger(t)\ .\end{aligned} \tag{2.57}$$

Let us expand and examine the double commutator and contract the evolution operators where possible. The first term out of the four in which the reduced density matrix sits on the most right-hand-side reads:

$$\begin{aligned}&\hat{U}_S(t)\mathrm{Tr}_B\big\{\hat{U}_S^\dagger(t)\hat{U}_B^\dagger(t)\hat{H}_{S-B}\hat{U}_B(t)\hat{U}_S(t)\\ &\qquad \hat{U}_S^\dagger(t-\tau)\hat{U}_B^\dagger(t-\tau)\hat{H}_{S-B}\hat{U}_S(t-\tau)\hat{U}_B(t-\tau) &(2.58)\\ &\qquad \hat{U}_S^\dagger(t)\hat{W}_{eq}\otimes\hat{\rho}(t)\hat{U}_S(t)\big\}\hat{U}_S^\dagger(t)\\ &=\mathrm{Tr}_B\Big\{\hat{U}_B^\dagger(t)\hat{H}_{S-B}\hat{U}_B^\dagger(-\tau)\hat{U}_S^\dagger(-\tau)\hat{H}_{S-B}\hat{U}_B(t-\tau)\hat{U}_S(-\tau)\hat{W}_{eq}\otimes\hat{\rho}(t)\Big\} &(2.59)\\ &=\mathrm{Tr}_B\Big\{\hat{H}_{S-B}\hat{U}_B^\dagger(-\tau)\hat{U}_S^\dagger(-\tau)\hat{H}_{S-B}\hat{U}_B(-\tau)\hat{U}_S(-\tau)\hat{W}_{eq}\otimes\hat{\rho}(t)\Big\} &(2.60)\\ &=\mathrm{Tr}_B\Big\{\hat{H}_{S-B}\hat{H}^{(I)}_{S-B}(-\tau)\hat{W}_{eq}\otimes\hat{\rho}(t)\Big\}\ . &(2.61)\end{aligned}$$

By repeating this procedure with each term of the expanded double commutator, we obtain the following expression:

$$\begin{aligned}&\mathrm{Tr}_B\Big\{\hat{H}_{S-B}\hat{H}^{(I)}_{S-B}(-\tau)\hat{W}_{eq}\otimes\hat{\rho}(t)\Big\}\\ -&\mathrm{Tr}_B\Big\{\hat{H}^{(I)}_{S-B}(-\tau)\hat{W}_{eq}\otimes\hat{\rho}(t)\hat{H}_{S-B}\Big\}\\ -&\mathrm{Tr}_B\Big\{\hat{H}_{S-B}\hat{W}_{eq}\otimes\hat{\rho}(t)\hat{H}^{(I)}_{S-B}(-\tau)\Big\}\\ &\mathrm{Tr}_B\Big\{\hat{W}_{eq}\otimes\hat{\rho}(t)\hat{H}^{(I)}_{S-B}(-\tau)\hat{H}_{S-B}\Big\}\ .\end{aligned} \tag{2.62}$$

[8]The difference and the point of transition between the term *quantum master equation* and the more general term *equation of motion for reduced density matrix in second-order of system-bath interaction* isn't quite settled and well-defined.

The final quantum master equation in the second order of system-bath interaction describing the dynamics of a reduced density matrix under the influence of a weakly coupled environment reads:

$$\frac{\partial}{\partial t}\hat{\rho}(t) = -i\big[\hat{H}_S, \hat{\rho}(t)\big] - \int_0^\infty \mathrm{d}\tau \begin{matrix} +\mathrm{Tr}_B\Big\{\hat{H}_{S-B}\hat{H}^{(I)}_{S-B}(-\tau)\hat{W}_{eq}\otimes\hat{\rho}(t)\Big\} \\ -\mathrm{Tr}_B\Big\{\hat{H}^{(I)}_{S-B}(-\tau)\hat{W}_{eq}\otimes\hat{\rho}(t)\hat{H}_{S-B}\Big\} \\ -\mathrm{Tr}_B\Big\{\hat{H}_{S-B}\hat{W}_{eq}\otimes\hat{\rho}(t)\hat{H}^{(I)}_{S-B}(-\tau)\Big\} \\ +\mathrm{Tr}_B\Big\{\hat{W}_{eq}\otimes\hat{\rho}(t)\hat{H}^{(I)}_{S-B}(-\tau)\hat{H}_{S-B}\Big\} \end{matrix} . \tag{2.63}$$

### 2.2.6 Bath correlation function

At this point, let's have a look at the system-bath interaction Hamiltonian. Since we factorised the total density matrix as:

$$\hat{W}(t) = \mathrm{Tr}_B\big\{\hat{W}(t)\big\}\otimes\hat{W}_{eq} = \hat{\rho}(t)\otimes\hat{W}_{eq}\,, \tag{2.64}$$

it'd be beneficial to do the same with $\hat{H}_{S-B}$, which also spans the combined Hilbert space $\mathcal{H}_S\otimes\mathcal{H}_B$. Let's assume the following factorization into, at this point still rather arbitrary, system ($\hat{K}\in\mathcal{H}_S$) and bath ($\hat{\Phi}\in\mathcal{H}_B$) operators:

$$\hat{H}_{S-B} = \sum_\nu \hat{K}_\nu\otimes\hat{\Phi}_\nu\,. \tag{2.65}$$

Another property of the interaction Hamiltonian that we've postulated during the derivation of the quantum master equation in (2.52) states that by averaging the operator with respect to the bath, we should obtain zero:

$$\big\langle\hat{H}_{S-B}\big\rangle = \mathrm{Tr}_B\big\{\hat{H}_{S-B}\hat{W}_{eq}\big\} = \sum_\nu \hat{K}_\nu\otimes\mathrm{Tr}_B\big\{\hat{\Phi}_\nu\hat{W}_{eq}\big\}\equiv 0\,. \tag{2.66}$$

Adopting the proposed form (2.65) of $\hat{H}_{S-B}$, the derived quantum master equation becomes:

$$\frac{\partial}{\partial t}\hat{\rho}(t) = -i\big[\hat{H}_S, \hat{\rho}(t)\big] - \sum_{\nu\nu'}\int_0^\infty \mathrm{d}\tau \begin{matrix} +\hat{K}_\nu\hat{K}^{(I)}_{\nu'}(-\tau)\hat{\rho}(t)\otimes\mathrm{Tr}_B\big\{\hat{\Phi}_\nu\hat{\Phi}^{(I)}_{\nu'}(-\tau)\hat{W}_{eq}\big\} \\ -\hat{K}^{(I)}_\nu(-\tau)\hat{\rho}(t)\hat{K}_{\nu'}\otimes\mathrm{Tr}_B\big\{\hat{\Phi}^{(I)}_\nu(-\tau)\hat{W}_{eq}\hat{\Phi}_{\nu'}\big\} \\ -\hat{K}_{\nu'}\hat{\rho}(t)\hat{K}^{(I)}_\nu(-\tau)\otimes\mathrm{Tr}_B\big\{\hat{\Phi}_\nu\hat{W}_{eq}\hat{\Phi}^{(I)}_{\nu'}(-\tau)\big\} \\ +\hat{\rho}(t)\hat{K}^{(I)}_{\nu'}(-\tau)\hat{K}_\nu\otimes\mathrm{Tr}_B\big\{\hat{W}_{eq}\hat{\Phi}^{(I)}_\nu(-\tau)\hat{\Phi}_{\nu'}\big\} \end{matrix} \tag{2.67}$$

$$= -i\big[\hat{H}_S, \hat{\rho}(t)\big] - \sum_{\nu\nu'}\int_0^\infty \mathrm{d}\tau \begin{matrix} +\hat{K}_\nu\hat{K}^{(I)}_{\nu'}(-\tau)\hat{\rho}(t)\otimes\mathrm{Tr}_B\big\{\hat{\Phi}_\nu\hat{\Phi}^{(I)}_{\nu'}(-\tau)\hat{W}_{eq}\big\} \\ -\hat{K}^{(I)}_\nu(-\tau)\hat{\rho}(t)\hat{K}_{\nu'}\otimes\mathrm{Tr}_B\big\{\hat{\Phi}_{\nu'}\hat{\Phi}^{(I)}_\nu(-\tau)\hat{W}_{eq}\big\} \\ -\hat{K}_{\nu'}\hat{\rho}(t)\hat{K}^{(I)}_\nu(-\tau)\otimes\mathrm{Tr}_B\big\{\hat{W}_{eq}\hat{\Phi}^{(I)}_{\nu'}(-\tau)\hat{\Phi}_\nu\big\} \\ +\hat{\rho}(t)\hat{K}^{(I)}_{\nu'}(-\tau)\hat{K}_\nu\otimes\mathrm{Tr}_B\big\{\hat{W}_{eq}\hat{\Phi}^{(I)}_\nu(-\tau)\hat{\Phi}_{\nu'}\big\} \end{matrix} . \tag{2.68}$$

Note that the Kronecker product symbol $\otimes$ was left in the expressions above (2.66–2.68) for the sake of clarity only to visually separate the terms that originate in the system and in the bath. Strictly speaking, the symbol is completely

redundant there since the trace over bath DOF is, by definition, reduced to the system Hilbert space only.

It can be shown that the traces on the first and second lines of (2.68) are complex conjugates of the ones on the third and fourth lines:

$$\left(\mathrm{Tr}_B\left\{\hat{W}_{eq}\hat{\Phi}^{(I)}_{\nu'}(-\tau)\hat{\Phi}_\nu\right\}\right)^* = \left(\left(\mathrm{Tr}_B\left\{\hat{W}_{eq}\hat{U}_B(\tau)\hat{\Phi}_{\nu'}\hat{U}^\dagger_B(\tau)\hat{\Phi}_\nu\right\}\right)^\top\right)^\dagger \tag{2.69}$$

$$= \left(\mathrm{Tr}_B\left\{\left(\hat{W}_{eq}\hat{U}_B(\tau)\hat{\Phi}_{\nu'}\hat{U}^\dagger_B(\tau)\hat{\Phi}_\nu\right)^\top\right\}\right)^\dagger \tag{2.70}$$

$$= \mathrm{Tr}_B\left\{\left(\hat{W}_{eq}\hat{U}_B(\tau)\hat{\Phi}_{\nu'}\hat{U}^\dagger_B(\tau)\hat{\Phi}_\nu\right)^\dagger\right\} \tag{2.71}$$

$$= \mathrm{Tr}_B\left\{\hat{\Phi}_\nu\hat{U}_B(\tau)\hat{\Phi}_{\nu'}\hat{U}^\dagger_B(\tau)\hat{W}_{eq}\right\} \tag{2.72}$$

$$= \mathrm{Tr}_B\left\{\hat{\Phi}_\nu\hat{\Phi}^{(I)}_{\nu'}(-\tau)\hat{W}_{eq}\right\}\,, \tag{2.73}$$

where we used the fact that Hermitian adjoint (denoted by $\dagger$) is composed of complex conjugation (denoted by $*$) followed by transposition (denoted by $\top$), the "diagonal" property of trace $(\mathrm{Tr}\{AB\})^\top = \mathrm{Tr}\left\{(AB)^\top\right\} = \mathrm{Tr}\{AB\}$, and we assumed operators $\hat{\Phi}$ are Hermitian.

For the sake of clarity, a simplified notation of $\mathrm{Tr}_B\{\cdot\} = \langle\cdot\rangle_B$ will be used from now on. Averaging over objects at two different times defines a two-time *bath correlation function* $C(t,0) = C(t)$:

$$\mathrm{Tr}_B\left\{\hat{\Phi}_\nu\hat{\Phi}^{(I)}_{\nu'}(-\tau)\hat{W}_{eq}\right\} = \left\langle\hat{\Phi}_\nu\hat{\Phi}^{(I)}_{\nu'}(-\tau)\right\rangle_B \tag{2.74}$$

$$= \left\langle\hat{\Phi}^{(I)}_\nu(\tau)\hat{\Phi}_{\nu'}\right\rangle_B = C_{\nu\nu'}(\tau)\,, \tag{2.75}$$

and

$$\mathrm{Tr}_B\left\{\hat{W}_{eq}\hat{\Phi}^{(I)}_{\nu'}(-\tau)\hat{\Phi}_\nu\right\} = C^*_{\nu\nu'}(\tau)\,. \tag{2.76}$$

From the lines (2.69) and (2.73) also follows:

$$C^*_{\nu'\nu}(-t) = C_{\nu\nu'}(t)\,. \tag{2.77}$$

### 2.2.7 Redfield theory

The quantum master equation now simplifies to:

$$\frac{\partial}{\partial t}\hat{\rho}(t) = -i\left[\hat{H}_S,\hat{\rho}(t)\right] - \sum_{\nu\nu'}\int_0^\infty \mathrm{d}\tau \begin{matrix} +\hat{K}_\nu\hat{K}^{(I)}_{\nu'}(-\tau)\hat{\rho}(t)C_{\nu\nu'}(\tau) \\ -\hat{K}^{(I)}_\nu(-\tau)\hat{\rho}(t)\hat{K}_{\nu'}C_{\nu'\nu}(\tau) \\ -\hat{K}_{\nu'}\hat{\rho}(t)\hat{K}^{(I)}_\nu(-\tau)C^*_{\nu\nu'}(\tau) \\ +\hat{\rho}(t)\hat{K}^{(I)}_{\nu'}(-\tau)\hat{K}_\nu C^*_{\nu'\nu}(\tau) \end{matrix} \tag{2.78}$$

$$= -i\left[\hat{H}_S,\hat{\rho}(t)\right] - \sum_\nu \begin{matrix} +\hat{K}_\nu\Lambda_\nu\hat{\rho}(t) \\ -\Lambda_\nu\hat{\rho}(t)\hat{K}_\nu \\ -\hat{K}_\nu\hat{\rho}(t)\Lambda^\dagger_\nu \\ +\hat{\rho}(t)\Lambda^\dagger_\nu\hat{K}_\nu \end{matrix} \tag{2.79}$$

$$= -i\left[\hat{H}_S,\hat{\rho}(t)\right] - \sum_\nu\left(\left[\hat{K}_\nu\,,\Lambda_\nu\hat{\rho}(t)\right] + \left[\hat{\rho}(t)\Lambda^\dagger_\nu,\hat{K}_\nu\right]\right) \tag{2.80}$$

where the new operators are defined as

$$\Lambda_\nu \equiv \sum_{\nu'} \int_0^\infty \mathrm{d}\tau C_{\nu\nu'}(\tau)\hat{K}^{(I)}_{\nu'}(-\tau)\,, \tag{2.81}$$

$$\Lambda^\dagger_\nu = \sum_{\nu'} \int_0^\infty \mathrm{d}\tau \hat{K}^{(I)}_{\nu'}(-\tau)C^*_{\nu'\nu}(\tau)\,. \tag{2.82}$$

were introduced. Note that a re-indexation $\nu \leftrightarrow \nu'$ was performed in the two middle lines of (2.79).

The equation derived in (2.80) is the most general form of a quantum master equation in the second order of the system-bath interaction without specifying pretty much any details about the model. To sum up the obtained expression, the time-local equation of motion has essentially two contributing terms. The commutator with the system Hamiltonian $\hat{H}_S$ governs the prevailing unitary dynamics of the quantum system since we're operating under the assumption of weak system-bath coupling. The second term comes from the second order of perturbation theory in the system-bath interaction. In particular, the second-order approximation was made in the evolution superoperator that describes the dynamics of our quantum system embedded in a much larger environment. The interaction itself isn't a subject of the approximation stemming from perturbation theory, though. However, several other approximations and assumptions were made.

Firstly, we factorised the entire system into two parts—system and bath—by performing a space reduction on the equation of motion. Secondly, we've reintroduced the Markovian property by adopting the Markov approximation, which disregards bath dynamics occurring on a long timescale. Thirdly, we postulated the system-bath interaction averages to zero with respect to bath. And finally, a factorisation of the system-bath interaction Hamiltonian was postulated as well.

This equation (2.80) belongs to the family of *Redfield equations* (Redfield, 1965). The compact and general form of the Redfield equation can be expressed in Liouville space in the following manner:

$$\frac{\partial}{\partial t}\hat{\rho}(t) = -i\breve{\mathcal{L}}_{\hat{H}_S}\hat{\rho}(t) - \breve{\mathcal{R}}\hat{\rho}(t)\,, \tag{2.83}$$

where $\breve{\mathcal{R}}$ is the *Redfield relaxation tensor*. In case the upper integration limit at (2.81) and (2.82) is set to the time $t$ instead of $\infty$, the operators become time-dependent. By doing so, we obtain the *time-dependent Redfield equation* with time-dependent Redfield relaxation tensor $\breve{\mathcal{R}}(t)$

### 2.2.8 Redfield theory in secular approximation

The Redfield relaxation superoperator can be expressed as a rank four tensor:

$$\mathcal{R}_{ijkl}\,, \tag{2.84}$$

assuming the Einstein summation convention from now on. Since it is a (super)operator, it can be represented in different bases. The most apparent choice of basis which provides the most insight is the basis of system Hamiltonian

eigenstates. This basis is sometimes called the *energy basis* or the *exciton basis*. The Redfield equation expressed in the energy basis reduces to:

$$\frac{\partial}{\partial t}\rho_{ij}(t) = -i\omega_{ij}\rho_{ij}(t) - \mathcal{R}_{ijkl}\rho_{kl}(t)\ , \tag{2.85}$$

where $\omega_{ij} = E_i - E_j$. The interaction picture can be once again adopted to get rid of the first term on the right-hand-side:

$$\rho^{(I)}_{jk}(t) = \left(\hat{U}^{\dagger}_S(t)\right)_{ij}\rho_{jk}\left(\hat{U}_S(t)\right)_{kl} = \delta_{ij}e^{iE_jt}\rho_{jk}e^{-iE_kt}\delta_{kl} = e^{i\omega_{jk}t}\rho_{jk}(t)\ . \tag{2.86}$$

We can now plug the following expression for $\rho(t)$:

$$\rho_{jk}(t) = e^{-i\omega_{jk}t}\rho^{(I)}_{jk}(t) \tag{2.87}$$

back to the Redfield equation, which then reads:

$$\frac{\partial}{\partial t}\rho^{(I)}_{ij}(t) = -e^{i\omega_{ij}t}\mathcal{R}_{ijkl}e^{-i\omega_{kl}t}\rho^{(I)}_{kl}(t) \tag{2.88}$$

$$= e^{i(\omega_{ij}-\omega_{kl})t}\mathcal{R}_{ijkl}\rho^{(I)}_{kl}(t)\ . \tag{2.89}$$

The equation (2.89) can be formally integrated which results in:

$$\rho^{(I)}_{ij}(t) = \rho^{(I)}_{ij}(t_0) - \mathcal{R}_{ijkl}\int_0^t \mathrm{d}\tau\ e^{i\Delta\omega\tau}\rho^{(I)}_{kl}(\tau) \tag{2.90}$$

$$\approx \rho^{(I)}_{ij}(t_0) - \mathcal{R}_{ijkl}\int_0^t \mathrm{d}\tau\ e^{i\Delta\omega\tau}\rho^{(I)}_{kl}(t) \tag{2.91}$$

$$= \rho^{(I)}_{ij}(t_0) - \mathcal{R}_{ijkl}\frac{1}{i\Delta\omega}\left(e^{i\Delta\omega t} - 1\right)\rho^{(I)}_{kl}(t)\ , \tag{2.92}$$

where we assumed $\rho^{(I)}_{kl}(\tau) \approx \rho^{(I)}_{kl}(t)$ since it evolves in the interaction picture slowly. Besides, the differential frequency $\Delta\omega = \omega_{ij} - \omega_{kl}$ was also introduced there. Let us now explore the behaviour of the result of integration performed in (2.92) with respect to the differential frequency $\Delta\omega$:

$$\lim_{\Delta\omega\to 0}\frac{1}{i\Delta\omega}\left(e^{i\Delta\omega t} - 1\right) \approx \frac{1 + i\Delta\omega t - 1}{i\Delta\omega} = t\ . \tag{2.93}$$

To sum up, if the differential frequency is close to zero, $\Delta\omega \approx 0$, the reduced density matrix dynamic boils down to:

$$\rho^{(I)}_{ij}(t) = \rho^{(I)}_{ij}(t_0) - \mathcal{R}_{ijkl}t\rho^{(I)}_{kl}(t)\ . \tag{2.94}$$

In other cases, i.e. $\Delta\omega \not\approx 0$, the term quickly diverges from the linear dependence on $t$, the real part of the term decreases as $\Delta\omega$ increases, and it also starts to oscillate around zero. The same occurs to the imaginary part, as can be seen in Figure 2.1.

As a result, in all the cases when the differential frequency isn't close to zero, the terms won't significantly contribute to the dynamics, or they can even be a source of numerical errors due to the quick oscillations. Hence, it sounds reasonable to disregard all the terms of the Redfield relaxation tensor that lead to non-cancelling frequencies.

The reduced density matrix has two types of elements—populations $\sum_i \rho_{ii}$, and coherences $\sum_{i,j(\neq i)}\rho_{ij}$. This leads to two sets of indices that will lead to the oscillation cancellation or no oscillations in the first place:

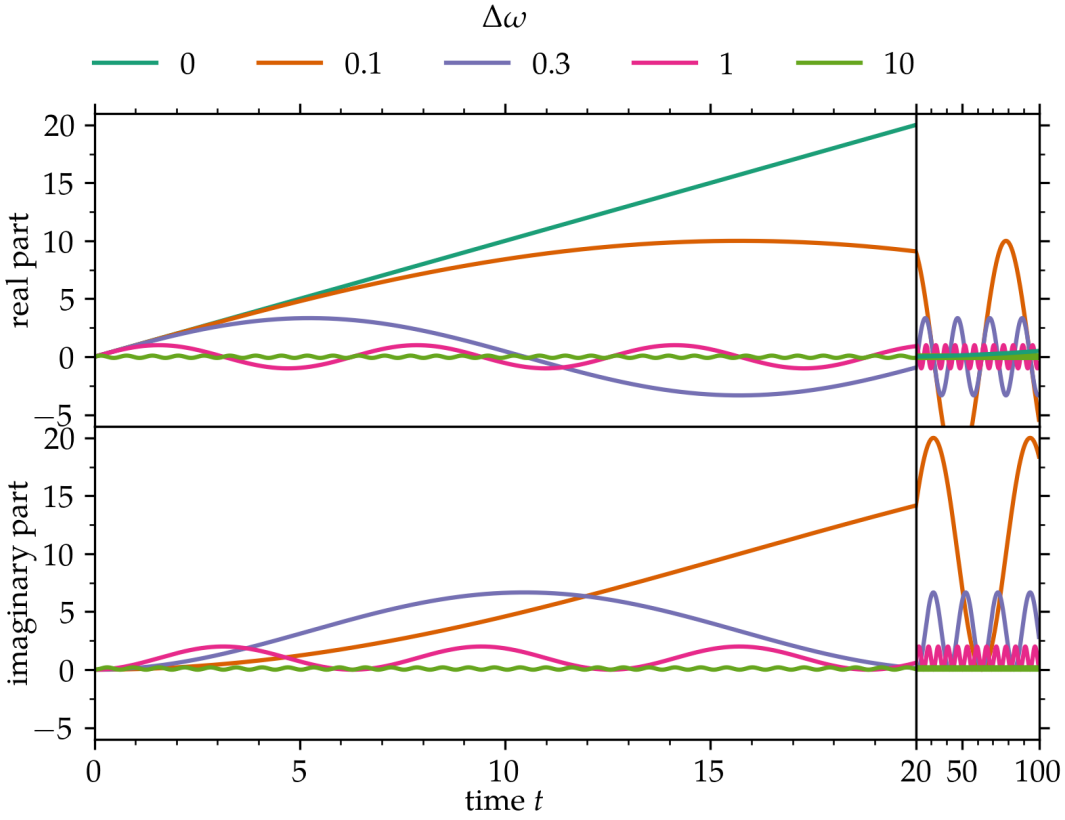


**Figure 2.1:** The evolution of the term $\frac{1}{i\Delta\omega}\left(e^{i\Delta\omega t}-1\right)$ for different values of $\Delta\omega$.

i) $\mathcal{R}_{iikk}\rho_{kk} \rightarrow \delta_{ij}\delta_{kl}$ for populations,

ii) $\mathcal{R}_{klkl}\rho_{kl} \rightarrow \delta_{ik}\delta_{jl}$ for coherences.

The first case describes the transfer or populations:

$$\frac{\partial}{\partial t}\rho_{ii}(t) = -\sum_{j}\mathcal{R}_{iijj}\rho_{jj}(t)\,, \tag{2.95}$$

where $\mathcal{R}_{iijj} = -K_{ij}$ is a negative value of a *transfer rate* from population $\rho_{jj} \rightarrow \rho_{ii}$ . Since the populations of a density matrix aren't subjects of any unitary evolution and oscillations, the rates will be real-valued.

The second case describes the process of *decoherence*—attenuation of the coherences due to the system relaxation:

$$\frac{\partial}{\partial t}\rho_{ij}(t) = -i\omega_{ij}\rho_{ij}(t) - \mathcal{R}_{ijij}\rho_{ij}(t)\,, \tag{2.96}$$

where $\mathcal{R}_{ijij}$ is a *decoherence rate* for a coherence $\rho_{ij}$.

Setting all other elements of the Redfield tensor to zero—leaving only the two types of elements discussed above—is called the *secular approximation*. The tensor elements that describe the abovementioned population transfer and decoherence are referred to as *secular* terms, and the rest is denoted as *nonsecular* terms.

## 2.3 The model

As explored in the introduction, the aim of this thesis is to construct a robust theoretical model of a chlorophyll molecule compatible with already existing theories developed for theoretical spectroscopy and for the study of complex molecular aggregates in general. The models that have been actively used so far pretty much always considered chlorophyll molecules to be two-level systems. Eventually, also three-level models were used (Niu et al., 2008) if the spectroscopic experiment demanded it.

### 2.3.1 Introduction

Let's start from the beginning and outline the framework of approximations we'll be working with. To begin with, the Hamiltonian of a molecule, which is a many-body system of electrons and nuclei, can be written as:

$$\hat{H}_S = \underbrace{\hat{T}_{nuc}(\mathbf{R})}_{\hat{H}_{nuc}(\mathbf{R})} + \hat{V}_{el-nuc}(\mathbf{r},\mathbf{R}) + \underbrace{\hat{T}_{el}(\mathbf{r}|\mathbf{R}) + \hat{V}_{el-el}(\mathbf{r}) + \hat{V}_{nuc-nuc}(\mathbf{R})}_{\hat{H}_{el}(\mathbf{r}|\mathbf{R})} \tag{2.97}$$

$$\begin{aligned} &= \sum_{\alpha} -\frac{1}{2M_\alpha}\nabla_\alpha^2 + \sum_{\alpha<\beta}\frac{Z_\alpha Z_\beta}{\left|R_\beta - R_\alpha\right|} \\ &+ \sum_i \left( -\frac{1}{2m_{el}}\nabla_i^2 + \sum_{j(<i)}\frac{1}{\left|r_i - r_j\right|} - \sum_\alpha \frac{Z_\alpha}{|r_i - R_\alpha|} \right), \end{aligned} \tag{2.98}$$

where $\hat{T}_{nuc}$ represents the kinetic energy of nuclei, $\hat{T}_{el}$ is the kinetic energy of electrons, and $\hat{V}_{el-el}$, $\hat{V}_{el-nuc}$, $\hat{V}_{nuc-nuc}$ are interaction potentials between electrons, between electrons and nuclei, and between nuclei, in the corresponding order. $\mathbf{r}$ are cartesian coordinates of the electrons, $\mathbf{R}$ are coordinates of the nuclei, and $Z_\alpha$ and $M_\alpha$ is a charge and a mass of $\alpha$th nuclei, correspondingly.

Since the mass of nuclei is much larger than that of the electrons, by a factor of ca 1836, the kinetic energy is by this factor smaller than that of the electrons:

$$\frac{E_{K,J}}{E_{K,el}} = \frac{p_J^2}{\underbrace{p_{el}^2}_{\mathbb{1}}}\frac{m_{el}}{m_J} = \frac{1}{1836} = 5.45\cdot 10^{-4}\,. \tag{2.99}$$

The kinetic energy of nuclei can be thus considered by means of a perturbation theory as a small perturbation to the electronic problem. The first approximation assigns nuclei a fixed position in space. For any position of the nuclei, the electronic part of the system will always remain in a stationary state given by the Schrödinger equation. That is, the electrons adiabatically react to changes in the position of nuclei. In this framework, the reorganization of nuclei cannot cause excitation to a higher electronic state. The total Hamiltonian $\hat{H}_S$ of such a system would be diagonal in the basis of electronic eigenstates of the electronic Hamiltonian $\hat{H}_{el}$:

$$\hat{H}_{el}\left|u_i^{(\mathrm{el})}\right\rangle = U_i^{(el)}\left|u_i^{(\mathrm{el})}\right\rangle. \tag{2.100}$$

The total wavefunction of such a system can be expanded in the basis of the electronic eigenstates:

$$|\Psi\rangle = \left( \sum_i \left|u_i^{(\mathrm{el})}\right\rangle \left\langle u_i^{(\mathrm{el})}\right| \right) |\Psi\rangle \tag{2.101}$$

$$= \sum_i \left|w_i^{(J)}\right\rangle \left|u_i^{(\mathrm{el})}\right\rangle, \tag{2.102}$$

where state $\left|w_i^{(J)}\right\rangle$ represent the nuclear wavefunction. By plugging this factorised form into the time-independent Schödinger equation $\hat{H}_S |\Psi\rangle = E|\Psi\rangle$ and multiplying the expression from the left by $\left\langle u_i^{(\mathrm{el})}\right|$, we obtain:

$$\left\langle u_i^{(\mathrm{el})}\right| \hat{H} |\Psi\rangle = \left\langle u_j^{(\mathrm{el})}\right| (\hat{T}_J + \hat{H}_{el}) \left( \sum_i \left|w_i^{(J)}\right\rangle \left|u_i^{(\mathrm{el})}\right\rangle \right) \tag{2.103}$$

$$= \sum_i \left\langle u_j^{(\mathrm{el})}\middle|\hat{T}_J\middle|u_i^{(\mathrm{el})}\right\rangle \left|w_i^{(\mathrm{J})}\right\rangle + \underbrace{\left\langle u_j^{(\mathrm{el})}\middle|\hat{H}_{el}\middle|u_i^{(\mathrm{el})}\right\rangle}_{U_i^{(el)}\delta_{ij}} \left|w_i^{(\mathrm{J})}\right\rangle \tag{2.104}$$

The matrix element of the kinetic energy operator can be expressed as follows:

$$\left\langle u_j^{(\mathrm{el})}\middle|\hat{T}_J\middle|u_i^{(\mathrm{el})}\right\rangle \left|w_i^{(\mathrm{J})}\right\rangle = \sum_\alpha -\frac{1}{2M_\alpha} \left\langle u_j^{(\mathrm{el})}\right| \left( \nabla_\alpha^2 \left|u_i^{(\mathrm{el})}\right\rangle \left|w_i^{(\mathrm{J})}\right\rangle \right) \tag{2.105}$$

$$\begin{aligned} = \sum_\alpha -\frac{1}{2M_\alpha} \Bigg( & \left( \left\langle u_j^{(\mathrm{el})}\middle|\nabla_\alpha^2\middle|u_i^{(\mathrm{el})}\right\rangle \right) \left|w_i^{(\mathrm{J})}\right\rangle \\ & + 2\left( \left\langle u_j^{(\mathrm{el})}\middle|\nabla_\alpha\middle|u_i^{(\mathrm{el})}\right\rangle \right) \left(\nabla_\alpha \left|w_i^{(\mathrm{J})}\right\rangle \right) \\ & + \underbrace{\left\langle u_j^{(\mathrm{el})}\middle|u_i^{(\mathrm{el})}\right\rangle}_{\delta_{ij}} \left(\nabla_\alpha^2 \left|w_i^{(\mathrm{J})}\right\rangle \right) \Bigg). \end{aligned} \tag{2.106}$$

An *operator of nonadiabaticity* can be introduced to simplify the notation:

$$\hat{\Theta}_{ji} = \left( \left\langle u_j^{(\mathrm{el})}\middle|\hat{T}_J\middle|u_i^{(\mathrm{el})}\right\rangle - \sum_\alpha \frac{1}{M_\alpha} \left\langle u_j^{(\mathrm{el})}\middle|\nabla_\alpha\middle|u_i^{(\mathrm{el})}\right\rangle \nabla_\alpha \right). \tag{2.107}$$

The equation (2.105) can be then again summed over $i$ and expressed as:

$$\sum_i \left\langle u_j^{(\mathrm{el})}\middle|\hat{T}_J\middle|u_i^{(\mathrm{el})}\right\rangle \left|w_i^{(\mathrm{J})}\right\rangle = \sum_{i(\neq j)} \hat{\Theta}_{ji} \left|w_i^{(\mathrm{J})}\right\rangle + \left( \hat{\Theta}_{jj} + \hat{T}_J \right) \left|w_j^{(\mathrm{J})}\right\rangle. \tag{2.108}$$

The Schródinger equation describing thy dynamics of nuclei finally becomes:

$$\left( \hat{T}_J + \underbrace{\hat{\Theta}_{jj} + U_j^{(\mathrm{el})}}_{\hat{W}_j} \right) \left|w_j^{(\mathrm{J})}\right\rangle = E \left|w_j^{(\mathrm{J})}\right\rangle - \sum_{i(\neq j)} \hat{\Theta}_{ji} \left|w_i^{(\mathrm{J})}\right\rangle. \tag{2.109}$$

The equation (2.109) is still exact; no approximations have been introduced yet. The operator $\hat{W}$ on the left-hand-side represents a *potential hypersurface*,

also known as potential energy surface (PES). At the beginning of this section, an adiabatic Hamiltonian was proposed to be diagonal in the eigenbasis of electronic states. That means the operator of nonadiabaticity needs to be zero. By neglecting it, we are adopting the so-called *adiabatic approximation*.

Generally speaking, the elements of the nonadiabatic operator $\Theta_{ji}$ $(i \neq j)$ can be expected to be zero if the electronic levels $i, j$ are well energetically separated, which usually applies to the first excited state and the ground state (May and Kühn, 2011). Hence, we can consider $i = 0$ and $\Theta_{0j} = 0$. This gives us:

$$\left(\hat{T}_J + \underbrace{\hat{\Theta}_{00} + U_0^{(\mathrm{el})}}_{\hat{W}_0} - E\right)\left|w_0^{(\mathrm{J})}\right\rangle = 0\,. \tag{2.110}$$

If the diagonal element of the nonadiabatic operator $\Theta_{jj}$ is committed as well, we arrive at the form of Hamiltonian in *Born-Oppenheimer approximation*:

$$\left(\hat{T}_J + U_0^{(\mathrm{el})} - E\right)\left|w_0^{(\mathrm{J})}\right\rangle = 0. \tag{2.111}$$

However, the first two excited states of the molecule of chlorophyll aren't that well energetically separated and hence a question arises whether it is appropriate to assume that the elements of the nonadiabatic operator $\Theta_{jj}$ will equal zero in the case of $i = Q_y, j = Q_x$. Following the previously used models of chlorophyll molecules (Reimers et al., 2013; Niu et al., 2008), the elements were considered nonzero between the first and second excited states. Following the approach of Reimers et al. (2013), the nonadiabatic terms, also called simply *diabatic*, were assumed to be linear in bath coordinate, as will be discussed further.

### 2.3.2 Model of the System

The quantum system of our interest consists of a single molecule of chlorophyll-like pigment. As discussed in Chapter 1, the two lowest-in-energy electronic transitions are expected to play a major role and are going to be included in the model. Along with the ground state, the molecule will be approximated by a *three-level system* (the levels are generally denoted by $g, e, f$). The two transitions are usually called $Q_y$ $(g \to e)$ and $Q_x$ $(g \to f)$, and they are roughly perpendicular to each. Hence the axes names that appear in subscript. The exact value of the angle, as well as the oscillator strength, i.e. amplitude, of the transitions, depend on the molecular chemical structure and on the solvent. For the sake of clarity, the corresponding electronic states will be denoted as $|g\rangle, \left|Q_y\right\rangle, |Q_x\rangle$.

Since our aim is to simulate and better understand the ultra-fast dynamics that are being observed between the two excited states $Q_y$ and $Q_x$, it is necessary to introduce to the system some kind of coupling that would bridge the interaction between them and open the door for the fast relaxation pathway.

The energy gap between $Q_y$ and $Q_x$ can be effectively decreased by introducing explicit vibrational modes to the system. The reasoning for that is given in the following subsection 2.3.3. For now, let us assume there are some vibrational modes which are expressed explicitly, and then there are some others that we will be treated otherwise.

The vibrational modes each belong to different Hilbert spaces that are also different from the Hilbert space of the electronic states. The addition of the modes to the electronic states is thus performed by a *tensor product*[9]. A similar operation called *tensor sum*[10] can also be defined. It can be used in formulations of objects that spread multiple Hilbert spaces. For the sake of simplicity, this operation will be explicitly used only sparsely, and the much simpler approach of implying this operation by a standard addition operator + between objects of different Hilbert spaces will be used predominantly.

For example, let's have an arbitrary matrix $A = \begin{pmatrix} a_1 & 0 \\ 0 & a_2 \end{pmatrix}$ of dimension $N_A \times N_A$, and a arbitrary matrix $B$ of dimensions $N_B \times N_B$. Let's now compare the tensor product $A \otimes B$ with the tensor sum $A \oplus B$:

$$A \otimes B = \begin{pmatrix} A_1 B & 0 \\ 0 & A_2 B \end{pmatrix}_{N_A N_B \times N_A N_B} , \tag{2.112}$$

$$A \oplus B = A \otimes \mathbb{1} + \mathbb{1} \otimes B \tag{2.113}$$

$$= \begin{pmatrix} A_1 + B & 0 \\ 0 & A_2 + B \end{pmatrix}_{N_A N_B \times N_A N_B} . \tag{2.114}$$

As can be seen, the addition of explicit vibrational modes to the system part of our problem dramatically increases the dimensions of the Hamiltonian and of the reduced density matrix. The resulting states that span both the electronic and a vibrational Hilbert space can be called *vibronic states*.

The explicit vibrational modes will be modelled by a quantum harmonic oscillator. Even though it's a rather rough approximation whose validity is limited to low excited states only around the potential minima at which the harmonic potential is centred, it still should provide sufficient insight into the modelled processes. The quantum harmonic oscillator Hamiltonian reads:

$$\hat{H}'_{Vi} = \frac{\Omega_{Vi}}{2} \left( \hat{P}^2_{Vi} + \hat{Q}^2_{Vi} \right) , \tag{2.115}$$

where $i$ is the index of the explicit vibrational mode included in the system, and $N_V$ is, from now, on, the number of such modes considered. In previous works (Reimers et al., 2013; Niu et al., 2008), up to one mode was added. However, we decided to explore also the case when two such modes are introduced. The reason for that was discussed in subsection 2.3.1.

The analytical representation of (2.115) is well-known and can be expressed as:

$$\hat{H}'_{Vi} = \Omega_{Vi} \left( \hat{a}^\dagger \hat{a} + \frac{1}{2} \right) \tag{2.116}$$

$$= \sum_{n}^{N_i} \Omega_{Vi} \left( n + \frac{1}{2} \right) |n\rangle\langle n| , \tag{2.117}$$

[9] Also known as *Kronecker* or *direct product*.
[10] Also known as *Kronecker* or *direct sum*

where $\hat{a}$ and $\hat{a}^\dagger$ are bosonic *annihilation* and *creation operators*, in corresponding order, defined as:

$$\begin{aligned} \hat{a} &= \frac{1}{\sqrt{2}} \left( \hat{q} + i\hat{p} \right) \ , \\ \hat{a}^\dagger &= \frac{1}{\sqrt{2}} \left( \hat{q} - i\hat{p} \right) \ . \end{aligned} \tag{2.118}$$

Besides, they obey the following relations:

$$\left[ \hat{a}_i, \hat{a}_j^\dagger \right] = \delta_{ij} \ , \tag{2.119}$$

$$\hat{a} \left| n \right\rangle = \sqrt{n} \left| n-1 \right\rangle \ , \tag{2.120}$$

$$\hat{a}^\dagger \left| n \right\rangle = \sqrt{n+1} \left| n+1 \right\rangle \ , \tag{2.121}$$

$$\hat{a} \left| \emptyset \right\rangle = 0 \left| \emptyset \right\rangle \ . \tag{2.122}$$

Also note that the Hamiltonian of the harmonic oscillator expressed in its eigenbasis in (2.117) was cropped into a finite dimension of $N_i$. The number of the modes included can be even further differentiated separately for each individual electronic state. Hence, notation $N_{i,j}$, where the index $i$ corresponds to different explicit modes and the index $j$ ($\in \{g,e,f\} = \left\{ g, \hat{Q}_y, \hat{Q}_x \right\}$) to different electronic states of the system, might be more appropriate.

The addition of explicit vibrational modes to the system should also be reflected in the model of the bath. Even though the details about the bath are discussed in the following subsection 2.3.3, for the sake of clarity, the interaction of the explicit vibrational modes with the bath will be discussed here and now.

The effect of the bath on the explicit vibrational modes should be causing relaxation in them. Since the Hamiltonian of the harmonic oscillator—the model for explicit vibrational modes—is purely diagonal, see (2.117), the vibrational bath can be assumed to be by-one off-diagonal so that the interaction may bridge the neighbouring energy levels. From (2.118) can be shown that one operator that would suit our intention is the operator of position $\hat{Q}$. Therefore, the interaction with the vibrational bath will be linear in $\hat{Q}$. Malý et al. (2016) proposed the following form of the $i$th harmonic mode interacting with its bath:

$$\hat{H}_{Vi} = \underbrace{\frac{\Omega_{Vi}}{2} \left( \hat{P}_{Vi}^2 + \hat{Q}_{Vi}^2 \right)}_{\hat{H}'_{Vi}} - \sqrt{2} \hat{Q}_{Vi} \otimes \hat{\Phi}_{B,Vi} \tag{2.123}$$

$$= \Omega_{Vi} \left( \hat{a}^\dagger \hat{a} + \frac{1}{2} \right) - \left( \hat{a} + \hat{a}^\dagger \right) \otimes \hat{\Phi}_{B,Vi} \tag{2.124}$$

$$= \sum_{n=0}^{N_V} \Omega_{Vi} \left( n + \frac{1}{2} \right) |n\rangle\langle n| - \underbrace{\sqrt{n+1} \Big( |n+1\rangle\langle n| + |n\rangle\langle n+1| \Big)}_{\hat{K}_{Vi}} \otimes \hat{\Phi}_{B,Vi} \ , \tag{2.125}$$

where $\hat{\Phi}_{B,Vi}$ is an operator of the bath which the modes are interacting with. The form of the operator will be revealed in the following subsection 2.3.3.

Nevertheless, just the addition of some explicit modes to the electronic states of the molecule still doesn't strictly result in a fast relaxation from $|Q_x\rangle$ to $\left|Q_y\right\rangle$. The relaxation would be happening in each of the modes independently and to their own vibrational ground states (assuming $\omega_{Vi} >> k_B T$).

To change that, the Born-Oppenheimer approximation has to be questioned. One way to mix the $\left|Q_y\right\rangle$ and $|Q_x\rangle$ states is—as published by (Reimers et al., 2013; Niu et al., 2008), for example—to introduce a linear diabatic coupling $\hat{H}_{el-vib,i}$ between the two electronic states:

$$\hat{H}_{el-vib,i} = \alpha_i \hat{Q}_{Vi} \left( \left|Q_y\right\rangle\!\left\langle Q_x\right| + \left|Q_x\right\rangle\!\left\langle Q_y\right| \right) , \tag{2.126}$$

where $\alpha_i$ is a constant representing the strength of the coupling, and $\hat{Q}_{Vi}$ is a coordinate of the $i$th vibrational mode explicitly included in the system Hamiltonian. In Figure 2.2, you can see the construction process of the system Hamiltonian with a single explicitly included vibrational mode.

### 2.3.3 Model of the bath

The standard approach for modelling the environment is to consider it as an infinite set of harmonic oscillators. There are multiple reasons that back this model up. Let's elaborate on the degrees of freedom the physical environment we are trying to model is expected to have.

The first constituent involves the vibrational degrees of freedom of both the physical environment and the molecule (the vibrational modes explicitly included in the system were sourced from there). Even though potential energy surfaces pertinent to the vibrations aren't harmonic, the actual potential can always be approximated by the harmonic one near its minima. This harmonic approximation tends to be valid for low-excited vibrational states only since it completely disregards the dissociation limit and incorrectly introduces equidistant energy levels.

The second constituent is the electromagnetic field that opens the channel for radiative transitions and radiative relaxation. It is purely bosonic and thus corresponds well to the statistics of harmonic oscillators.

The third constituent of the bath is a little more conceptual and essentially exists on top of the two already mentioned. Since we are dealing with molecules or molecular aggregates in solvents, the sample is undergoing a perpetual chaotic motion that may influence and shift the energetic transitions. Most of the processes in concern have Gaussian distribution of fluctuations, which corresponds to bosonic statistics and to the harmonic model once again.

Let us consider an infinite set of bath coordinates $\{\hat{q}_k\}_k^\infty$ (they can be viewed as coordinates of the vibrational normal modes) and a corresponding set of momenta $\{\hat{p}_k\}_k^\infty$. The general bath Hamiltonian $\hat{H}_B$ modelled by the infinite set of dimensionless quantum harmonic oscillators then reads:

$$\hat{H}_B = \sum_k^\infty \frac{\omega_k}{2} \left( \hat{p}_k^2 + \hat{q}_k^2 \right) \tag{2.127}$$

$$= \sum_k^\infty \omega_k \left( \underbrace{\hat{a}_k^\dagger \hat{a}_k}_{\hat{n}_k} + \frac{1}{2} \right) . \tag{2.128}$$

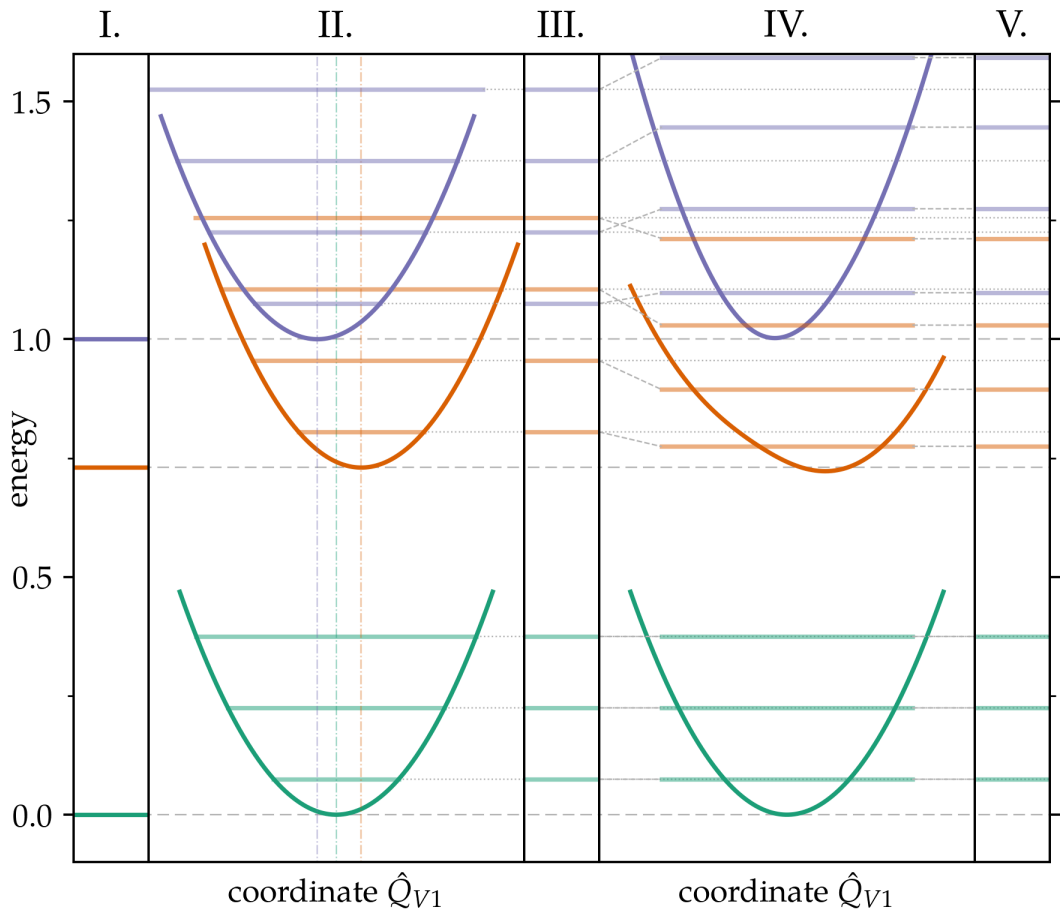


**Figure 2.2:** A schematic representation of the system Hamiltonian construction steps. In panel I., only electronic states of our three-level model are present. Moving one step (and panel) right, one explicit vibrational mode was added to the system. Its energies are depicted on the energy level diagram in panel III. By moving to the panel labelled IV., the linear diabatic coupling $H_{el-vib,i}$ is added, and the whole system Hamiltonian is diagonalised. The eigenenergies of vibronic states are depicted in the right diagram V. The colour selection for vibronic energy levels and hence their assignment to the diabatic states (as indicated by non-horizontal dashed lines between energy levels of panels III. and IV.) were based on the single most dominant contribution (i.e. the maximum squared values of the Hamiltonian-diagonalising matrix $S$, such that $\hat{S}^{\dagger}\hat{H}_S\hat{S} = E\mathbb{1}$, were calculated). The parameters used for this exemplary model were chosen arbitrarily and for illustration only. The parameters are included in the appendix section A.2.

In the theory of molecular aggregates, an assumption about local, independent baths is made based on the argument the molecules are somewhat separated in space, and their mutual interaction through the bath can be neglected. In our case, this argument can no longer be used since the system consists of a single molecule. Hence, this assumption cannot be made.

As a result, a common bath coordinate can be found for all three electronic states. However, the potentials belonging to different electronic states cannot be expected to be perfectly aligned. The harmonic potential energy surfaces will be thus shifted by an arbitrary constant $d_k$. We arrive at this set of equations

defining the bath Hamiltonian for the individual electronic states:

$$\hat{H}_B^{(g)} = \sum_k^{\infty} \frac{\omega_k}{2} \left(\hat{p}_k^2 + \hat{q}_k^2\right) , \tag{2.129}$$

$$\hat{H}_B^{(Q_y)} = \sum_k^{\infty} \frac{\omega_k}{2} \left(\hat{p}_k^2 + \left(\hat{q}_k - d_k^{(Q_y)}\right)^2\right) \tag{2.130}$$

$$= \hat{H}_B^{(g)} + \underbrace{\sum_k^{\infty} \frac{\omega_k}{2} \left(d_k^{(Q_y)}\right)^2}_{\lambda^{(Q_y)}} \underbrace{- \sum_k^{\infty} \omega_k \hat{q}_k d_k^{(Q_y)}}_{\Delta\hat{V}^{(Q_y)}} , \tag{2.131}$$

$$\hat{H}_B^{(Q_x)} = \sum_k^{\infty} \frac{\omega_k}{2} \left(\hat{p}_k^2 + \left(\hat{q}_k - d_k^{(Q_x)}\right)^2\right) \tag{2.132}$$

$$= \hat{H}_B^{(g)} + \underbrace{\sum_k^{\infty} \frac{\omega_k}{2} \left(d_k^{(Q_x)}\right)^2}_{\lambda^{(Q_x)}} \underbrace{- \sum_k^{\infty} \omega_k \hat{q}_k d_k^{(Q_x)}}_{\Delta\hat{V}^{(Q_y)}} . \tag{2.133}$$

Several new quantities and operators were introduced in the equations (2.130)–(2.133). $\lambda^{(Q_y)}$ and $\lambda^{(Q_x)}$ are called *reorganisation energies*, and they are real-valued constants pertinent to the two electronic states denoted by $Q_y$ and $Q_x$. The reorganisation energy represents an energetic shift occurring during vertical transitions between the misaligned but identical potential energy surfaces. For a schematic representation, please see Figure 2.2. An alternative quantity that is frequently used is the *Huang-Rhys factor S* defined as:

$$S^{(j)} = \sum_k^{\infty} S_k = \sum_k^{\infty} \frac{\lambda_k^{(j)}}{\omega_k} = \sum_k^{\infty} \frac{1}{2} \left(d_k^{(j)}\right)^2 . \tag{2.134}$$

The Huang-Rhys factor $S_k$ essentially expresses the reorganisation energy $\lambda_k$ in the units of frequency $\omega_k$. Operators $\Delta\hat{V}^{(Q_y)}$ and $\Delta\hat{V}^{(Q_x)}$ represent a system-bath interaction of the electronic state $\left|Q_y\right\rangle$ and $|Q_x\rangle$, correspondingly, with the infinite set of harmonic oscillators forming the bath.

In the previous section, a formal differentiation between an electronic and vibrational bath was introduced (the terms reflect the system degrees of freedom the bath is interacting with). However, the model of both of the baths will be the same for the reasons discussed at the beginning of this section. The operator $\hat{\Phi}_{B,Vi}$ should be then viewed as a variant of the term $\Delta\hat{V}$ defined above. That is, $\hat{\Phi}_{B,Vi}$ is linear in the bath coordinate $\hat{q}_k$. The vibrational bath that interacts with *i*th explicit vibrational mode can be expressed in a similar manner as the electronic one discussed so far:

$$\hat{H}_B^{(Vi)} = \hat{H}_B^{(g)} + \lambda^{(Vi)} + \hat{\Phi}_{B,Vi} . \tag{2.135}$$

The Hamiltonian of the bath can be summed up as follows:

$$\begin{aligned}\hat{H}_B &= \hat{H}_B^{(g)} \otimes |g\rangle\langle g| + \hat{H}_B^{(Q_y)} \otimes \left|Q_y\right\rangle\left\langle Q_y\right| + \hat{H}_B^{(Q_x)} \otimes |Q_x\rangle\langle Q_x| \\ &\quad + \sum_i^I \hat{H}_{B,Vi} \otimes \hat{K}_{Vi} \end{aligned} \tag{2.136}$$

$$\begin{aligned}&= \hat{H}_B^{(g)} \otimes \mathbb{1}_{el} \otimes \mathbb{1}_V + \left(\lambda^{(Q_y)} + \Delta\hat{V}^{(Q_y)}\right) \otimes \left|Q_y\right\rangle\left\langle Q_y\right| \\ &\quad + \left(\lambda^{(Q_x)} + \Delta\hat{V}^{(Q_x)}\right) \otimes |Q_x\rangle\langle Q_x| + \underbrace{\sum_i^I \left(\lambda^{(Vi)} + \hat{\Phi}_{B,Vi}\right) \otimes \hat{K}_{Vi}}_{\text{already in } \hat{H}_{Vi}} . \end{aligned} \tag{2.137}$$

In equation (2.52), we postulated the system-bath interaction Hamiltonian $\hat{H}_{S-B}$ should average to zero with respect to the bath degrees of freedom:

$$\left\langle \hat{H}_{S-B} \right\rangle_B = \mathrm{Tr}_B\left\{\hat{H}_{S-B}\hat{W}_{eq}\right\} \equiv 0 , \tag{2.138}$$

where $\hat{W}_{eq}$ is a bath density matrix in thermal equilibrium. Using the Boltzmann distribution and the Hamiltonian in the form of (2.128), we can express $\hat{W}_{eq}$ as follows:

$$\hat{W}_{eq} = \frac{1}{Z}\exp\left\{-\beta\hat{H}_B^{(g)}\right\} \tag{2.139}$$

$$= \frac{1}{Z}\prod_k^\infty \exp\left\{-\beta\omega_k\left(\hat{n}_k + \frac{1}{2}\right)\right\} \tag{2.140}$$

$$= \frac{1}{Z}\prod_k^\infty \sum_{n_k}^\infty \exp\left\{-\beta\omega_k\left(n_k + \frac{1}{2}\right)\right\} |n_k\rangle\langle n_k| , \tag{2.141}$$

where $Z = \mathrm{Tr}_B\left\{\hat{W}_{eq}\right\}$. Similarly, the system-bath interaction term derived in (2.133), after expressing the coordinate $\hat{q}_k$ in terms of the annihilation and creation operators (2.118), yields:

$$\Delta\hat{V}^{(Q_x)} = -\sum_k^\infty \frac{\omega_k}{\sqrt{2}}\left(\hat{a}_k + \hat{a}_k^\dagger\right) d_k^{(Q_x)} . \tag{2.142}$$

The averaging of $\Delta\hat{V}^{(Q_x)}$ then yields:

$$\left\langle \Delta\hat{V}^{(Q_x)} \right\rangle_B = \mathrm{Tr}_B\left\{\left(-\sum_k^\infty \frac{\omega_k}{\sqrt{2}}\left(\hat{a}_k + \hat{a}_k^\dagger\right) d_k^{(Q_x)}\right)\left(\frac{1}{Z}\prod_{k'}^\infty \exp\left\{-\beta\omega_{k'}\left(\hat{n}_{k'} + \frac{1}{2}\right)\right\}\right)\right\} \tag{2.143}$$

$$= -\sum_{m,k}^\infty \frac{\omega_k d_k^{(Q_x)}}{\sqrt{2}Z_k}\left\langle m\left|\left(\hat{a}_k + \hat{a}_k^\dagger\right)\sum_{n_k}^\infty \exp\left\{-\beta\omega_k\left(n_k + \frac{1}{2}\right)\right\}\right|n_k\right\rangle \underbrace{\langle n_k|m\rangle}_{\delta_{n_k m}} \tag{2.144}$$

$$= -\sum_{k,n_k}^\infty \frac{\omega_k d_k^{(Q_x)}}{\sqrt{2}Z_k}\underbrace{\left\langle n_k\right|\left(\hat{a}_k + \hat{a}_k^\dagger\right)\left|n_k\right\rangle}_{=0}\exp\left\{-\beta\omega_k\left(n_k + \frac{1}{2}\right)\right\} \tag{2.145}$$

$$= 0 , \tag{2.146}$$

where $Z_k = \mathrm{Tr}_B\{\exp\{-\beta\omega_k\left(\hat{n}_k + \frac{1}{2}\right)\}\}$. The same applies to $\Delta\hat{V}(Q_y)$ as well. Hence, we can see that the operator $\Delta\hat{V}$ complies with the already made assumptions, and it can be used as a part of the system-bath interaction Hamiltonian. It's also possible to fulfil the requirement (2.52) in a more general manner by setting up the bath operator as a fluctuation around its averaged value. Consider an arbitrary bath operator $\hat{V}$ ($\in \mathcal{H}_B$), then the energy gap fluctuation operator could be constructed as follows:

$$\Delta\hat{V} = \hat{V} - \left\langle \hat{V} \right\rangle_B , \tag{2.147}$$

since

$$\left\langle \Delta\hat{V} \right\rangle_B = \left\langle \hat{V} - \left\langle \hat{V} \right\rangle_B \right\rangle_B = \left\langle \hat{V} \right\rangle_B - \left\langle \hat{V} \right\rangle_B = 0 . \tag{2.148}$$

The system-bath interaction term also satisfies another assumption made in (2.65), and that is the factorisation into separate system and bath parts. In our case, the interaction term in its entirety reads:

$$\hat{H}_{S-B} = \underbrace{\Delta\hat{V}^{(Q_y)}}_{\in\mathcal{H}_B} \otimes \underbrace{|Q_y\rangle\langle Q_y|}_{\in\mathcal{H}_S} + \underbrace{\Delta\hat{V}^{(Q_x)}}_{\in\mathcal{H}_B} \otimes \underbrace{|Q_x\rangle\langle Q_x|}_{\in\mathcal{H}_S} . \tag{2.149}$$

### 2.3.4 The Hamiltonian

All constituents of the total Hamiltonian have been specified by now so we can put them together. The total Hamiltonian consists of three parts:

$$\hat{H} = \hat{H}_S + \hat{H}_B + \hat{H}_{S-B} . \tag{2.150}$$

The system Hamiltonian $\hat{H}_S$ has three general parts—the electronic ($\in \mathcal{H}_{el}$), the vibrational ($\in \mathcal{H}_{vib}$), and the adiabatic coupling ($\in \mathcal{H}_{el-vib} = \mathcal{H}_{el} \otimes \mathcal{H}_{vib}$). The electronic part of our three-level system can be expressed using the energies of each state as:

$$\hat{H}_{S,el} = E_g |g\rangle\langle g| + E_{Q_y} |Q_y\rangle\langle Q_y| + E_{Q_x} |Q_x\rangle\langle Q_x| . \tag{2.151}$$

The vibrational part, which includes $I$ number of vibrational modes modelled by $N_{i,j}$ states of a harmonic oscillator for $j$th electronic state, reads:

$$\hat{H}_{S,vib} = \sum_i^I \sum_{n_i=0}^{N_{i,j}} \Omega_i \left(n_i + \frac{1}{2}\right) |n_i\rangle\langle n_i| \otimes |j\rangle\langle j| . \tag{2.152}$$

The assumed linear diabatic coupling defined in (2.126) has the following form as the coordinate is expressed using (2.118):

$$\hat{H}_{el-vib,i} = \frac{\alpha_i}{\sqrt{2}} \left(\hat{a}_{Vi} + \hat{a}_{Vi}^\dagger\right) \left(|Q_y\rangle\langle Q_x| + |Q_x\rangle\langle Q_y|\right) \tag{2.153}$$

$$= \frac{\alpha_i}{\sqrt{2}} \sum_{n_i=0}^{N_i} \sqrt{n_i+1} \Big( |n_i\rangle\langle n_i+1| + |n_i+1\rangle\langle n_i| \Big) \left(|Q_y\rangle\langle Q_x| + |Q_x\rangle\langle Q_y|\right) , \tag{2.154}$$

where $N_i = \inf\left\{N_{i,Q_y}, N_{i,Q_x}\right\}$. The total coupling that involves all explicitly included vibrational modes is obtained by performing a tensor summation of the vibrational parts ($\hat{H}_{el-vib} \in \mathcal{H}_{el} \otimes \mathcal{H}_{vib} = \mathcal{H}_{el} \otimes \left(\bigotimes_i^{N_i} \mathcal{H}_{vib,i}\right)$):

$$\hat{H}_{el-vib} = \bigoplus_i^I \hat{H}_{el-vib,i} \,. \tag{2.155}$$

The system Hamiltonian is then obtained as a sum of all parts:

$$\hat{H}_S = \hat{H}_{S,el} + \hat{H}_{S,vib} + \hat{H}_{el-vib} \,. \tag{2.156}$$

### 2.3.5 Correlation functions & spectral densities

A quantity called *bath correlation function* was introduced back in subsection 2.2.6 in (2.75):

$$C_{jj'}(t) = \left\langle \hat{\Phi}_j^{(I)}(t)\hat{\Phi}_{j'} \right\rangle_B \,, \tag{2.157}$$

where $\hat{\Phi}_j$ was considered an operator of the bath degrees of freedom of a factorised system-bath interaction Hamiltonian, as postulated in (2.65). By comparison with the adopted form of the system-bath interaction expressed in (2.149), the term that corresponds to $\hat{\Phi}_\nu(t)$ is the energy gap fluctuation operator $\Delta\hat{V}^{(j)}$ of the $j$th system state. It was defined in (2.130) as:

$$\Delta\hat{V}^{(j)} = -\sum_k^\infty \omega_k \hat{q}_k d_k^{(j)} \,. \tag{2.158}$$

Plugging (2.158) into (2.157) yields:

$$\begin{aligned} C_{jj'}(t) &= \left\langle \Delta\hat{V}^{(j)}(t)\Delta\hat{V}^{(j')} \right\rangle_B && (2.159)\\ &= \sum_k \sum_{k'} \omega_k \omega_{k'} d_k^{(j)} d^{(j')} \underbrace{\langle \hat{q}_k(t)\hat{q}_{k'} \rangle_B}_{\to \delta_{kk'}} \delta_{jj'} && (2.160)\\ &= \sum_k \omega_k^2 \left(d_k^{(j)}\right)^2 \langle \hat{q}_k(t)\hat{q}_k \rangle_B \,. && (2.161) \end{aligned}$$

Indices $j$ correspond to different parts of the system (e.g. electronic, vibrational) that are interacting with the bath. In equation (2.160) we introduced an assumption that cross-correlations between different system parts ($j \neq j'$) equal zero. The last term of (2.161) can be expressed in terms of annihilation and creation operators using relations from (2.118):

$$\begin{aligned} \langle \hat{q}_k(t)\hat{q}_k \rangle_B &= \frac{1}{2}\mathrm{Tr}_B\left\{ e^{i\hat{H}t}\left(\hat{a}_k + \hat{a}_k^\dagger\right) e^{-i\hat{H}t}\left(\hat{a}_k + \hat{a}_k^\dagger\right)\hat{W}_{eq} \right\} && (2.162)\\ &= \frac{1}{2}\sum_n \langle n| \Big( (n+1) e^{iE_n t} |n\rangle \langle n+1| e^{i(E_{n+1}))t} |n+1\rangle \langle n| \\ &\quad + n\, e^{iE_n t} |n\rangle \langle n-1| e^{-iE_{n-1}t} |n-1\rangle \langle n| \frac{1}{Z}\exp\{-\beta E_n\}\Big) |n\rangle && (2.163)\\ &= \frac{1}{2}\left( \langle \hat{n} \rangle_B e^{i\omega t} + (\langle \hat{n} \rangle_B + 1) e^{-i\omega t} \right) \,. && (2.164) \end{aligned}$$

The bath correlation function for a harmonic oscillator bath model thus reads:

$$C_j(t) = \sum_k \frac{\omega_k^2 \left(d_k^{(j)}\right)^2}{2} \left( \langle \hat{n}_k \rangle_B e^{i\omega t} + \left( \langle \hat{n}_k \rangle_B + 1 \right) e^{-i\omega t} \right) . \tag{2.165}$$

Using the Bose-Einstein distribution

$$\langle \hat{n} \rangle_B = \frac{1}{e^{\beta\omega} - 1} \tag{2.166}$$

and the relations for hyperbolic cotangent $\coth \frac{\beta\omega}{2} = 2 \langle \hat{n} \rangle_B + 1$, and for complex exponential $e^{-i\omega t} = \cos \omega t - i \sin \omega t$, the correlation function above can also be expressed as follows:

$$C_j(t) = \sum_k \frac{\omega_k^2 \left(d_k^{(j)}\right)^2}{2} \left( \underbrace{\coth \frac{\beta\omega_k}{2} \cos \omega_k t}_{\to \mathrm{Re}\,[C(t)]} \underbrace{- i \sin \omega_k t}_{\to \mathrm{Im}\,[C(t)]} \right) . \tag{2.167}$$

It is worth a note that the imaginary part of the correlation function doesn't depend on $\beta$, i.e. the temperature $T$. A useful quantity is the correlation function in the frequency domain:

$$\begin{aligned} C_j(\omega) &= \mathrm{FT}\left[ C_j(t) \right] && (2.168)\\ &= \int_{-\infty}^{\infty} \mathrm{d}t \, C_j(t) e^{i\omega t} && (2.169)\\ &= \sum_k 2\pi \frac{\omega_k^2 \left(d_k^{(j)}\right)^2}{2} \Big( \langle \hat{n}_k \rangle_B \, \delta(\omega + \omega_k) + \langle \hat{n}_k + 1 \rangle_B \, \delta(\omega - \omega_k) \Big) . && (2.170) \end{aligned}$$

Yet another useful quantity can be identified in (2.170) called the *spectral density* $J(\omega)$:

$$J(\omega) = \sum_k \frac{(d_k)^2}{2} \delta(\omega - \omega_k) . \tag{2.171}$$

Spectral density, as the name suggests, describes the density of available modes of the bath at frequency $\omega$. The correlation function then simplifies to:

$$\begin{aligned} C_j(\omega) &= 2\pi\omega^2 \left( \langle n \rangle_B + 1 \right) \Big( J(\omega) - J(-\omega) \Big) && (2.172)\\ &= \pi\omega^2 \left( 1 + \coth \frac{\beta\omega}{2} \right) \Big( J(\omega) - J(-\omega) \Big) . && (2.173) \end{aligned}$$

By performing a Fourier transformation on the real and imaginary parts of the correlation function separately, the following relation can be derived:

$$\begin{aligned} C(\omega) &= \mathrm{FT}\left[ \mathrm{Re}\left[ C(t) \right] \right] + \mathrm{FT}\left[ i \, \mathrm{Im}\left[ C(t) \right] \right] && (2.174)\\ &= C'(\omega) + C''(\omega) && (2.175)\\ &= \left( 1 + \coth\left( \frac{\beta\omega}{2} \right) \right) C''(\omega) . && (2.176) \end{aligned}$$

Therefore, the correlation function in the frequency domain satisfies the detailed balance condition[11] since:

$$C(\omega) = e^{\beta\omega} C(-\omega) \,. \tag{2.177}$$

The terminology here is once again rather unsettled. The terms used so far are based on May and Kühn (2011). It's important to point out, though, that some other authors (Mukamel, 1995; Valkunas et al., 2013) tend to use different naming conventions since they use the same names for different objects. In their case, the term *spectral density* is used for the imaginary part of the correlation function in the frequency domain FT $\left[ i \,\mathrm{Im}\left[\hat{C}(t)\right]\right] \equiv \hat{C}''(\omega)$. Both forms and definitions of the spectral density are frequently used, and they can be converted between each other by a simple relation:

$$C''(\omega) = 2\pi\omega^2 \Big( J(\omega) - J(-\omega) \Big) \,. \tag{2.178}$$

Since the physical properties of the bath—the correlation function included—are difficult to obtain from experiments, and the theoretical methods like molecular dynamics can be computationally very demanding, a different approach is usually adopted here. An analytical spectral density model is postulated and used to find the correlation function $C(t)$ afterwards.

### 2.3.6 Spectral density models

There are essentially two types of spectral density forms based on their general shape. The profile can be either Gaussian or Lorentz. The most often utilised is the Lorentz-shaped spectral density:

$$J(\omega) = \frac{1}{\pi} \frac{1}{(\omega - \omega_0)^2 + (2\ln 2)\gamma^2} \,, \tag{2.179}$$

or alternatively expressed as:

$$C''(\omega) = \frac{4\omega\omega_0\gamma}{\left(\omega^2 - \omega_0^2 - \gamma^2\right)^2 + 4\omega^2\gamma^2} \,. \tag{2.180}$$

$\omega_0$ is the central carrying frequency of the model, $\gamma = \frac{1}{\tau_c}$ is a relaxation rate, i.e. the reciprocal value of the characteristic correlation time $\tau_c$ of the bath, which relates to the friction present in the environment.

Various approximations that correspond to different limit cases of the parameters occurring in (2.180) can be made. In our case, the limit of strong friction was adopted, which is usually appropriate for baths with a macroscopic

[11] The detailed balance condition says, in its full generality, that system is in equilibrium if and only if the flow of probability into a microstate is equal to the flow from the microstate. As thermal equilibrium and thermal harmonic baths are considered, the condition can be formulated around the Boltzmann factor, as every reversed process with a negative overall change of energy is weighed by a corresponding Boltzmann factor. In the case of the thermally equilibrated harmonic oscillator, this reads $\forall n > m, k_{m\leftarrow n} = e^{\beta(E_n - E_m)} k_{n\leftarrow m}$, where $k_{m\leftarrow n}$ is a transfer rate from level $n$ to $m$.

solvent (Mukamel, 1995). The limit of $\gamma \gg 2\omega_0$ leads to the so-called *overdamped Brownian oscillator model* whose spectral density adopted in the simulations has the following form:

$$C''(\omega) = 2\frac{\lambda}{\tau_c}\frac{\omega}{\omega^2 + \left(\frac{1}{\tau_c}\right)^2}\,. \tag{2.181}$$

The parameter $\lambda$ represents the reorganisation energy of the bath. In the time domain, the correlation function of an overdamped Brownian oscillator becomes:

$$C(t) = \frac{\lambda}{\tau_c}\cot\left(\frac{\beta}{\tau_c}\right)e^{-\frac{t}{\tau_c}} - i\frac{\lambda}{\tau_c}e^{-\frac{t}{\tau_c}} + \frac{4\lambda}{\beta\tau_c}\sum_{n=1}^{\infty}\frac{\nu_n e^{-\nu_n t}}{\nu_n^2 - \left(\frac{1}{\tau_c}\right)^2}\,. \tag{2.182}$$

The last term with the sum in (2.182) corresponds to the so-called *Matsubara frequencies* with $\nu_n = \frac{2\pi n}{\beta}$ (Weiss, 2008). The upper summation boundary is cut off at a finite number of $N_{Mats}$. In the simulations I performed, the number of Matsubara frequencies included in the correlations functions was fixed at a converged value of 100.

To sum up, the overdamped Brownian oscillator model was used to represent the bath degrees of freedom. Three parameters enter its definition in (2.182): the bath reorganisation energy $\lambda$ and the correlation time $\tau_c$, which can be alternatively expressed also as a bath relaxation rate $\gamma = \frac{1}{\tau_c}$.

This model was adopted for both of the formally distinguished bath components: the electronic and the vibrational (as assumed in subsection 2.3.2). The reorganisation energy for the vibrational bath, however, does not have a straightforward interpretation and might have an unphysical meaning. To preclude that, a formally redefined model was used for the vibrational bath named the *scaled overdamped Brownian oscillator* model. Instead of the reorganisation energy $\lambda$, which still could have been easily used as an arbitrary numerical parameter, introducing a new parameter with specific physical meaning named (*targeted*) *vibrational relaxation time* was preferred. The idea behind this model is to specify the relaxation time between the first excited and the ground state of the vibrational mode the bath is interacting with. The Redfield relaxation tensor (as defined in (2.80)) for the vibrational mode interacting with a standard overdamped Brownian model as a bath is calculated, and the reorganisation energy that entered the standard overdamped Brownian model is then rescaled by the ratio of the obtained relaxation time (inverse of relaxation tensor element) and the targeted one. The newly rescaled reorganisation energy $\lambda'$ then enters the definition (2.182) to get the rescaled correlation function. Other used parameters remain unchanged.

To conclude, this newly defined model has four parameters: the bath correlation time $\tau_c$, the targeted relaxation time $\tau_T$, and the frequency $\Omega_{Vi}$ (*cf.* eq. (2.123)) and Huang-Rhys factor $S_{Vi}$ belonging to the coupled vibrational mode to perform the simulation. Besides, there is one additional parameter specifying the number of vibrational states to be considered in the Redfield tensor calculation. In this thesis, a converged number of 10 levels was used steadily.

## 2.4 Theoretical molecular spectroscopy

Standard theoretical approaches to calculate the linear absorption spectra were used in the simulations. The details about the theory and the derivation can be found in, e.g., in Mukamel (1995) and Valkunas et al. (2013).

### 2.4.1 Introduction to theoretical molecular spectroscopy

Molecular spectroscopy has some specificities that clearly distinguish it from other spectroscopic fields like atomic spectroscopy or condensed-matter spectroscopy. The most important difference comes from the size of the particles that are interacting with the electromagnetic field we are probing the sample with. Since the on-average size of the molecules is much smaller than the wavelength of the light, $\lambda \gg \bar{d}$ (in case of Chl*a*, the chlorin diameter is roughly 1 nm and the usual wavelength of light used in spectroscopic experiments is in Vis-IR region of 500–800 nm), the spatial dependence of the light can be neglected and each molecule floating in some solvent can be considered to be placed in a homogeneous electromagnetic field. This assumption is usually called by the term *dipole approximation*. However, each molecule will perceive a different field at each given time since they are separated in space. On top of that, each of the molecules can be oriented differently and can have a slightly different molecular environment which may affect its spectroscopic properties. To sum up, to characterise a macroscopic quantity that would describe the spectroscopic properties of the entire sample, an averaging over all the degrees of freedom just mentioned has to be performed:

$$\mathbf{P}(\mathbf{r}, t) = \left\langle \left\langle \left\langle \langle \boldsymbol{\mu} \rangle_r \right\rangle_{\Delta V} \right\rangle_E \right\rangle_\Omega , \tag{2.183}$$

where $\mathbf{P}(\mathbf{r}, t)$ is the macroscopic polarisation of the sample, $\langle \cdot \rangle$ denotes averaging over the dimension of each molecule ($r$), varying energetic shifts ($\Delta V$), the electric field ($E$), and over different spatial orientations of the molecules ($\Omega$). See the great review of Andrews (2004) for more details about how it is done.

Another important approximation considers the disproportionality of masses of electrons and nuclei and assumes that transition dipole moments of some electronic transition don't depend on the nuclear degrees of freedom of the molecule. Alternatively, it is (not particularly well) interpreted as electronic transitions happening faster than the nuclear degrees of freedom (DOF) can react and thus they appear as vertical transitions on the diagrams of energy levels and potential energy surfaces. The thing is, even when we excite some system slowly, the approximation still holds and doesn't depend on the time scale. The interaction Hamiltonian between the system and the electromagnetic field is usually expressed in the following form:

$$\hat{H}_{int}(t) = -\hat{\mu} \cdot \hat{E}(t) , \tag{2.184}$$

which is sometimes referred to as an interaction Hamiltonian in *lenght gauge*, or as an interaction Hamiltonian in dipole approximation.

Techniques of molecular spectroscopy can be generally viewed as perturbative in different orders of the interaction of the transition dipole moment operator with the incoming field. The first order in interaction corresponds to absorption spectroscopy (the resulting equation is in the second order of $\hat{\mu}$).

### 2.4.2 Linear spectroscopy

The general relation for linear absorption spectrum $\alpha(\omega)$ reads:

$$\alpha(\omega) = \sum_n 2\frac{\omega}{n(\omega)}\left|d_{ng}\right|^2 \mathrm{Re}\left[\int_0^\infty \mathrm{d}t\, e^{-g_n(t)-i(\omega-\omega_{ng})t-\frac{1}{2}K_n(t)}\right], \tag{2.185}$$

where $g_n(t) = \int_0^t \mathrm{d}\tau \int_0^\tau \mathrm{d}\tau'\, C_n(\tau')$ is the so-called *lineshape function*[12], $K_n(t) = -\sum_{m\neq n} R_{mg,ng}(t)$ is a dephasing rate obtained from the relaxation tensor $R(t)$. However, in our case, the absorption spectrum was calculated from simulations by evaluating the following terms directly:

$$\left\langle \vec{d}_{gn} \mathcal{U}_{ng,mg}(t) \vec{d}_{mg} \right\rangle = \left\langle \vec{d}_{gn} \vec{d}_{mg} \right\rangle \mathcal{U}_{ng,mg}(t) \tag{2.186}$$

$$= \frac{d_n^{(x)} d_m^{(x)} + d_n^{(y)} d_m^{(y)} + d_n^{(z)} d_m^{(z)}}{3} \mathcal{U}_{ng,mg}(t)\,. \tag{2.187}$$

As can be seen, three separate simulations have to be performed for each cartesian element of the transition dipole matrix. The density matrix in thermal equilibrium is excited by the first interaction, and it is propagated to time $t$ when it interacts with the second matrix. The results are then summed up, and Fourier transformed. The absorption spectrum $\alpha(\omega)$ is obtained by multiplying the previous result by $\omega$, which comes from the analysis of Maxwell equations, and by the factor of $\frac{1}{3}$, which comes from orientational averaging (see Andrews, 2004).

[12] Not to be confused with a quantity called just a "lineshape", usually denoted as $G(\omega)$ which stands for the integral occurring in (2.185).

## 2.5 Software tools

The one and only computational tool used during the project was Python programming language and its publicly available libraries. Namely, the following libraries were intensely used, tested, or experimented with: `Numpy`, `Scipy`, `Cupy`, `joblib`, `mayavi`. Besides, the library `quantarhei` developed in the research group was also used.

The coding part of this project went through two phases. First, a brand new from-scratch implementation of the Redfield equations was created. The main purpose of it was to focus on possible optimisation and look into possible ways to accelerate the computations since large molecular systems are planned to be computed in the near future. Two main approaches were taken to the problem: mathematical/physical ones in which the subjects of improvement were the equations, and then the purely computational optimisations.

In general, the equations were expressed using tensors where possible, but great care had to be made regarding memory utilisation. This turned out to be a problem especially in the attempts of computing on graphics processing unit (GPU) using CUDA, Nvidia libraries, and `Cupy` library. More successful turned out to be parallelisation using, e.g. the `joblib` library.

Another type of optimisation to deal with the memory utilisation problems was the implementation of `Numpy`-compatible class of array-like objects named DiskArray that behaves like `Numpy` array but the data are stored on disk, not only in memory.

The last optimisation that was implemented reduces the dimensions of the system Hamiltonian, and all other pertinent operators, thus again lowering the demands on memory. Mathematical details of this approach are in section B.1.

After lowering the computational demands necessary to perform the computations, the implemented form was introduced into the `quantarhei` library (so far only locally) which provides the user with many useful tools to work with and perform simulations of open quantum systems.

There are, however, some problems that still need someone to look into. Mainly, at this point, it is the methodology for curve-fitting and spectra optimisations. The approaches used so far involved either manual manipulation with the parameters which is tremendously time-consuming, or fitting functions provided by the library `Scipy`, which can be quite unreliable and unstable in some cases, as will be mentioned in Chapter 3.

# 3. Results

The spectroscopic model of a chlorophyll molecule was treated by the time-dependent Redfield theory, and the linear absorption spectra were calculated from the simulated dynamics of optical coherence elements of the system's density matrix. To parameterize the model, the simulated absorption spectra were fitted to experiential data sets obtained from the literature. It is important to stress that despite the term "parameters" being used here for the numerical values that enter the theoretical model, each of them corresponds to some physical property or feature of the physical system. Therefore, they should not be viewed as arbitrary numerical constants with dubious interpretations but rather as actual physical variables.

The Chl*a* molecule soluted in two different solvents—diethyl ether and pyridine—was chosen to be modelled. Both data sets of the experimental linear absorption spectra measured at room temperature were taken from Rätsep et al. (2009). The simulations were done in multiple different setups and constraints.

Firstly, the number of explicitly included vibrational modes in the system Hamiltonian ($N_V$) was varied from zero—which corresponds to a three-level electronic system only—to two modes in total. Secondly, each such setup was performed with two different constraints on the parameters.

(i) In order to be able to compare the validity of our model with other authors (Reimers et al., 2013), one of the simulations was always constrained in terms of the parameters they used and found to be optimal (see section A.1). Only the parameters that weren't used by them were subjected to the fitting procedure then.

(ii) In the other simulations, any constraints on the parameters (up to an extent, as will be mentioned shortly) were released. Only the initial guess of the parameters remained the same as in (i).

The initial guess of parameters was obtained by manually varying the parameters. One-dimensional scans through the parameter space were used to facilitate this procedure. After achieving acceptable—but still rather rough—correspondence, the optimisation curve-fitting function from a Python library Scipy was adopted to find the optimal values by means of nonlinear least-squares method. The Table A.1 in the Appendix summarises the parameter space for all the various setups and constraints mentioned above.

After finding the optimal values, further inspection of the parameter space was performed by "optimising scans". That is, the value of one particular selected parameter (or a group of coupled parameters) was iteratively dragged from its optimal value. At each point, a new optimisation and curve-fitting with respect to all other parameters, i.e. excluding the one that is being scanned, was performed by the algorithm. A new set of optimal parameters was obtained this way, the scanned parameter was increased/decreased, and the procedure was repeated until the scan was completed. This approach was used to scan the relations between the parameters and possibly identify the indefiniteness between linear absorption spectra and the set of parameters.

## 3.1 Chlorophyll *a* in diethyl ether

To better understand the importance and function of each component included in the model system Hamiltonian, a bottom-up approach was used, and the simplest model stripped of any vibrational modes was simulated and fitted first.

### 3.1.1 No vibrational modes

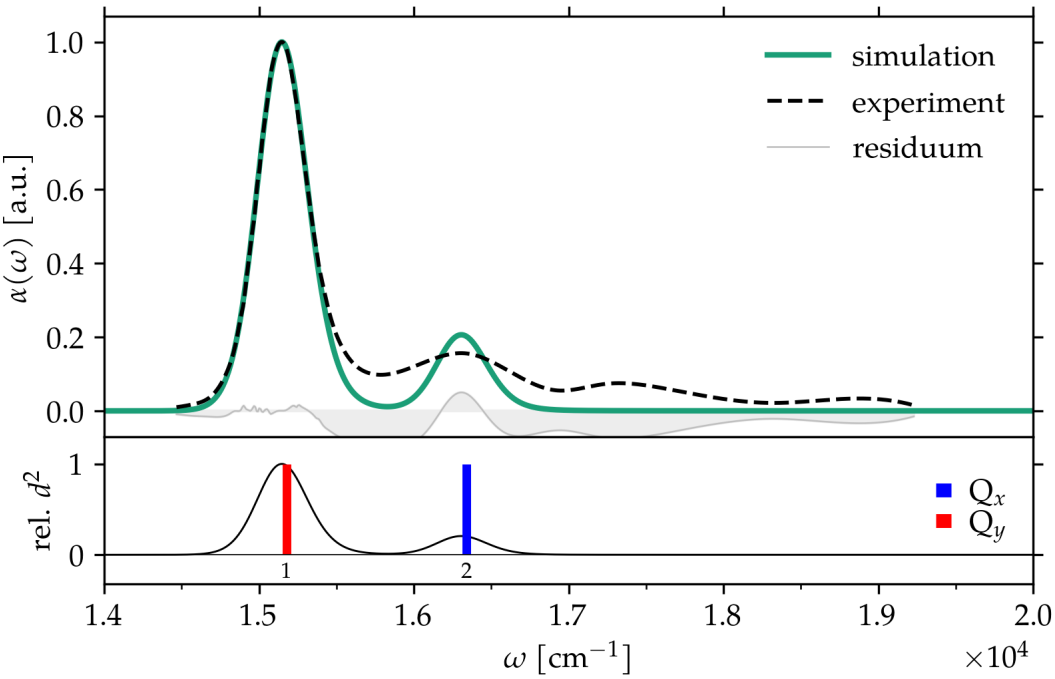


**Figure 3.1:** Simulated linear absorption spectra of a three-level system molecule in diethyl ether. The top subfigure presents the simulated absorption spectrum (green solid line) as compared to the experimental data of reference (black dashed line; Rätsep et al., 2009). A shaded grey line displays the residuum of the fit. The bottom subfigure shows the position of the two electronic transitions. The black line represents the absorption spectrum plotted above.

Figure 3.1 presents the simplest case of our model—a three-level system consisting of three electronic states and two possible transitions from the ground state. We can clearly see that the three-level model alone simply can't be used with our current theoretical tools to quantitatively reproduce the experimental data. Besides, since there is no coupling included, no interaction between the two states (the system Hamiltonian is diagonal in the site basis), and a weak system-bath coupling is assumed, the populations of the states won't change in time, and the system won't relax. In order to overcome this issue, a different theory of quantum dynamics would need to be adopted, or the system has to be enlarged and diversified.

### 3.1.2 Single vibrational mode

A leap step ahead in terms of the Hamiltonian's structure can be made by identifying in the bath some notable intermolecular vibrational modes that deserve to be included in the system Hamiltonian. When a diabatic coupling between different excited electronic states is introduced as well—Figure 3.2—the spectrum gains more structure (even though in this figure the spectrum wasn't fitted to see the influence of another feature better, as to be mentioned shortly). Also, the plot of dynamics of populations represented in the eigenbasis of the system Hamiltonian started behaving as roughly expected. That is, a relaxation process on the timescale of hundreds of femtoseconds can be seen. However, we can also see a general problem of reduced density matrix approaches as the populations are leaking out of the zero to one interval.

This effect even reinforces as we add a coupling between the explicit vibrational modes and the bath and enable a pathway for fast relaxation within the modes. The absorption spectra that can be obtained at this level of the model complexity fit the experimentally obtained one rather well; see Figure 3.3. Meanwhile, the dynamics of the populations went out of control. The adoption of the secular approximation corrects this issue as displayed in Figure 3.4. The spectra displayed in Figures 3.2–3.4 used the same set of parameters as optimised in Figure 3.3.

A plethora of scans through the parameter space, with or without concurrent optimisation, were performed. Only a sparse selection of them can get the space to be presented here. In Figure 3.5 and belonging Figure 3.6, an optimising scan through the value of targeted relaxation time in the vibrational mode $\tau_{T,1}$, a parameter that enters the scaled overdamped Brownian oscillator model of the bath correlation function, as defined on page 39. A one-dimensional scan without the optimisation procedure (see section A.3 in Appendix) pointed out that this parameter has quite some influence on the width, position, and relative separation of the absorption bands.

The influence of fixation of some parameters can be seen in the comparison of Figure 3.6 with Figure 3.8, and Figure 3.6 with Figure 3.8. As long as the spectral line is close to its optimum, the constraint-free optimisation gives slightly better results. But as the difference increase, the optimisation of a higher number of parameters tends to become unstable and result in diverging.

Besides that, we can conclude that even though the parameter itself has quite an impact on the spectra, other parameters can rather successfully compensate for its changes in value.

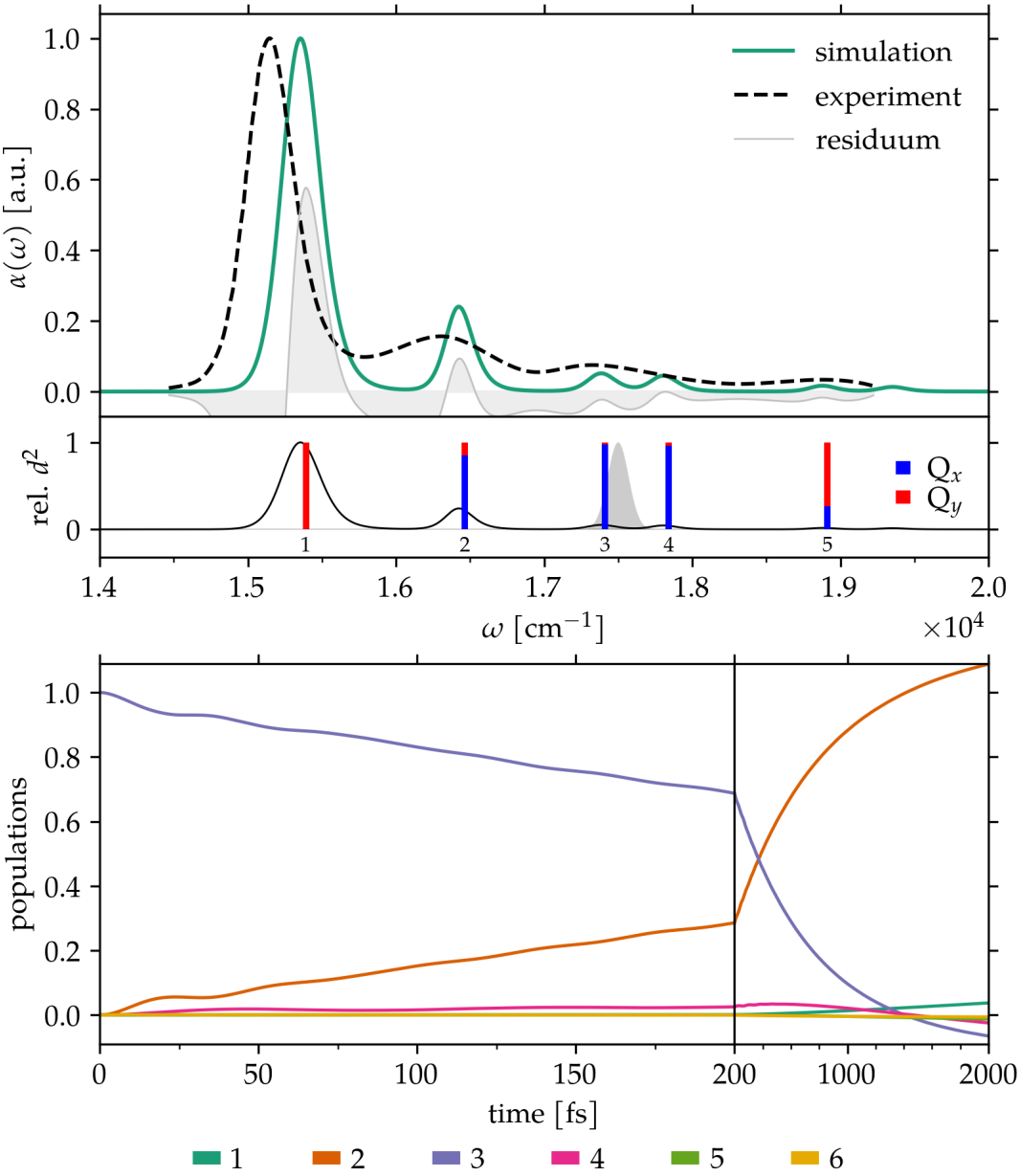


**Figure 3.2:** Linear absorption spectra of a model of Chl*a* molecule in diethyl ether with one explicit vibrational mode ($N_V = 1$) that doesn't interact with the bath. The top figure presents the simulated absorption line (green solid line), the experimental data of reference (black dashed line; Rätsep et al., 2009), and a residuum of the fit is shaded in grey. The middle subfigure shows the position of energetic transition energies obtained from a diagonalised system Hamiltonian as enumerated bars. Their colouring corresponds to the ratio of vibronic mixing between the $Q_y$ (red) and $Q_x$ (blue) diabatic states. The black line represents the absorption spectrum plotted above. The Gaussian profile shaded in grey represents the excitation pulse (FWHM = 100 cm$^{-1}$, $\omega_0$ = 17500 cm$^{-1}$) used in the simulation to invoke excited state dynamics displayed in the bottom subfigure. The bottom subfigure shows the simulated dynamics of populations (in the system Hamiltonian eigenbasis) after excitation in the $Q_x$ region of spectra.

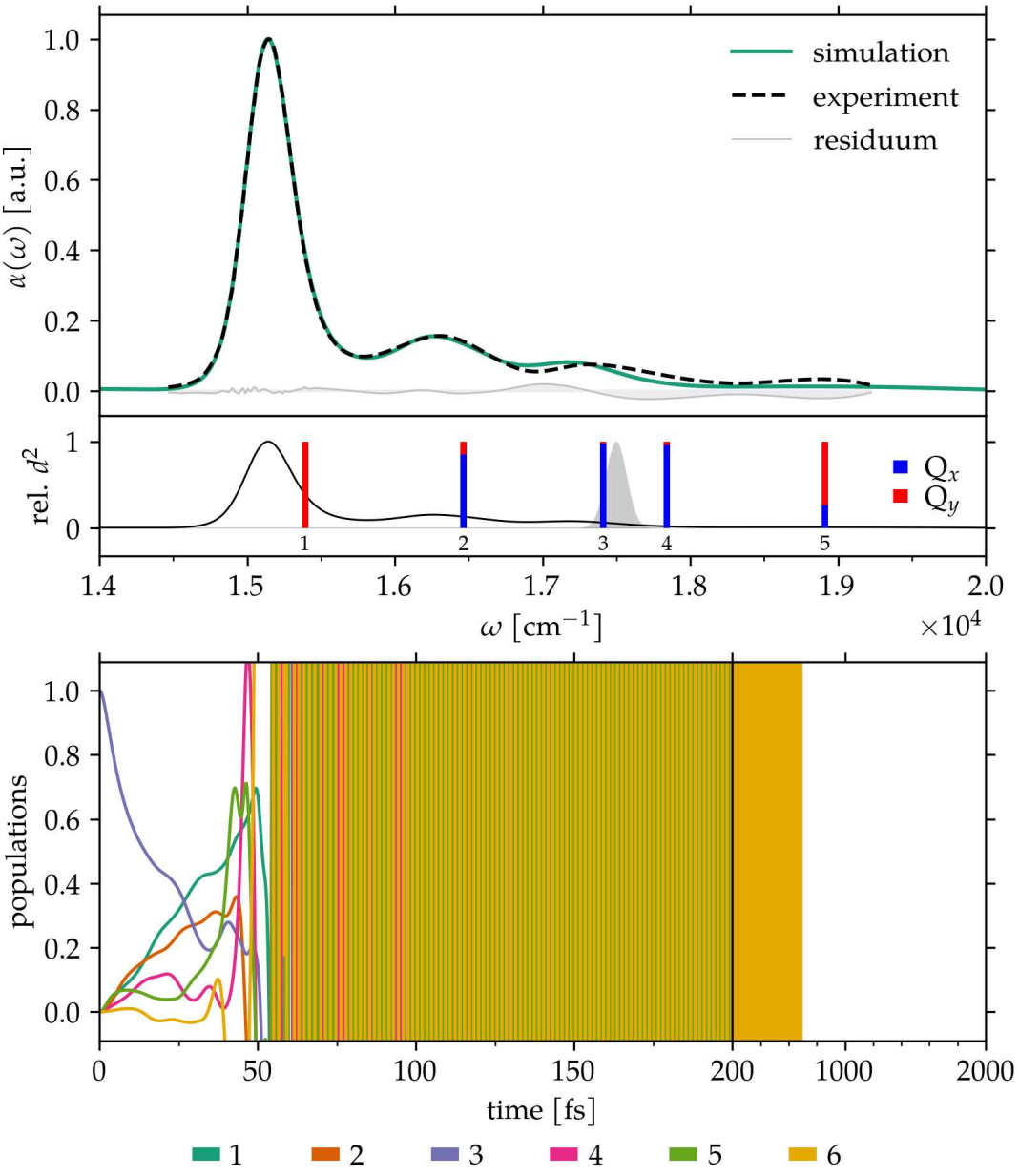


**Figure 3.3:** The optimised linear absorption spectrum of a model of Chl*a* molecule in diethyl ether with one explicit vibrational mode ($N_V = 1$). For more details on the figure, please see the caption of Figure 3.2 on page 46.

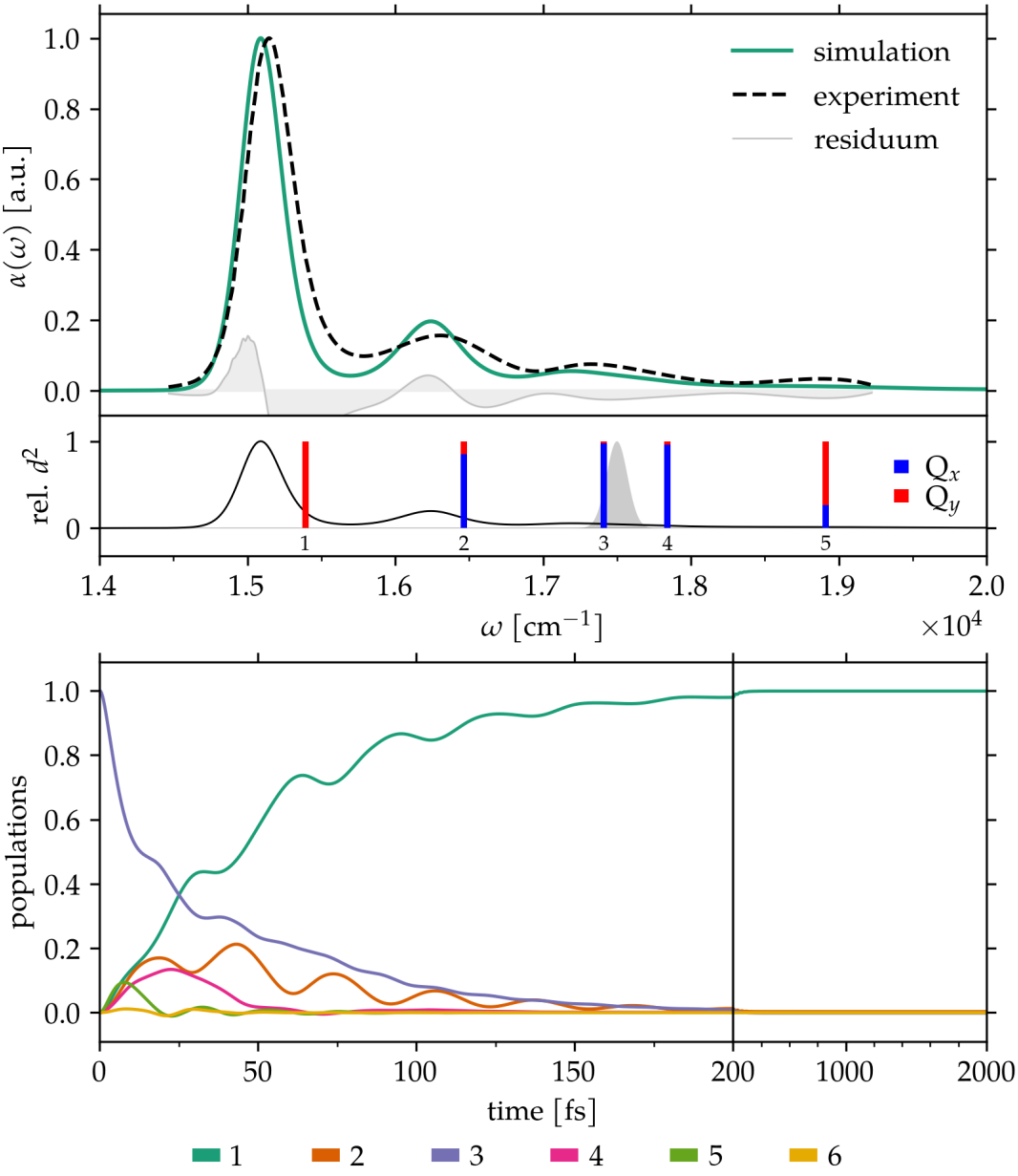


**Figure 3.4:** Linear absorption spectra of a model of Chl*a* molecule in diethyl ether with one explicit vibrational mode ($N_V = 1$) and the secular approximation adopted. For more details on the figure, please see the caption of Figure 3.2 on page 46.

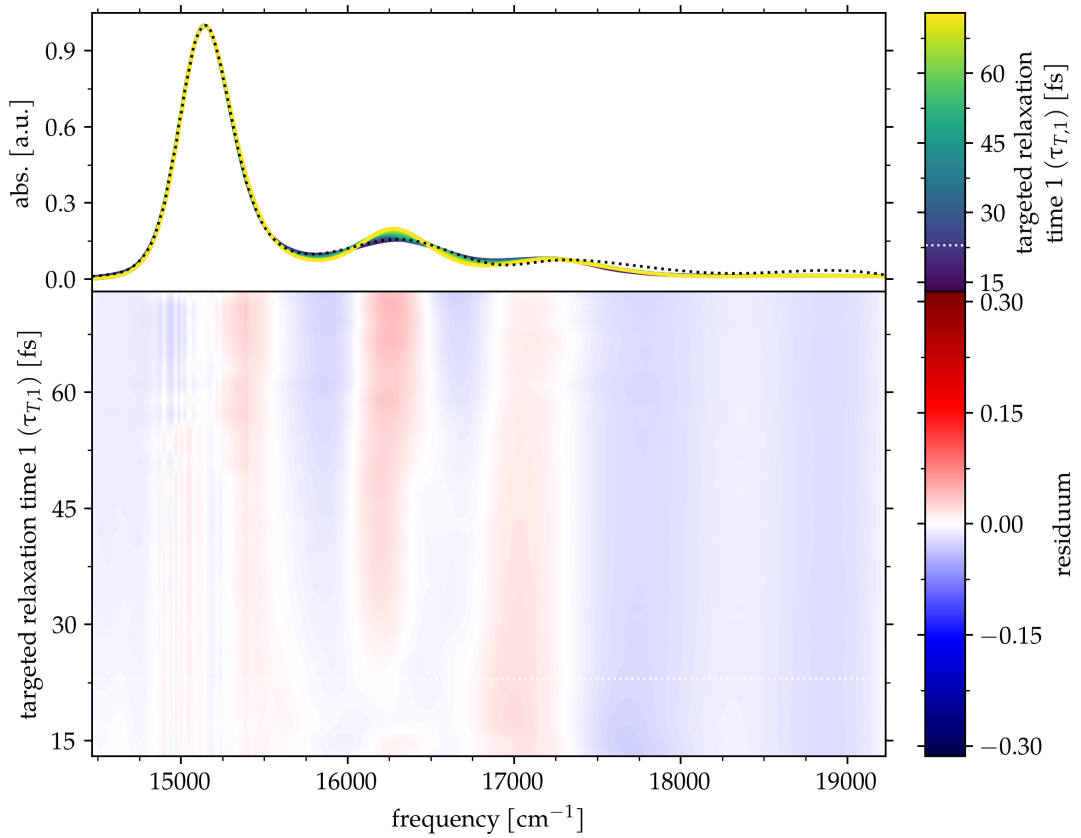


**Figure 3.5:** The results of linear absorption spectra fitting that was combined with a scan in a single parameter—the targeted relaxation time $\tau_{T,1}$ in the vibrational mode belonging to the first electronic excited state $Q_y$—as described in the text. The scan was performed with both positive and negative increments of 2 fs. All obtained absorption lineshapes are displayed on top of each other in the top subfigure. The value of the scanned parameter they belong to is encoded in their colour. The bottom subfigure shows essentially the same data but in a different representation. The experimental data of reference of Chl*a* in diethyl ether (Rätsep et al., 2009) were subtracted from the simulated ones, and the obtained residuum was plotted as a 2D map assigning the values of the scanned parameter to the $y$-axis. The initial parameter, and thus the initial absorption spectrum, is denoted in the figure by a white dotted line.

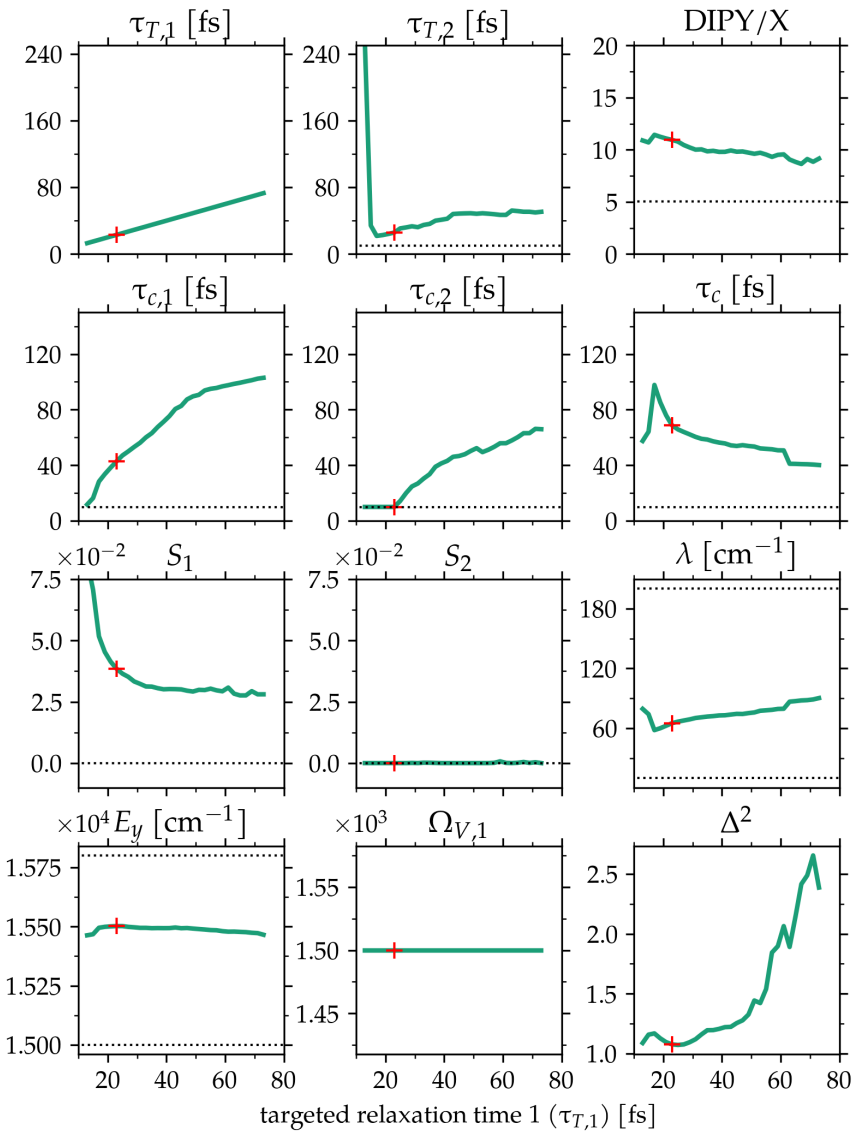


**Figure 3.6:** An overview of selected parameters that play the major role in specifying the shape of the spectrum as the parameter $\tau_{T,1}$ is scanned (see also Figure 3.5). Namely, the depicted parameters are (from left to right, top to bottom): the targeted relaxation times in the vibrational mode belonging to the first ($\tau_{T,1}$) and second ($\tau_{T,2}$) excited electronic states, the ratio of squares of the transition dipole moments $\frac{|\vec{d}_y|^2}{|\vec{d}_x|^2}$, bath correlation times belonging to vibrations of the first ($\tau_{c,1}$) and second ($\tau_{c,2}$) excited el. states, bath correlation function of the electronic part of the system ($\tau_c$), Huang-Rhys factors ($S$) for the explicit vibrational mode on the first and second excited electronic state, the bath reorganization energy $\lambda$, the energy of the first excited electronic state $E_y$, the frequency of the single explicit vibrational mode $\Omega_{V,1}$ [cm$^{-1}$], and finally, the square of the residual sum (a row-wise sum performed on the 2D map of Figure 3.5). The dotted lines represent boundary conditions for each parameter during the fitting procedure. The red cross denotes the initial position–the initially known optimum in terms of the correspondence with the experimental data.

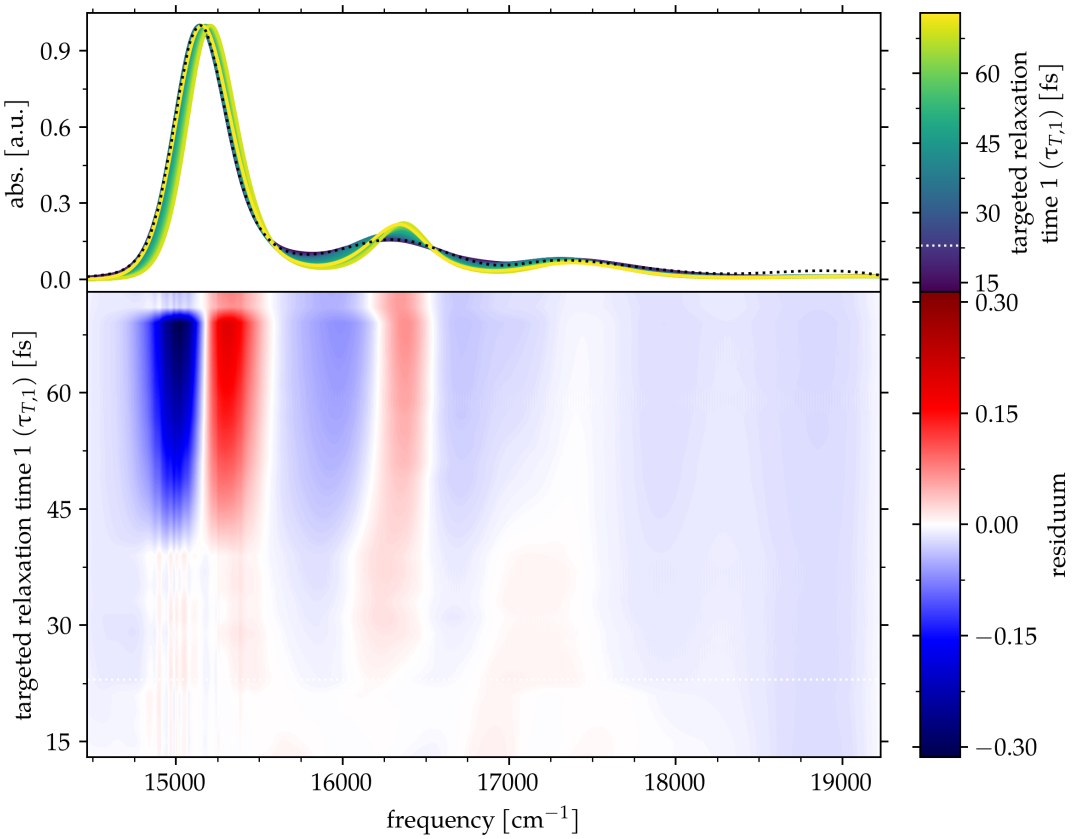


**Figure 3.7:** The results of linear absorption spectra fitting for Chl*a* in diethyl ether ($N_V = 1$) without any constraints, that was combined with a scan in a single parameter—the targeted relaxation time $\tau_{T,1}$ in the vibrational mode belonging to the first electronic excited state $Q_y$. The scan was performed with both positive and negative increments of 2 fs. For more details on the figure, please see the caption of Figure 3.5 on page 49.

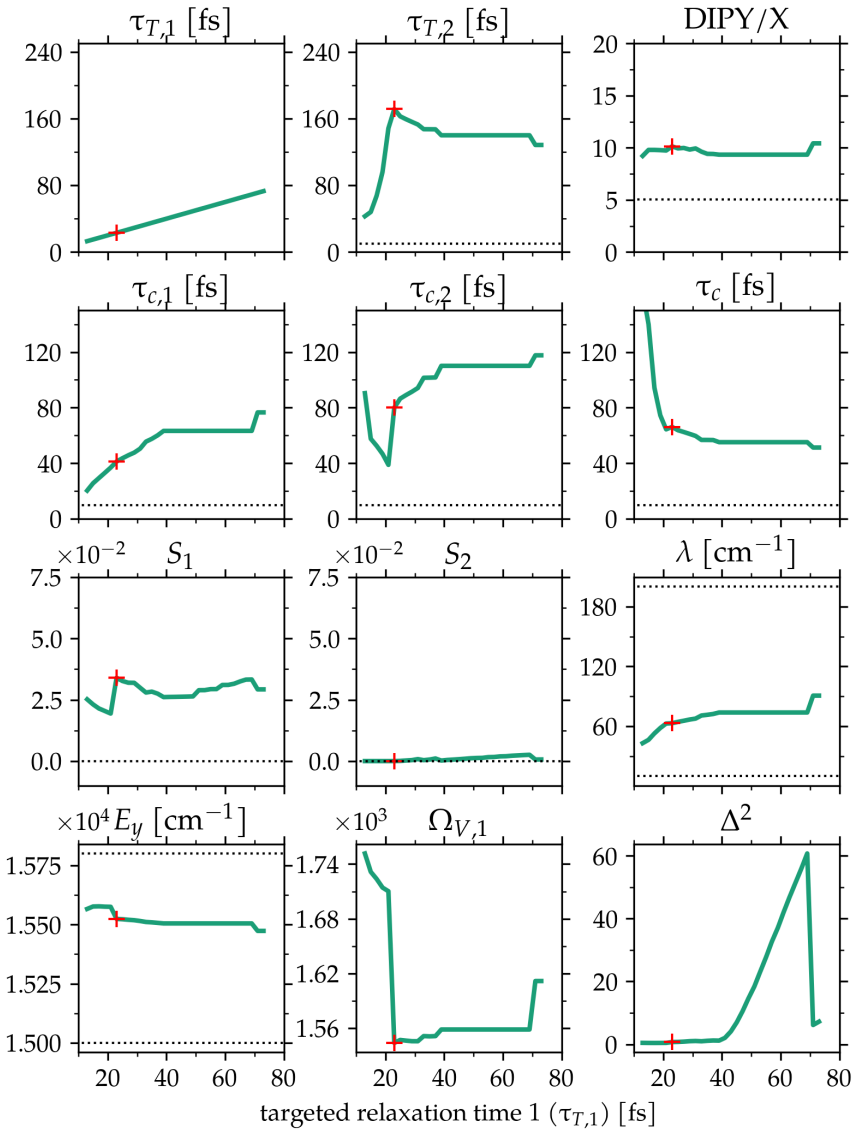


**Figure 3.8:** An overview of selected parameters as they evolve during the scan of parameter $\tau_{T,1}$ combined with optimisations. No constraints were applied to the parameters. For more details on the figure, please see the caption of Figure 3.6 on page 50.

### 3.1.3 Two vibrational modes

By adding a second vibrational mode to the system Hamiltonian, the number of states significantly increases, as does the number of parameters entering our model. At this point, it is desirable to start reducing the parameter space size since the general curve-fitting algorithms generally struggle with a surplus of free degrees of freedom. One-dimensional scans through individual parameters were used to identify those parameters that have an insignificant effect on the absorption spectrum shape. They were then fixed for optimisation.

Figure 3.9 shows pretty much perfect correspondence with the experimental data. The secular approximation introduced in Figure 3.10 shows only a minor effect on the absorption spectrum but a major improvement on the dynamics.

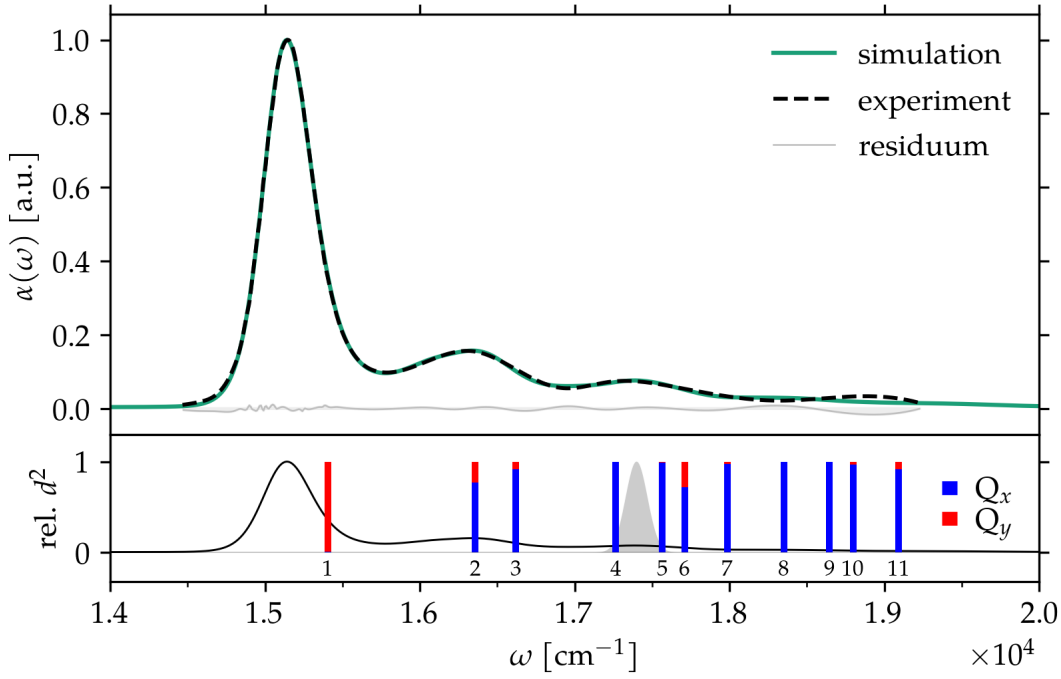


**Figure 3.9:** The optimised linear absorption spectra of a model of Chl*a* molecule in diethyl ether with two explicit vibrational modes ($N_V = 2$). For more details on the figure, please see the caption of Figure 3.2 on page 46.

The optimisation scans in $\tau_{T,1}$ depicted in Figures 3.11–3.14 show again how well other parameters can adapt without much of a change in the simulated absorption spectrum. The changes in the plotted parameters also reflect show the increased instability of the curve-fitting procedure, which persists even after shortening the steps of the scan. Hence, it can be concluded that the instability results from two facts. Some of the parameters entering the model have negligible impact on the shape of the linear absorption spectra, and aside from that, the sheer number of parameters added along with the second explicit vibrational mode usually causes troubles to optimisation algorithms.

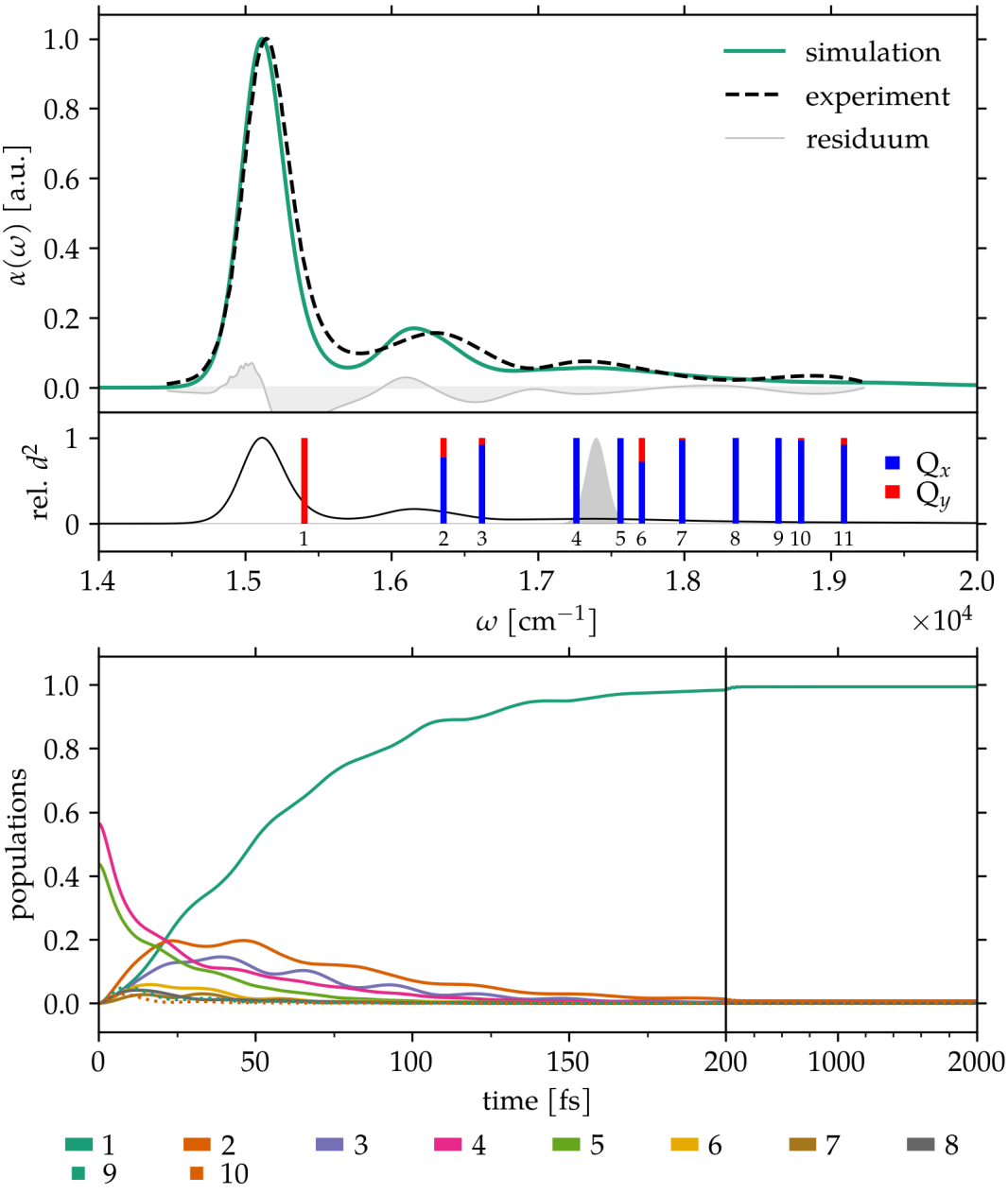


**Figure 3.10:** Linear absorption spectra of a model of Chl*a* molecule in diethyl ether with two explicit vibrational modes ($N_V = 2$). The secular approximation was used in the simulation of dynamics. For more details on the figure, please see the caption of Figure 3.2 on page 46.

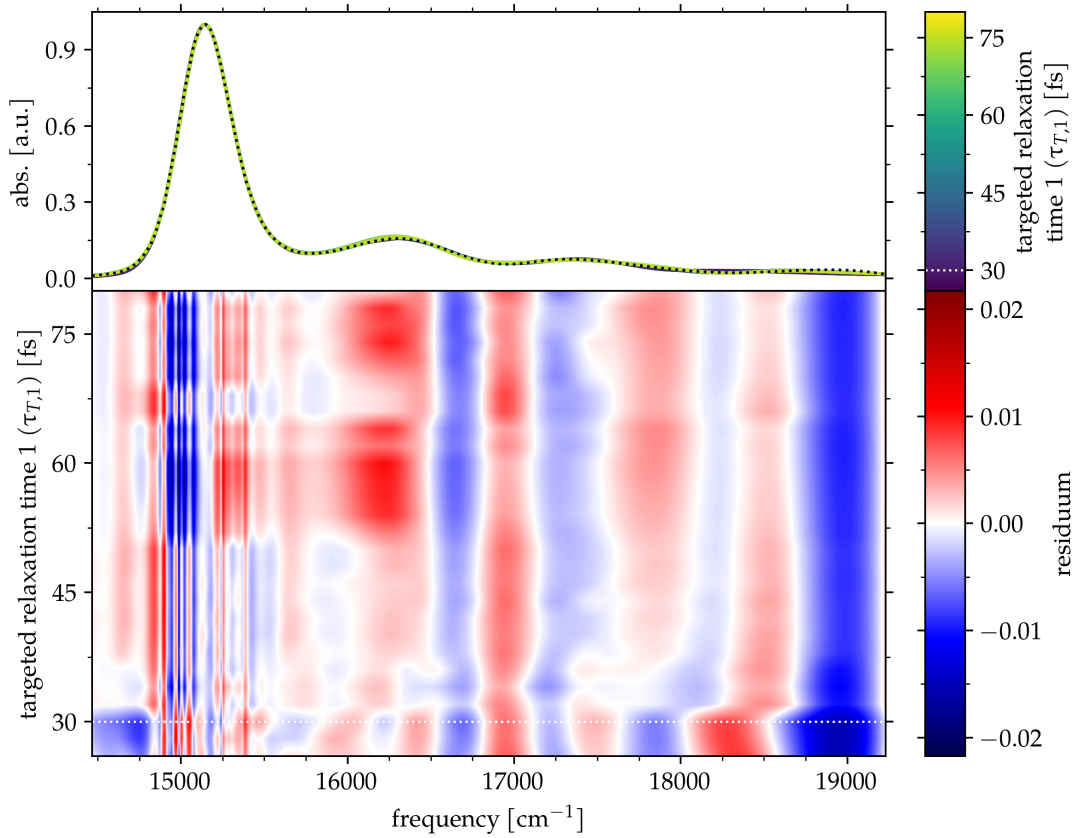


**Figure 3.11:** The results of linear absorption spectra simulation (Chl*a* in diethyl ether, $N_V = 2$) and fitting with constraints on the first vibrational mode as used by Reimers et al. (2013). The fitting procedure was combined with a scan in a single parameter—the targeted relaxation time $\tau_{T,1}$ in the vibrational mode belonging to the first electronic excited state $Q_y$. The scan was performed with both positive and negative increments of 2 fs. For more details on the figure, please see the caption of Figure 3.5 on page 49.

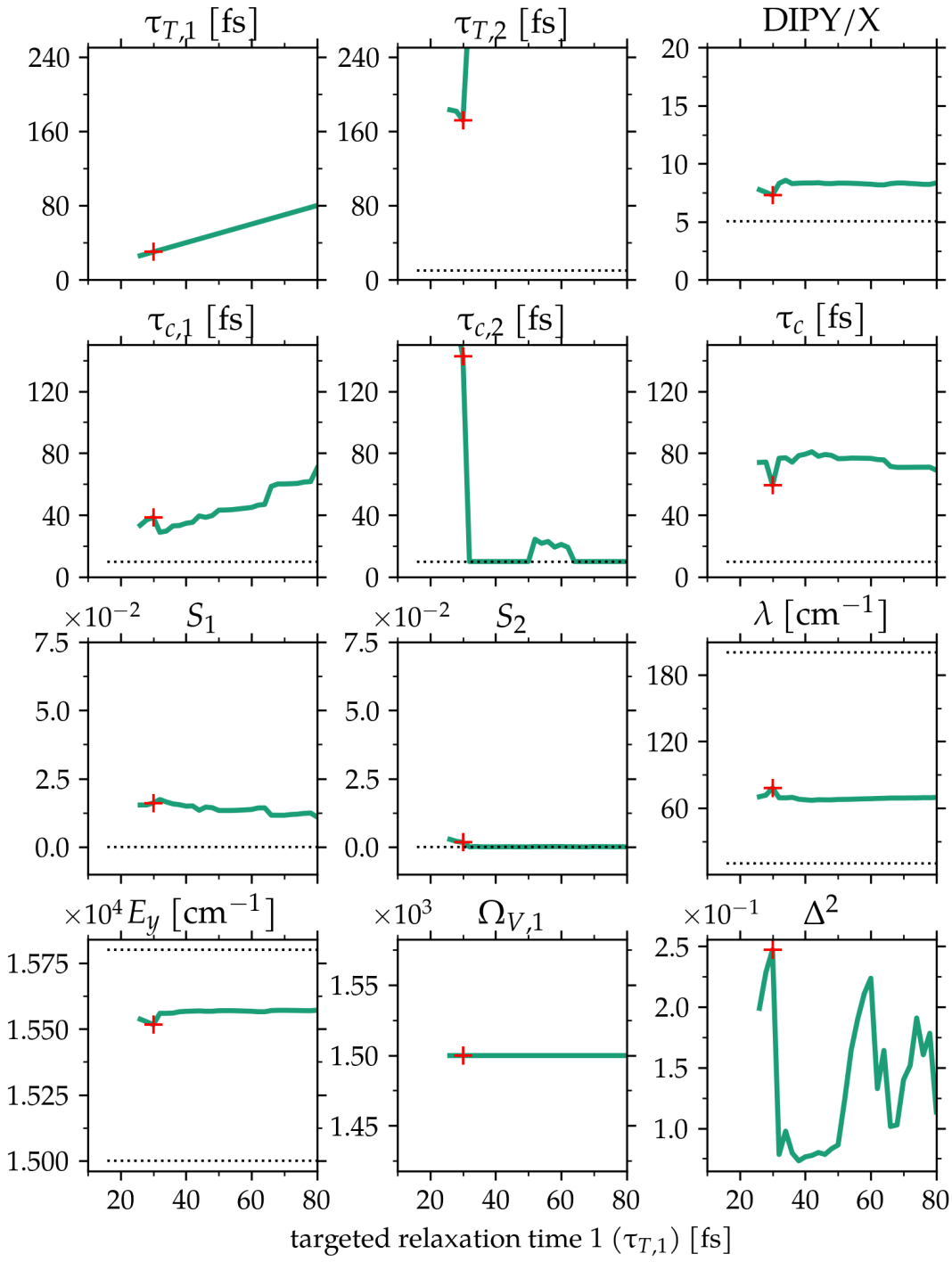


**Figure 3.12:** An overview of selected parameters as they evolve during the scan of parameter $\tau_{T,1}$ combined with optimisations. Constraints on the first vibrational mode were made as used by Reimers et al. (2013). This Figure belongs to Figure 3.11. For more details on the figure, please see the caption of Figure 3.6 on page 50.

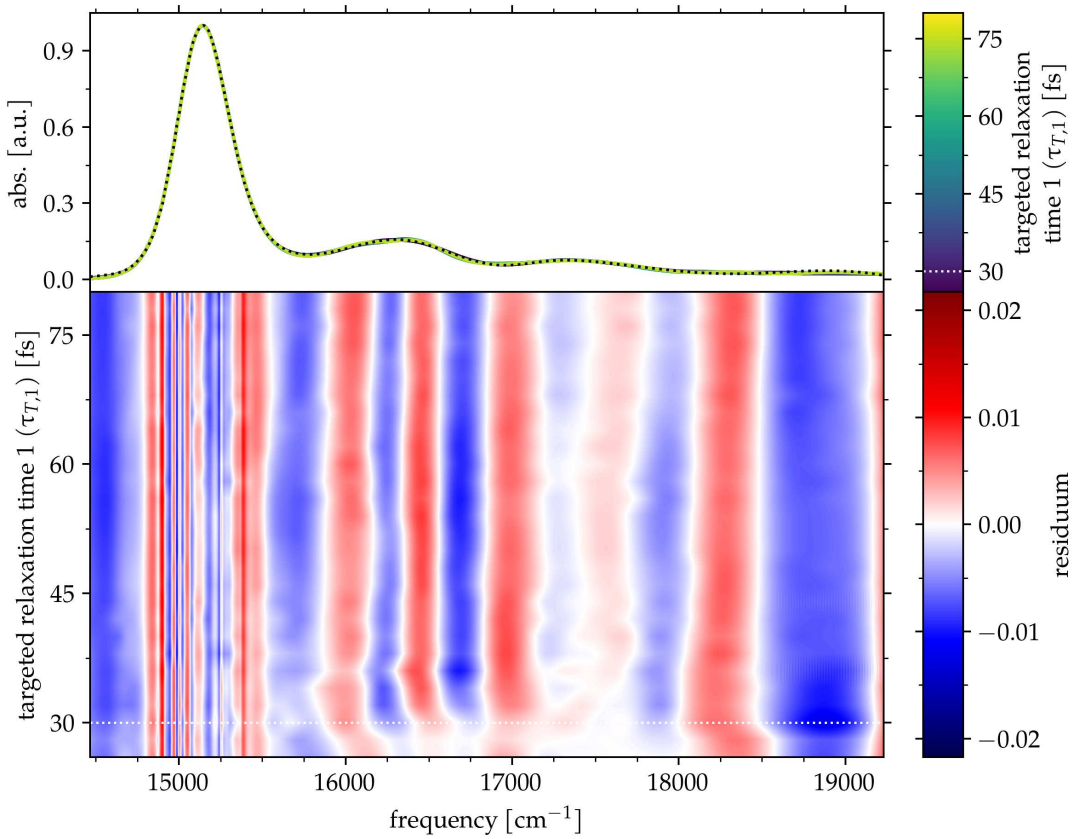


**Figure 3.13:** The results of linear absorption spectra simulation (Chl*a* in diethyl ether, $N_V = 2$) and fitting without any constraint. The fitting procedure was combined with a scan in a single parameter—the targeted relaxation time $\tau_{T,1}$ in the vibrational mode belonging to the first electronic excited state $Q_y$. The scan was performed with both positive and negative increments of 2 fs. For more details on the figure, please see the caption of Figure 3.5 on page 49.

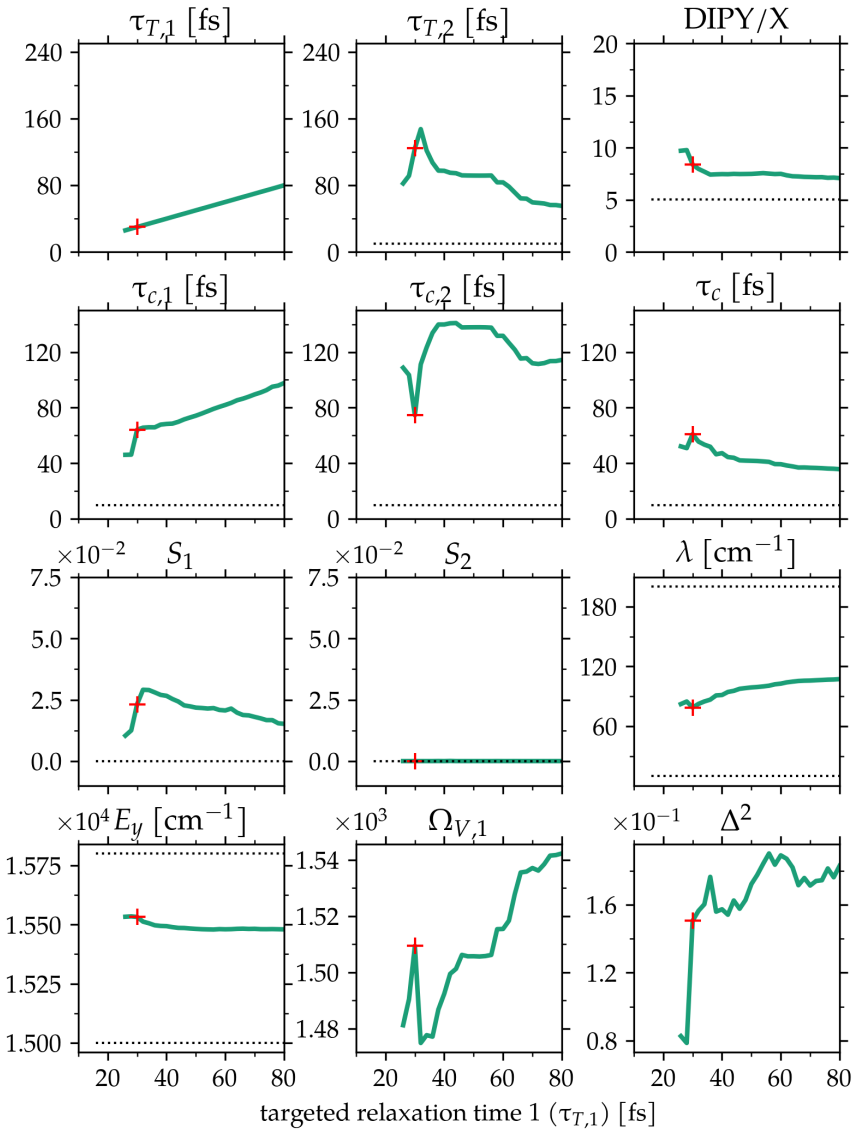


**Figure 3.14:** An overview of selected parameters as they evolve during the scan of parameter $\tau_{T,1}$ combined with optimisations. No constraints were applied to the parameters in this case. This Figure belongs to Figure 3.13. For more details on the figure, please see the caption of Figure 3.6 on page 50.

## 3.2 Chlorophyll *a* in pyridine

Pyridine as a solvent for Chl*a* was chosen for its distinctly different spectroscopic signature when compared with the diethyl ether solvent shown in the previous section. Instead of still quite distinguishable absorption sidebands present in the absorption spectra of Chl*a* in diethyl ether, pyridine renders the spectrum much more uniform and considerably more difficult for curve-fitting procedures to process. Indeed, this theory got confirmed since many of the optimisations failed, diverged, or got stuck.

### 3.2.1 No vibrational modes

Let us start with the simplest case in which our model can be reduced to—the bare three-level system. As can be again seen in Figure 3.15, the three-level model doesn't provide enough means, when combined with the theoretical apparatus used here, to reproduce the absorption spectrum of Chl*a*.

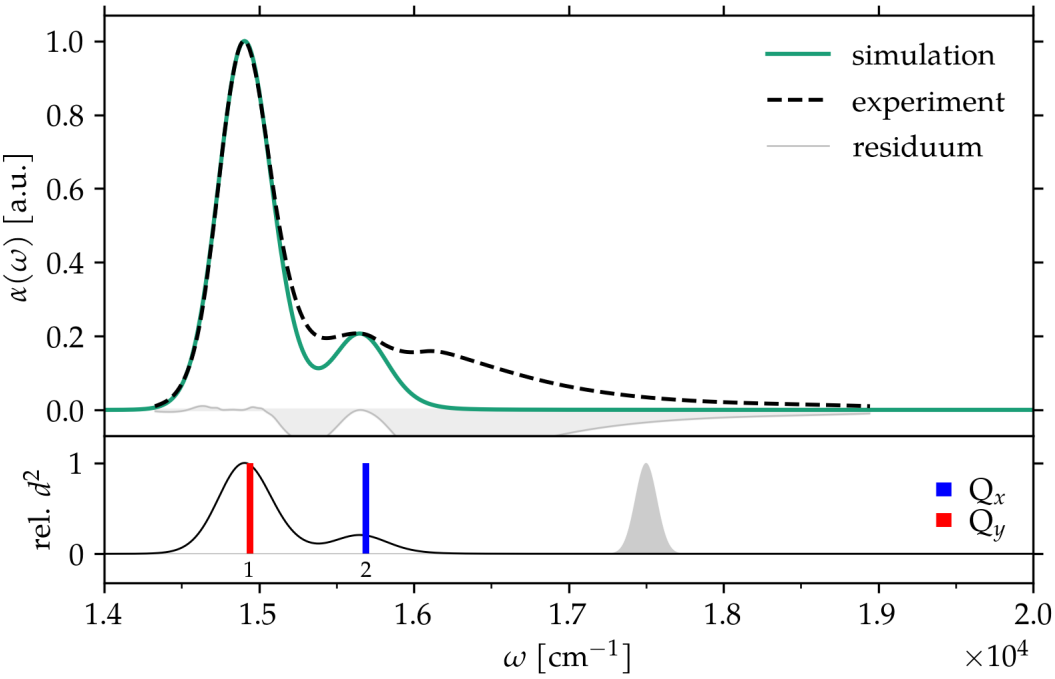


**Figure 3.15:** Simulated linear absorption spectra of a three-level system molecule in pyridine solvent. For more details on the figure, please see the caption of Figure 3.2 on page 46.

### 3.2.2 Single vibrational mode

Once at least a single vibrational mode is included in the model, the spectrum can be fitted with a decent precision to the experimental data as shown in Figure 3.16. Despite the numerical artefact occurring out of the region subjected to the fitting. However, the population dynamics are far from perfect even when the secular approximation is adopted as depicted in Figure 3.17.

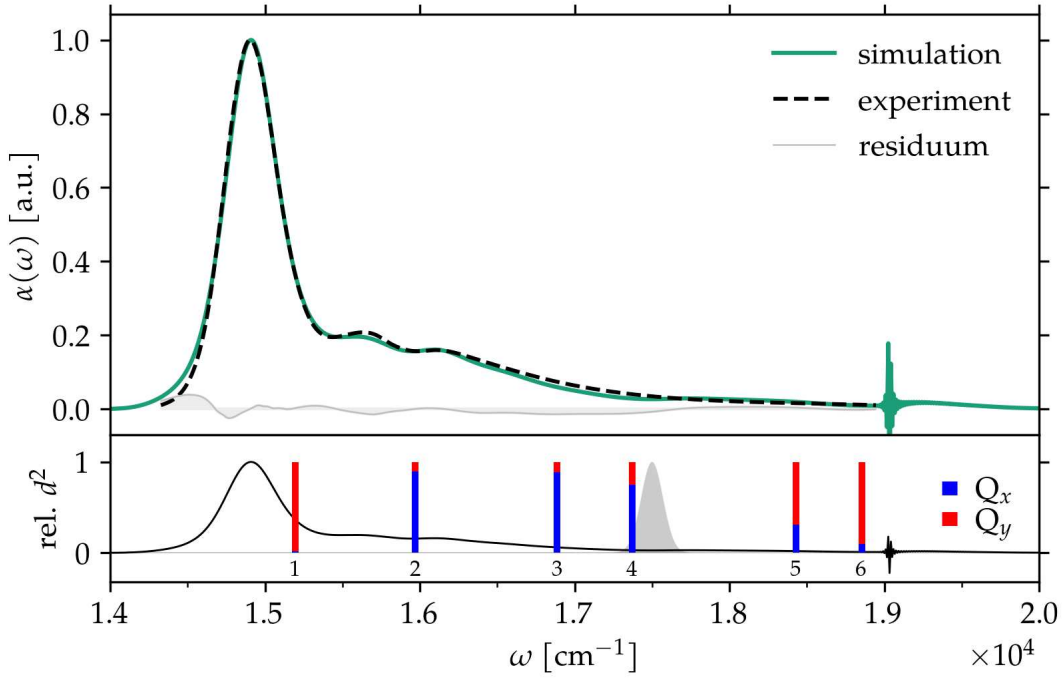


**Figure 3.16:** The optimised linear absorption spectrum of a model of Chl*a* molecule in pyridine solvent with one explicit vibrational mode ($N_V = 1$). For more details on the figure, please see the caption of Figure 3.2 on page 46.

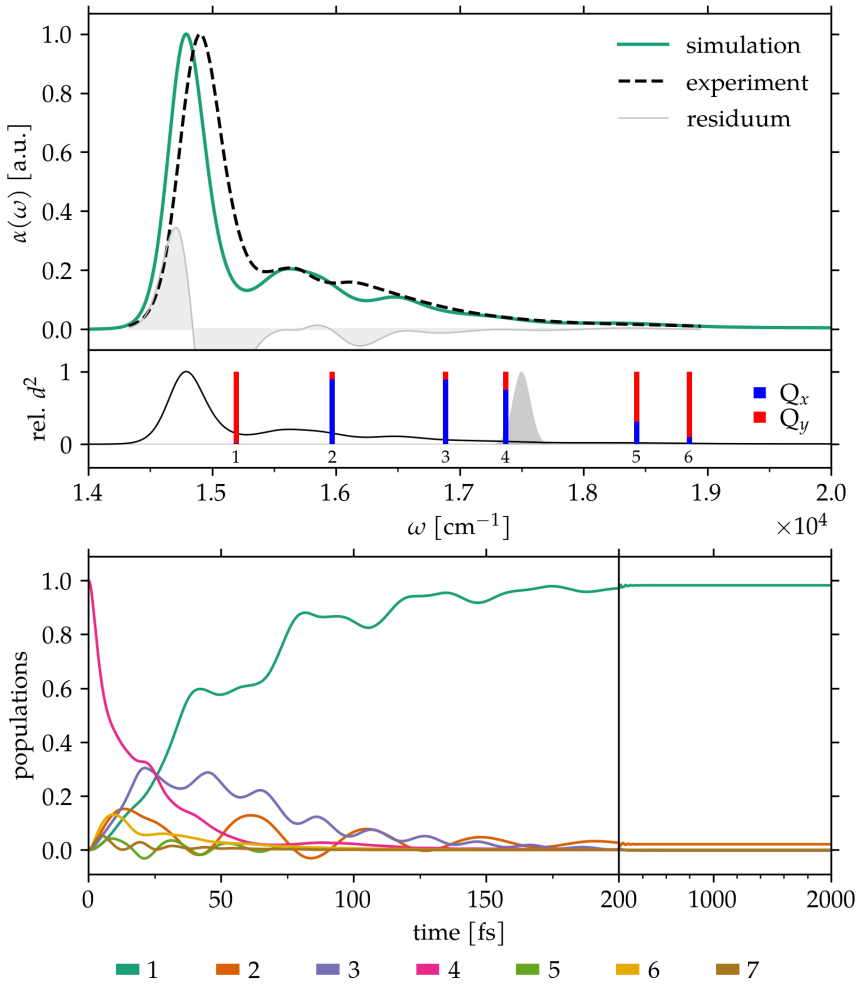


**Figure 3.17:** Simulated linear absorption spectrum of a model of Chl*a* molecule in pyridine solvent and with one explicit vibrational mode ($N_V = 1$). The secular approximation was adopted in the simulation. For more details on the figure, please see the caption of Figure 3.2 on page 46.

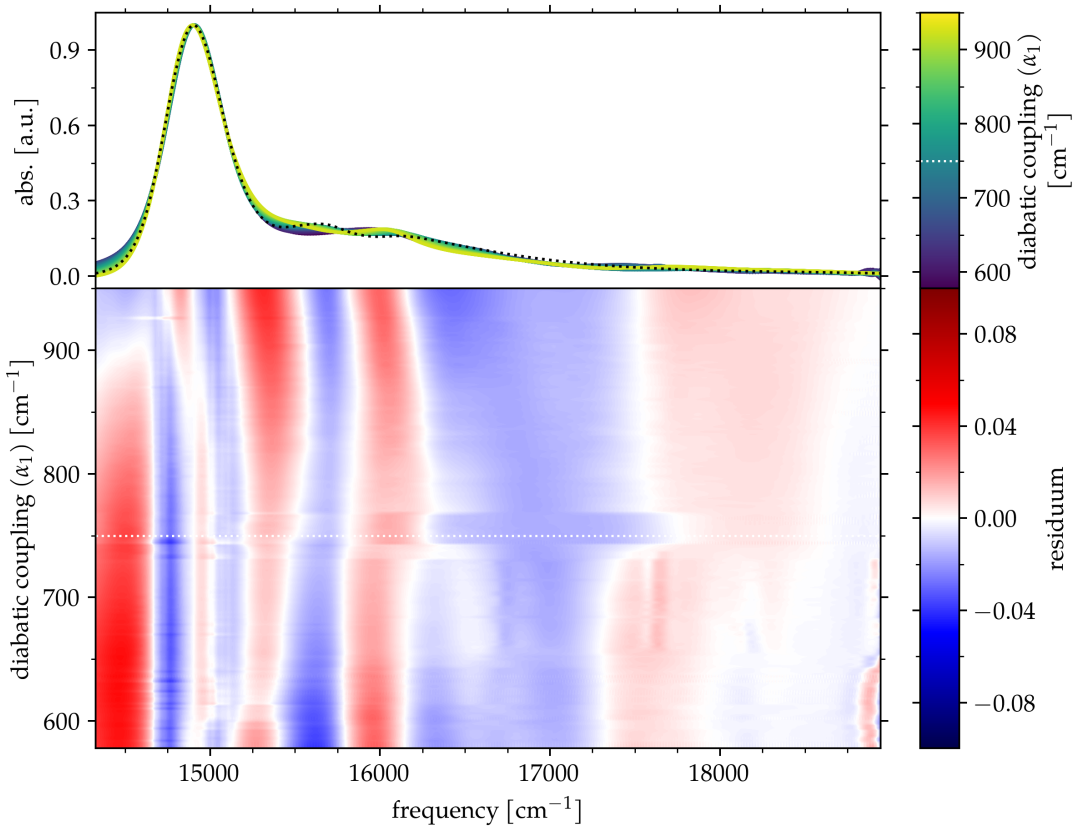


**Figure 3.18:** The results of a linear absorption spectra simulation (Chl*a* in pyridine, $N_V = 1$) and fitting with constraints according to Reimers et al. (2013). The fitting procedure was combined with a scan in a single parameter—the diabatic coupling $\alpha_1$, belonging to the first explicit vibrational mode included in the system Hamiltonian. The scan was performed with both positive and negative increments of 2 cm$^{-1}$. For more details on the figure, please see the caption of Figure 3.5 on page 49.

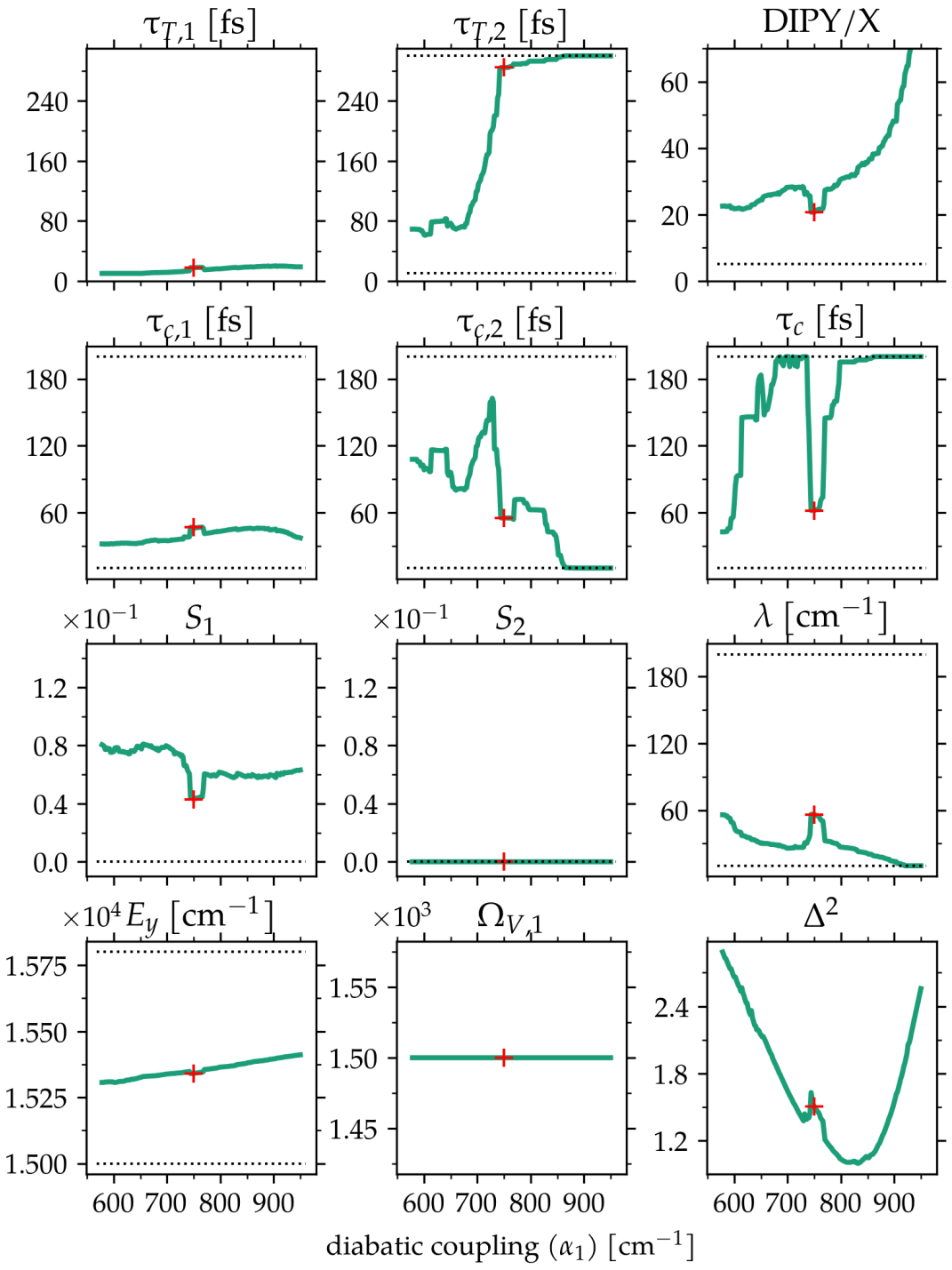


**Figure 3.19:** An overview of selected parameters as they evolve during the scan of the diabatic coupling $\alpha_1$, belonging to the first explicit vibrational mode included in the system Hamiltonian, as combined with optimisations. Constraints on the first vibrational mode were made as used by Reimers et al. (2013). This Figure belongs to Figure 3.11. For more details on the figure, please see the caption of Figure 3.6 on page 50.

### 3.2.3 Two vibrational modes

Two explicitly included vibrational modes result in a decent fit, as can be seen in Figure 3.20, only the small humps at around 15600 $cm^{-1}$ aren't that resolved. Also, note the large amount of vibronic mixing in the bottom subfigure. When compared with the single-vibrational-mode case, there are much more states that mix $Q_y$ and $Q_x$ about equally.

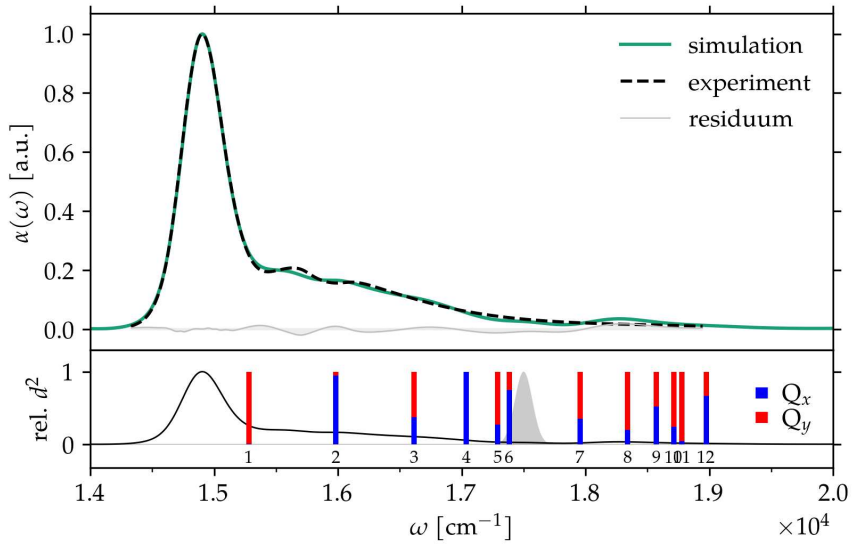


**Figure 3.20:** Optimised Simulated linear absorption spectrum of a model of Chl*a* molecule in pyridine solvent and with two explicit vibrational modes ($N_V = 2$). For more details on the figure, please see the caption of Figure 3.2 on page 46.

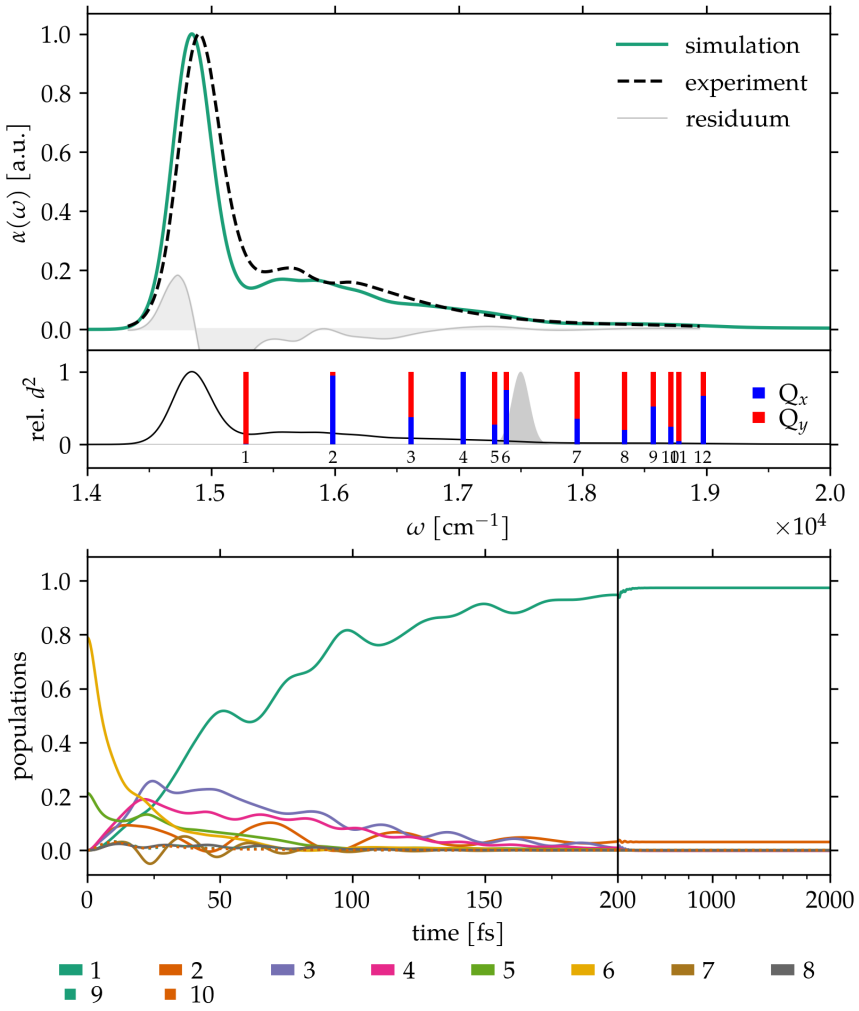


**Figure 3.21:** Simulated linear absorption spectrum of a model of Chl*a* molecule in pyridine solvent and with two explicit vibrational modes ($N_V = 2$). The secular approximation was adopted in the simulation. For more details on the figure, please see the caption of Figure 3.2 on page 46.

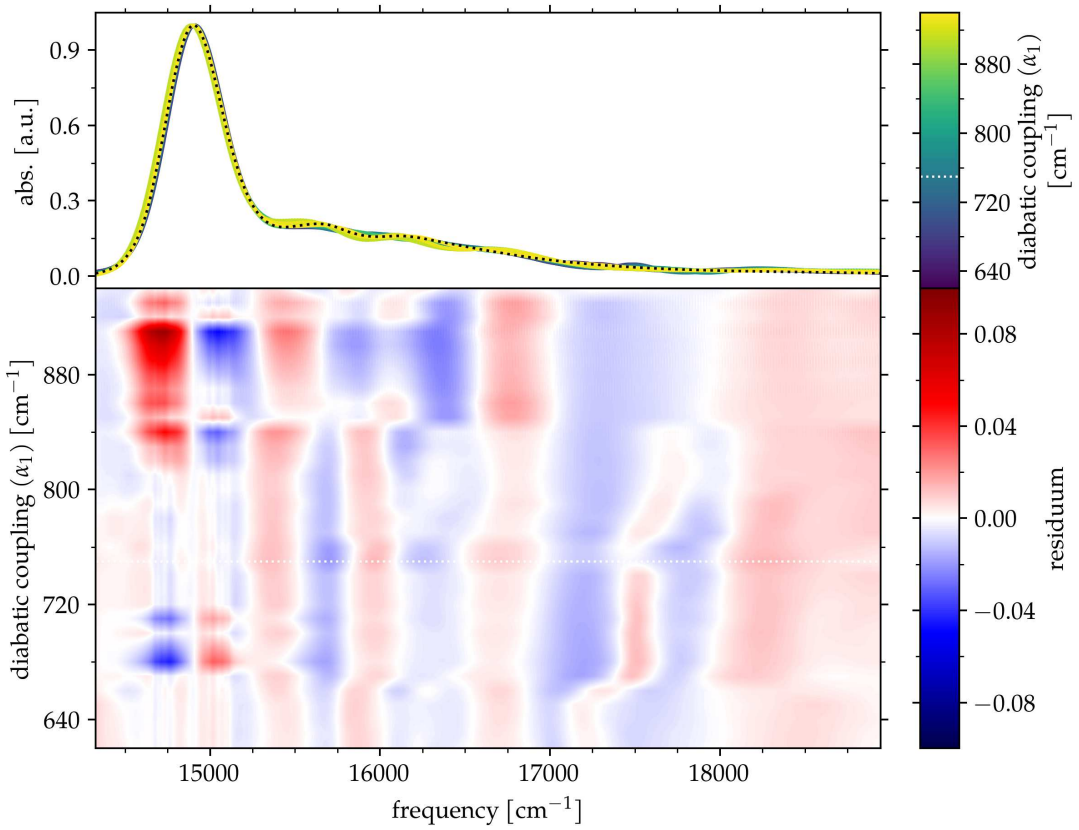


**Figure 3.22:** The results of linear absorption spectra simulation (Chl*a* in pyridine, $N_V = 2$) and fitting with constraints on the first vibrational mode as used by Reimers et al. (2013). The fitting procedure was combined with a scan in a single parameter—the diabatic coupling $\alpha_1$ belonging to the first vibrational mode. The scan was performed with both positive and negative increments of 10 cm$^{-1}$. For more details on the figure, please see the caption of Figure 3.5 on page 49.

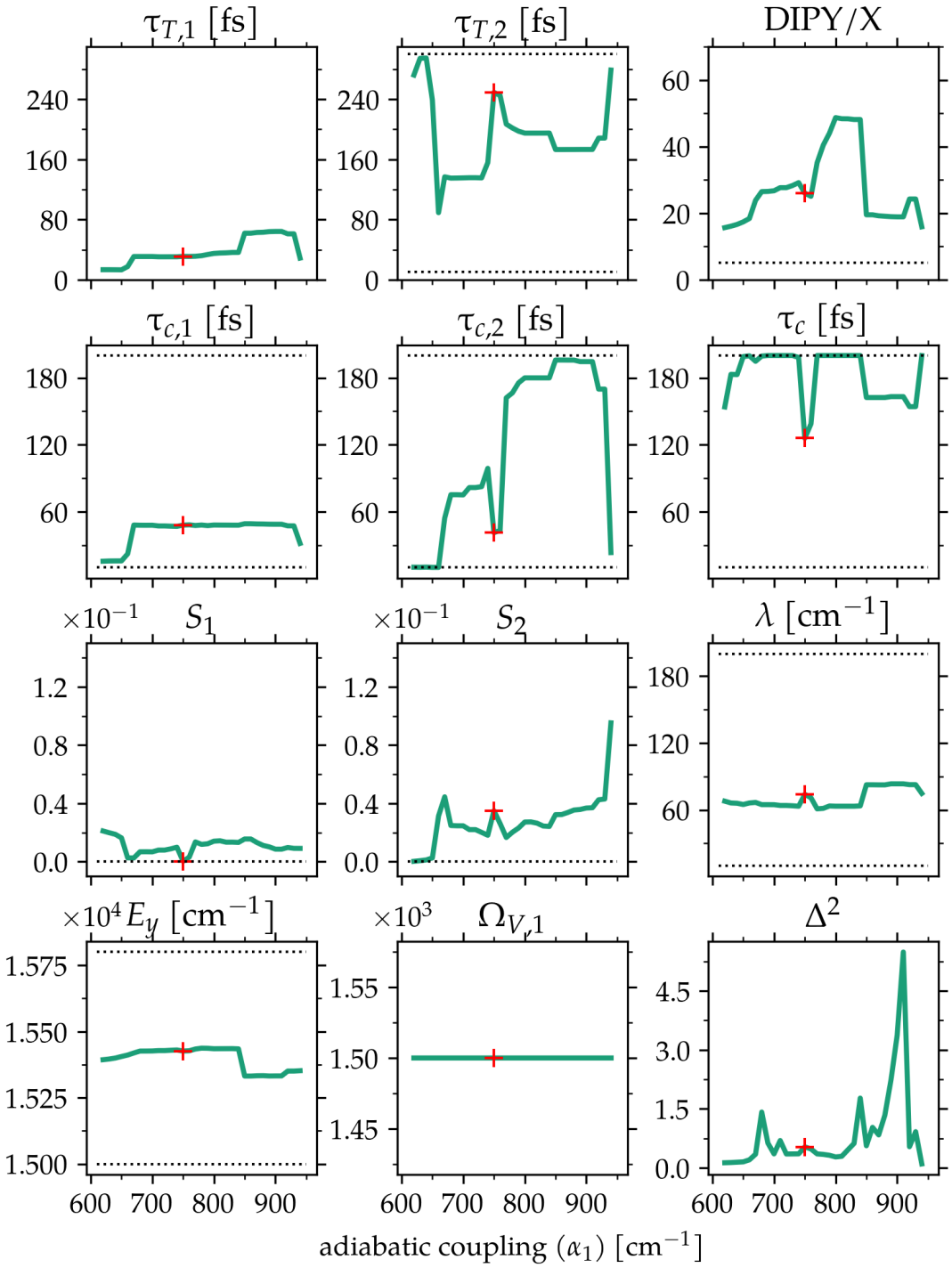


**Figure 3.23:** An overview of selected parameters as they evolve during the scan of parameter $\alpha_1$ combined with optimisations. Constraints on the first vibrational mode were made as used by Reimers et al. (2013). This Figure belongs to Figure 3.22. For more details on the figure, please see the caption of Figure 3.6 on page 50.

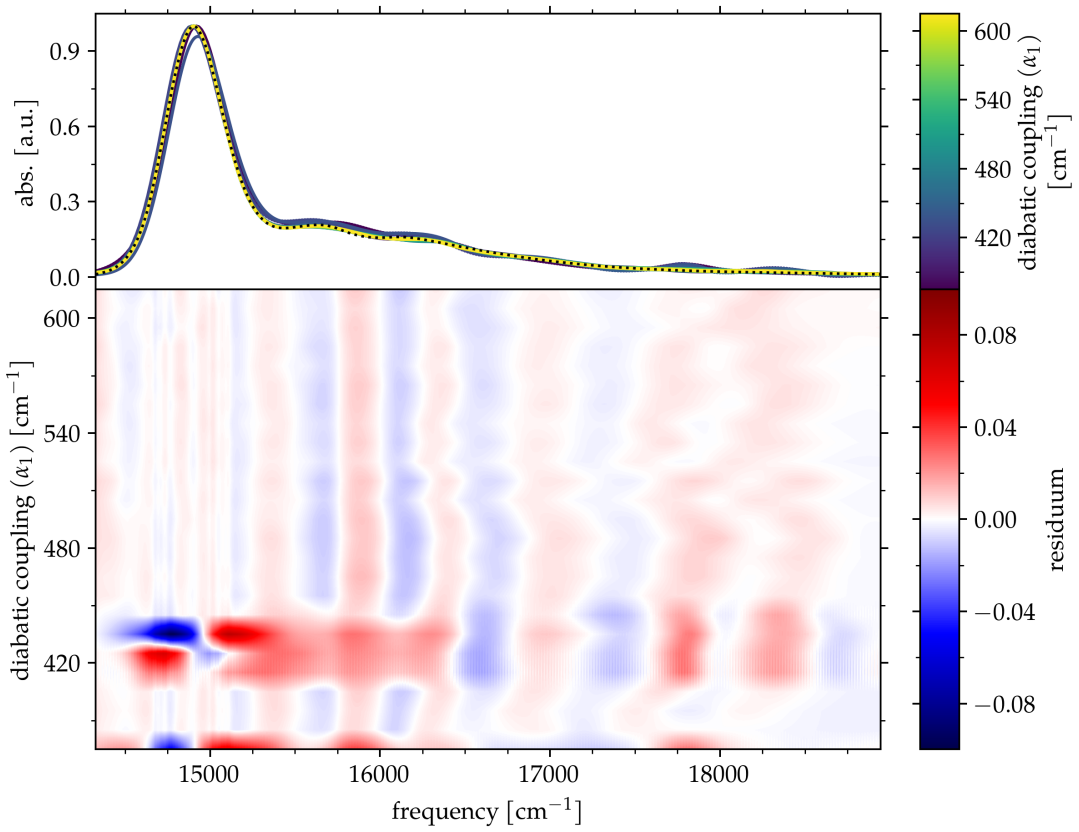


**Figure 3.24:** The results of linear absorption spectra simulation (Chl*a* in pyridine, $N_V = 2$) and fitting without any constraint. The fitting procedure was combined with a scan in a single parameter—the diabatic coupling $\alpha_1$ belonging to the first vibrational mode. The scan was performed with both positive and negative increments of 10 cm$^{-1}$. For more details on the figure, please see the caption of Figure 3.5 on page 49.

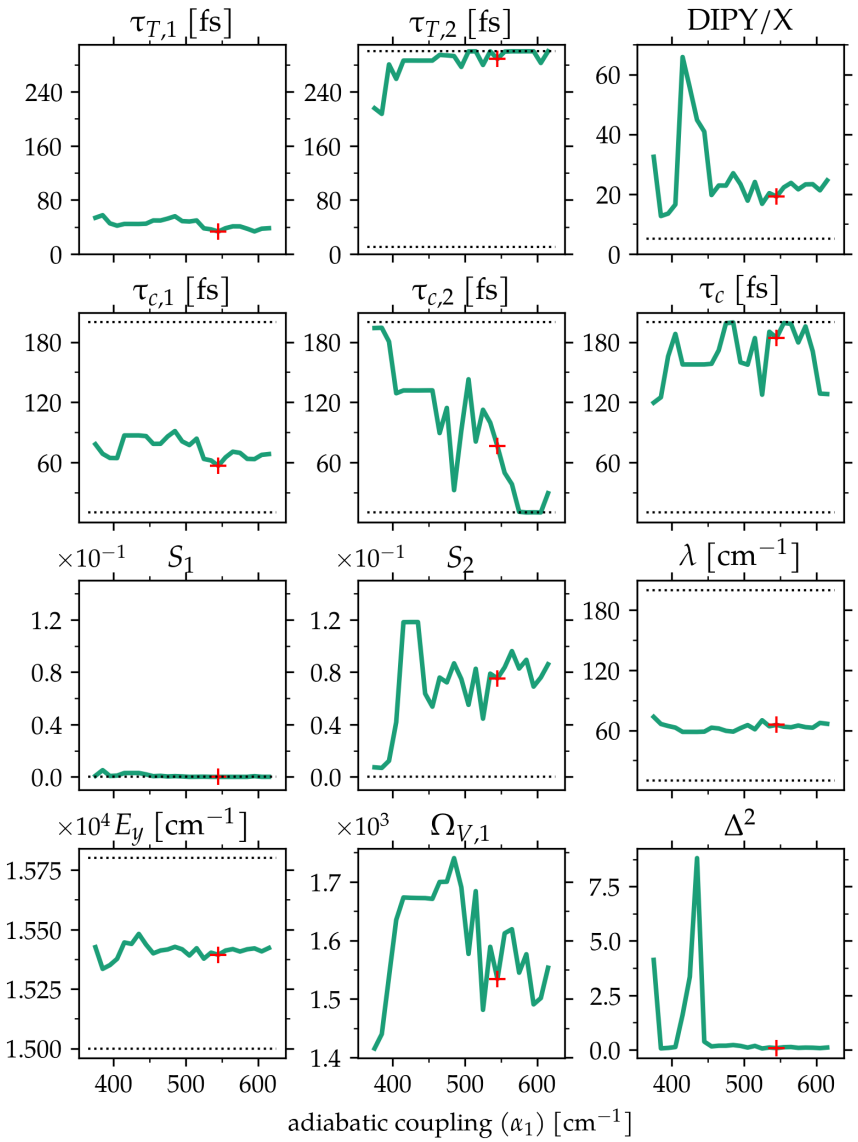


**Figure 3.25:** An overview of selected parameters as they evolve during the scan of parameter $\alpha_1$ combined with optimisations. No constraints were applied to the parameters in this case. This Figure belongs to Figure 3.24. For more details on the figure, please see the caption of Figure 3.6 on page 50.

# 4. Discussion

The spectroscopic model of a chlorophyll-like molecule as formulated in Chapter 2 was able to quantitatively reproduce both of the selected experimental data while all parameters remained in physically meaningful values. This is an important piece of information since the parameters seem to correctly characterise the molecular system and thus have a physical interpretation.

However, as will be discussed shortly, the parameterised model can be only as good for any generalisations as the experimental data that were used to optimise it are restrictive to the parameters. That is, the physical meaning of the parameters of our model might not be correct if there is too much indefiniteness invoked by too general experimental data. A possible answer to this question might provide section 4.3 below.

## 4.1 Curve fitting

A core method used throughout this project was curve-fitting, or, to be more precise, function-fitting to a curve. The curve that was subjected to the fitting procedure was just an output from some function that calculated the absorption spectra based on the input parameters of our spectroscopic model and technical parameters of the simulation like the duration of the simulation, time step, secular approximation, or some of the performance-improving approximations mentioned in section 2.5. For the lack of experience in the field of multidimensional optimisation techniques, an already implemented function from the Python library `Scipy`, namely `scipy.optimize.curve_fit`, was adopted. This function uses the nonlinear least squares method to find the best set of arguments for the function.

As it turned out, it has some serious drawbacks and limitations. Firstly, a really good initial guess of the function arguments has to be provided to return usable data. Secondly, it is very prone to stability issues. For example, in many of the optimising scans performed, the parameters tend to jump or even oscillate as another parameter is varied, meanwhile, other parameters instantly dropped to the minimum or maximum value as manually set limits allowed. This behaviour worsened as the number of parameters grew.

To overcome this issue, two approaches will be done in the following part of the research. First, the parameter space will be scanned more thoroughly, possibly multidimensional, to identify as many parameters that do not alter the simulated experiment significantly as possible and either approximate them by some function of another parameter or assign to them a constant value. The second approach that will be endeavoured will be the implementation of an entirely new function-fitting algorithm that would better suit our needs and would enable us, in an ideal case, to assign different importance weights to different parts of the experimental data so that those sections will be optimised with a higher priority.

## 4.2 Simulated absorption spectra

Despite the difficulties with the optimisation algorithm, all experimental data were successfully reproduced with great precision. The model was able to function even with only one explicit vibrational level included and thus be fully correspondent to the model used by (Reimers et al., 2013). Even though their model was similar, and in fact, it had set foundations for the model developed here, their method of calculation of the linear absorption was very different. Hence, it might be reasonable to assume the model formulated here will provide credible results even if a different method for describing the quantum dynamics of an open quantum system will be used. This will be one of the subjects of our following research.

There are other aspects of the performed simulations that also need further inspection. One of them is the spectral shift induced to the quantum system by adding the vibrational bath to the explicitly included vibrational modes. The shift can be seen when Figure 3.2 is compared with Figure 3.3. In the former figure, where the vibrational bath isn't included in the model, the absorption bands are aligned with the transition energies from the ground state. Meanwhile, in the latter figure, the bands are red-shifted to the left from the actual transition energies denoted by the red and blue bars. This is a consequence of some form of "reorganisation energy" taking a toll on the energy, even though, as discussed in subsection 2.3.6, reorganisation energy doesn't represent the intended physical quantity here as there are no transitions between states taking places.

Another influence on spectra has the secular approximation as shown in Figure 3.4 and Figure 3.10 for Chl*a* in diethyl ether, and in Figure 3.17 and Figure 3.21 for Chl*a* in pyridine. In both cases, the secular approximation had a smaller impact on the spectra if there were more vibrational modes.

## 4.3 The parameter space

The parameter spaces of our model with one or two explicitly included vibrational levels were thoroughly explored, even though only a selection of data was presented in Chapter 3. The remaining data and corresponding scripts will be stored on the GitHub repository `https://github.com/MichalPt/MScThesis`. Nevertheless, the parameter space scans presented here have tons of information to tell us about the formulated spectroscopic model and the relevance of simulating linear absorption spectra.

On pages 3.5–3.8, a parameter of the vibrational bath assigned to the single explicit vibrational mode included in the system Hamiltonian, at first excited electronic state—named *targeted relaxation time* $\tau_{T,1}$ (see 39)—was scanned while optimisation of all other parameters, to fit the simulated spectrum to the experimental data, was performed at each consecutive step. By comparison, in section A.3 of Appendix, essentially the same scan was performed but without the optimisations.

Even though the parameter had quite some influence on various characteristics of the calculated absorption spectrum in the second case, the first case tells a completely different story. We can see already in Figure 3.6 with only one

mode included that other parameters of the model can successfully compensate to any changes in its value. This idea is even better depicted in the two-mode case in Figure 3.14 and Figure 3.14. We can clearly see residuum is pretty much constant throughout the scan even though the parameters are changing only slightly. But they are definitely changing. The most notable ones appear to be the reorganisation energy of the electronic bath $\lambda$ and also the other parameters of the vibrational bath $(\tau_{T,2}, \tau_{c,1}, \tau_{c,2})$.

A similar effect can also be seen in the case of Chl*a* in pyridine. The diabatic coupling $\alpha_1$ assigned to the first vibrational mode was chosen to be shown there. As far as only one vibrational mode is concerned in the model (Figure 3.18 and Figure 3.19), an optimisation scan with a smoother step of 2 $\mathrm{cm}^{-1}$ was feasible to compute in a reasonable time. The 2D map thus provides a very detailed insight into sudden changes in lineshapes. Besides that, we can also see a little bit smoother evolution of the parameters, as can be seen in the other figure. In this case, however, the parameters are changing on much larger timescales and some of them; namely, the Huang-Rhys factor $S_1$, dipole moments (DIPY/X), and correlation time of the bath $\tau_c$ appear to be negatively correlated with the reorganisation energy $\lambda$ .

The case of two explicit vibrational levels shows a less detailed picture of the situation due to the higher computational cost and as well as overall higher instability of the optimisations. Despite that, the Figures on pages 67–70 can still tell us which parameters tend to evolve $(\tau_{c,2}, S_2, \Omega_{V,1})$ and which rather not $(\tau_{c,1}, S_1, \tau_{T,1}, \lambda,)$. Hence, the part of the system that is affected the most by the diabatic coupling and needs to optimize its parameters is the vibrational bath of the higher-in-energy $Q_x$ state.

## 4.4 Excited states dynamics

A separate part of the simulations was the calculation of excited state dynamics to evaluate at which timescales the internal conversion between $Q_x$ and $Q_y$ states occur. The simulations for that were based on the same parameters as obtained from the fitting of the calculated absorption spectra to the experimental one. It is important to point out that the simulations there were performed for the purpose of calculating absorption spectra were different from the ones that regarded excited state dynamics. The computational details about simulating the absorption spectra are listed in section 2.4.

As can be seen in a majority of the population dynamics presented in Chapter 3, rather strong oscillations were always obtained in the evolutions. Even after introducing the secular approximation, which should have gotten rid of oscillatory nonsecular terms, some kind of oscillation persisted (see for example Figure 3.21). There are several possible explanations for that.

First, a strong coupling of vibrational modes included in the system to the vibrational bath may render our system out of the boundaries of initial assumptions when deriving the Redfield equations. That is the assumption of a weak system-bath interaction. A clue might provide testing of different theories to describe the dynamics.

Second, as was pointed out in section 4.3, the parameterization of the model based on experimental data of linear absorption spectra only might not provide the correct physical form of the model. As it was discussed, many different combinations of the parameter values can result in mostly identical absorption spectra. Hence, as it is going to be again a subject of our future research, a possible solution for improving the dynamics of the excited state would be to use different experimental data, or use even combinations of them, to parameterize the model. A more suitable would be models that actually capture the processes on the femtosecond timescale such 2DES with femtosecond resolution, a pump-probe experiments. Especially the polarisation-resolved techniques (e.g. Zahn et al., 2022) might be a source of important information about the orientation of the transition dipole moments and about mixing of the states due to the diabatic coupling.

## 4.5 Ultrafast internal conversion

Due to the problems with strong oscillation in the evolution of populations in excited state dynamics simulations mentioned in the previous section, the interpretation of these dynamics has to be done with great care. All the presented dynamics in secular approximation seem to have similar timescales of relaxations to the $Q_y$ state of roughly 100 fs, with much faster intermediate relaxations in the modes. Such a number would be in great correspondence with both the experimental and theoretical findings, as discussed in greater detail in section 1.2. The best correspondence would be with the results of Meneghin et al. (2017) since they as well observed intermediate vibrations-involving relaxation in the 40 fs window.

Nevertheless, one shouldn't consider these results to be the final contribution to the topic of ultrafast internal conversion in chlorophyll molecules. It might be even the exact opposite since the thorough data about the parameter space gathered so far, using the newly formulated model, weren't even fully employed yet.

# Conclusion

A new spectroscopic model for chlorophyll-like molecules was formulated, implemented, and tested on simulations of linear absorption spectroscopic experiments. The model was parameterised by fitting the simulated spectrum to the experimental data—Chl*a* soluted in two different solvents, diethyl ether and pyridine—obtained from the literature (Rätsep et al., 2009). By introducing constraints on the parameters to maximally correspond parameter-wise with an older work that used in principle the same, but simpler version of our model (Reimers et al., 2013), the fitted simulated spectrum still well reproduced the experimental data (see Figure 3.3, Figure 3.16) and thus confirmed the validity of our model and its backwards compatibility with simpler models used prior to this work.

The time-dependent Redfield theory was implemented and optimised for performance (as discussed insection 2.5) to make calculations of larger systems feasible. The theory was used to calculate not only the linear absorption spectra from relations presented in section 2.4, but also the excited state population dynamics. However, since the parameterization of the model turned out to be too "loose" and indefinite (myriads of the physical parameters can be changed without affecting the linear absorption spectrum as discussed in section 4.3) with respect to the absorption spectrum, we didn't delve in great detail into the discussion of the energy relaxation times (i.e. transfer rates) as it is most probably necessary to use more specific and short-timescale oriented experiments to parameterise the model with first.

Nevertheless, the parameter space of linear absorption spectra simulations was explored in great detail and the obtained results will be used in the following research to better understand the relations between the parameters of the formulated model and the system photoinduced dynamics.

# Bibliography


Andrews, S. S. (2004). Using Rotational Averaging To Calculate the Bulk Response of Isotropic and Anisotropic Samples from Molecular Parameters. *Journal of Chemical Education*, 81:877. https://doi.org/10.1021/ed081p877.

Björn, L. O. and Ghiradella, H. (2014). Photobiology, The Science of Light and Life. pages 97–117. https://doi.org/10.1007/978-1-4939-1468-5_9.

Blankenship, R. E. (2014). *Molecular Mechanisms of Photosynthesis*. Wiley Blackwell.

Bricker, W. P., Shenai, P. M., Ghosh, A., Liu, Z., Enriquez, M. G. M., Lambrev, P. H., Tan, H.-S., Lo, C. S., Tretiak, S., Fernandez-Alberti, S., and Zhao, Y. (2015). Non-radiative relaxation of photoexcited chlorophylls: theoretical and experimental study. *Scientific Reports*, 5:13625. https://doi.org/10.1038/srep13625.

Brixner, T., Mančal, T., Stiopkin, I. V., and Fleming, G. R. (2004). Phase-stabilized two-dimensional electronic spectroscopy. *The Journal of Chemical Physics*, 121:4221–4236. https://doi.org/10.1063/1.1776112.

Cai, Z.-L., Crossley, M. J., Reimers, J. R., Kobayashi, R., and Amos, R. D. (2006). Density Functional Theory for Charge Transfer: The Nature of the N-Bands of Porphyrins and Chlorophylls Revealed through CAM-B3LYP, CASPT2, and SAC-CI Calculations. *The Journal of Physical Chemistry B*, 110: 15624–15632. https://doi.org/10.1021/jp063376t.

Cignoni, E., Slama, V., Cupellini, L., and Mennucci, B. (2022). The atomistic modeling of light-harvesting complexes from the physical models to the computational protocol. *The Journal of Chemical Physics*, 156:120901. https://doi.org/10.1063/5.0086275.

Croce, R., van Grondelle, R., van Amerongen, H., and van Stokkum, I. (2018). *Light Harvesting in Photosynthesis*. CRC Press.

Curutchet, C. and Mennucci, B. (2017). Quantum Chemical Studies of Light Harvesting. *Chemical Reviews*, 117:294–343. https://doi.org/10.1021/acs.chemrev.5b00700.

Dong, L.-Q., Niu, K., and Cong, S.-L. (2006). Theoretical study of vibrational relaxation and internal conversion dynamics of chlorophyll-a in ethyl acetate solvent in femtosecond laser fields. *Chemical Physics Letters*, 432:286–290. https://doi.org/10.1016/j.cplett.2006.10.040.

Dong, L.-Q., Niu, K., and Cong, S.-L. (2007a). Theoretical analysis of internal conversion pathways and vibrational relaxation process of chlorophyll-a in ethyl ether solvent. *Chemical Physics Letters*, 440:150–154. https://doi.org/10.1016/j.cplett.2007.04.021.

Dong, L.-Q., NIU, K., and Cong, S.-L. (2007b). Theoretical investigation of ultrafast dynamics of the rhodamine-700 molecule in solvents. *Journal of Theoretical and Computational Chemistry*, 6:885–892. https://doi.org/10.1142/s0219633607003490.

Fresch, E. and Collini, E. (2020). Relaxation Dynamics of Chlorophyll b in the Sub-ps Ultrafast Timescale Measured by 2D Electronic Spectroscopy. *International Journal of Molecular Sciences*, 21:2836. https://doi.org/10.3390/ijms21082836.

Gouterman, M. (1961). Spectra of porphyrins. *Journal of Molecular Spectroscopy*, 6:138–163. https://doi.org/10.1016/0022-2852(61)90236-3.

Gouterman, M., Wagnière, G. H., and Snyder, L. C. (1963). Spectra of porphyrins Part II. Four orbital model. *Journal of Molecular Spectroscopy*, 11: 108–127. https://doi.org/10.1016/0022-2852(63)90011-0.

Gyamfi, J. A. (2020). Fundamentals of quantum mechanics in Liouville space. *European Journal of Physics*, 41:063002. https://doi.org/10.1088/1361-6404/ab9fdd.

Harris, C. R., Millman, K. J., van der Walt, S. J., Gommers, R., Virtanen, P., Cournapeau, D., Wieser, E., Taylor, J., Berg, S., Smith, N. J., Kern, R., Picus, M., Hoyer, S., van Kerkwijk, M. H., Brett, M., Haldane, A., del Río, J. F., Wiebe, M., Peterson, P., Ǵerard-Marchant, P., Sheppard, K., Reddy, T., Weckesser, W., Abbasi, H., Gohlke, C., and Oliphant, T. E. (2020). Array programming with NumPy. *Nature*, 585:357–362. https://doi.org/10.1038/s41586-020-2649-2.

Heard, A. W., Bekker, A., Kovalick, A., Tsikos, H., Ireland, T., and Dauphas, N. (2022). Oxygen production and rapid iron oxidation in stromatolites immediately predating the Great Oxidation Event. *Earth and Planetary Science Letters*, 582:117416. https://doi.org/10.1016/j.epsl.2022.117416.

Maiuri, M., Garavelli, M., and Cerullo, G. (2020). Ultrafast Spectroscopy: State of the Art and Open Challenges. *Journal of the American Chemical Society*, 142: 3–15. https://doi.org/10.1021/jacs.9b10533.

Malý, P., Somsen, O. J. G., Novoderezhkin, V. I., Mančal, T., and van Grondelle, R. (2016). The Role of Resonant Vibrations in Electronic Energy Transfer. *ChemPhysChem*, 17:1356–1368. https://doi.org/10.1002/cphc.201500965.

May, V. and Kühn, O. (2011). *Charge and Energy Transfer Dynamics in Molecular Systems*. Wiley-VCH.

Meneghin, E., Leonardo, C., Volpato, A., Bolzonello, L., and Collini, E. (2017). Mechanistic insight into internal conversion process within Q-bands of chlorophyll a. *Scientific Reports*, 7:11389. https://doi.org/10.1038/s41598-017-11621-2.

Meneghin, E., Pedron, D., and Collini, E. (2018). Raman and 2D electronic spectroscopies: A fruitful alliance for the investigation of ground and excited state vibrations in chlorophyll a. *Chemical Physics*, 514:132–140. https://doi.org/10.1016/j.chemphys.2018.03.003.

Mennucci, B. and Curutchet, C. (2011). The role of the environment in electronic energy transfer: a molecular modeling perspective. *Physical Chemistry Chemical Physics*, 13:11538–11550. https://doi.org/10.1039/c1cp20601j.

Moca, R., Meech, S. R., and Heisler, I. A. (2015). Two-Dimensional Electronic Spectroscopy of Chlorophyll a: Solvent Dependent Spectral Evolution. *The Journal of Physical Chemistry B*, 119:8623–8630. https://doi.org/10.1021/acs.jpcb.5b04339.

Mukamel, S. (1995). *Principles of Nonlinear Optical Spectroscopy*. Oxford University Press.

Niedringhaus, A., Policht, V. R., Sechrist, R., Konar, A., Laible, P. D., Bocian, D. F., Holten, D., Kirmaier, C., and Ogilvie, J. P. (2018). Primary processes in the bacterial reaction center probed by two-dimensional electronic spectroscopy. *Proceedings of the National Academy of Sciences*, 115:201721927. https://doi.org/10.1073/pnas.1721927115.

Niu, K., Dong, L.-Q., and Cong, S.-L. (2008). Internal Conversion Process of Chlorophyll a in Solvents in Femtosecond Pump-Probe Laser Fields. *Chinese Journal of Chemical Physics*, 21:211–216. https://doi.org/10.1088/1674-0068/21/03/211-216.

Nonomura, Y., Igarashi, S., Yoshioka, N., and Inoue, H. (1997). Spectroscopic properties of chlorophylls and their derivatives. Influence of molecular structure on the electronic state. *Chemical Physics*, 220:155–166. https://doi.org/10.1016/s0301-0104(97)00087-6.

Padilla, M., Kolbe, B., and Chakraborty, A. (2017). The Nearest Hermitian Inverse Eigenvalue Problem Solution with Respect to the 2-Norm. *arXiv*. https://doi.org/10.48550/arxiv.1703.00829.

Policht, V. R., Niedringhaus, A., Willow, R., Laible, P. D., Bocian, D. F., Kirmaier, C., Holten, D., Mančal, T., and Ogilvie, J. P. (2022). Hidden vibronic and excitonic structure and vibronic coherence transfer in the bacterial reaction center. *Science Advances*, 8:eabk0953. https://doi.org/10.1126/sciadv.abk0953.

Redfield, A. (1965). The Theory of Relaxation Processes. *Advances in Magnetic and Optical Resonance*, 1:1–32. https://doi.org/10.1016/b978-1-4832-3114-3.50007-6.

Reimers, J. R., Cai, Z.-L., Kobayashi, R., Rätsep, M., Freiberg, A., and Krausz, E. (2013). Assignment of the Q-Bands of the Chlorophylls: Coherence Loss via Qx − Qy Mixing. *Scientific Reports*, 3:2761. https://doi.org/10.1038/srep02761.

Reimers, J. R., Cai, Z.-L., Kobayashi, R., Rätsep, M., Freiberg, A., and Krausz, E. (2014). The role of high-level calculations in the assignment of the Q-band spectra of chlorophyll. *AIP Conference Proceedings*, 1618:18–22. https://doi.org/10.1063/1.4897663.

Rätsep, M., Linnanto, J., and Freiberg, A. (2009). Mirror symmetry and vibrational structure in optical spectra of chlorophyll a. *The Journal of Chemical Physics*, 130:194501. https://doi.org/10.1063/1.3125183.

Rätsep, M., Linnanto, J. M., Muru, R., Biczysko, M., Reimers, J. R., and Freiberg, A. (2019). Absorption-emission symmetry breaking and the different origins of vibrational structures of the 1Qy and 1Qx electronic transitions of pheophytin a. *The Journal of Chemical Physics*, 151:165102. https://doi.org/10.1063/1.5116265.

Scheer, H. (2003). Light-Harvesting Antennas in Photosynthesis. *Advances in Photosynthesis and Respiration*, pages 29–81. https://doi.org/10.1007/978-94-017-2087-8_2.

Segatta, F., Cupellini, L., Garavelli, M., and Mennucci, B. (2019). Quantum Chemical Modeling of the Photoinduced Activity of Multichromophoric Biosystems. *Chemical Reviews*, 119:9361–9380. https://doi.org/10.1021/acs.chemrev.9b00135.

Shi, Y., Liu, J.-Y., and Han, K.-L. (2005). Investigation of the internal conversion time of the chlorophyll a from S3, S2 to S1. *Chemical Physics Letters*, 410: 260–263. https://doi.org/10.1016/j.cplett.2005.05.017.

Shi, Y., Shiu, Y. J., Su, C., Lin, S. H., and li Han, K. (2006). Transient Absorption of the Chlorophyll a in Ethanol. *Chinese Journal of Chemical Physics*, 19:6–10. https://doi.org/10.1360/cjcp2006.19(1).6.5.

Sirohiwal, A., Berraud-Pache, R., Neese, F., Izsák, R., and Pantazis, D. A. (2020). Accurate Computation of the Absorption Spectrum of Chlorophyll a with Pair Natural Orbital Coupled Cluster Methods. *The Journal of Physical Chemistry. B*, 124:8761–8771. https://doi.org/10.1021/acs.jpcb.0c05761.

Thompson, K. J., Kenward, P. A., Bauer, K. W., Warchola, T., Gauger, T., Martinez, R., Simister, R. L., Michiels, C. C., Llirós, M., Reinhard, C. T., Kappler, A., Konhauser, K. O., and Crowe, S. A. (2019). Photoferrotrophy, deposition of banded iron formations, and methane production in Archean oceans. *Science Advances*, 5. https://doi.org/10.1126/sciadv.aav2869.

Umetsu, M., Wang, Z.-Y., Kobayashi, M., and Nozawa, T. (1999). Interaction of photosynthetic pigments with various organic solvents Magnetic circular dichroism approach and application to chlorosomes. *Biochimica et Biophysica Acta (BBA) - Bioenergetics*, 1410:19–31. https://doi.org/10.1016/s0005-2728(98)00170-4.

Valkunas, L., Abramavicius, D., and Mančal, T. (2013). *Molecular Excitation Dynamics and Relaxation*. Wiley-VCH.

Weiss, U. (2008). *Quantum Dissipative Systems*. World Scientific. https://doi.org/10.1142/6738.

Zahn, C., Stensitzki, T., and Heyne, K. (2022). Femtosecond anisotropy excitation spectroscopy to disentangle the Q x and Q y absorption in chlorophyll a. *Chemical Science*, 13:12426–12432. https://doi.org/10.1039/d2sc03538c.

Zakutauskaite, K., Macernis, M., Nguyen, H., Ogilvie, J. P., and Abramavicius, D. (2022). Extracting the excitonic Hamiltonian of a Chlorophyll dimer from broadband two-dimensional electronic spectroscopy. *The Journal of Chemical Physics*. https://doi.org/10.1063/5.0108166.

# List of Abbreviations

| | |
|---|---|
| 2DES | two-dimensional electronic spectroscopy |
| Chl*a* | chlorophyll *a* |
| Chl*b* | chlorophyll *b* |
| DFT | density functional theory |
| DMF | dimethylformamide |
| DOF | degrees of freedom |
| FLN | fluorescence line-narrowing spectroscopy |
| GPU | graphics processing unit |
| HOMO | highest occupied molecular orbital |
| LUMO | lowest unoccupied molecular orbital |
| MD | molecular dynamics |
| NA-ESMD | nonadiabatic excited-state molecular dynamics |
| PES | potential energy surface |
| QCh | quantum chemistry |
| TEA | triethylamine |
| THF | tetrahydrofuran |

# A. Attachments

## A.1 Parameter space of the physical model for various constraints

The optimised parameters of the model are available on the GitHub repository: `https://github.com/MichalPt/MScThesis`

**Table A.1:** Summary of the parameters that are subjected to a fitting procedure. The uppermost row denotes the number of vibrational modes explicitly included in the model. Single asterisks $(*)$ mark quantities, there were optimised by Reimers et al. (2013) and thus were subjected to a constraint on their value for some of the simulations presented in this thesis to compare both models. The quantity $\Delta$ represents here an energy gap defined as $\Delta = E_x - E_y$. $\phi$ is an angle in degrees between $Q_x$ and $Q_y$ transition dipole moments.

| $N_V$ | | 0 | 1 | 2 |
|---|---|---|---|---|
| $^*E$ | $g$ | | $E_g$ | |
| | $Q_y$ | | $E_y$ | |
| | $^*Q_x - Q_y$ | | $\Delta$ | |
| tr. dipoles | $Q_y$ | | $\left(d_y, d_x, \phi\right)$ | |
| | $Q_x$ | | | |
| N | $g$ | – | $N_g$ | |
| | $Q_y$ | – | $N_y$ | |
| | $Q_x$ | – | $N_x$ | |
| $^*\Omega_V$ | | – | $\Omega_1$ | $(\Omega_1, \Omega_2)$ |
| $^*\alpha$ | | – | $\alpha_1$ | $(\alpha_1, \alpha_2)$ |
| $S$ (HR) | $Q_y$ | – | $S_1$ | $(S_{11}, S_{12})$ |
| | $Q_x$ | – | $S_2$ | $(S_{21}, S_{22})$ |
| EL BATH | | | $\lambda$ | |
| | | | $\tau_c$ | |
| VIB BATH | $Q_y$ | – | $\begin{pmatrix}\tau_T\\ \tau_c\end{pmatrix}_1$ | $\begin{pmatrix}\tau_T\\ \tau_c\end{pmatrix}_{11}$ $\begin{pmatrix}\tau_T\\ \tau_c\end{pmatrix}_{12}$ |
| | $Q_x$ | – | $\begin{pmatrix}\tau_T\\ \tau_c\end{pmatrix}_2$ | $\begin{pmatrix}\tau_T\\ \tau_c\end{pmatrix}_{21}$ $\begin{pmatrix}\tau_T\\ \tau_c\end{pmatrix}_{22}$ |

## A.2 Parameters of the model from Figure 2.2

- electronic energies: (0.0, 0.73, 1.0)
- number of vibrational levels: (3,4,4)
- displacement of the potential: (0, 0.4, -0.3)
  Alternatively, Huang-Rhys factors can be used instead: (0, 0.16, 0.09) .
- vibrational mode frequency $\Omega_V$: 0.15
- diabatic coupling $\alpha$: 0.1

The Python script for the Figure 2.2 is published on my GitHub repository at: `https://github.com/MichalPt/MScThesis` .

## A.3 One-dimensional scans through the parameter space

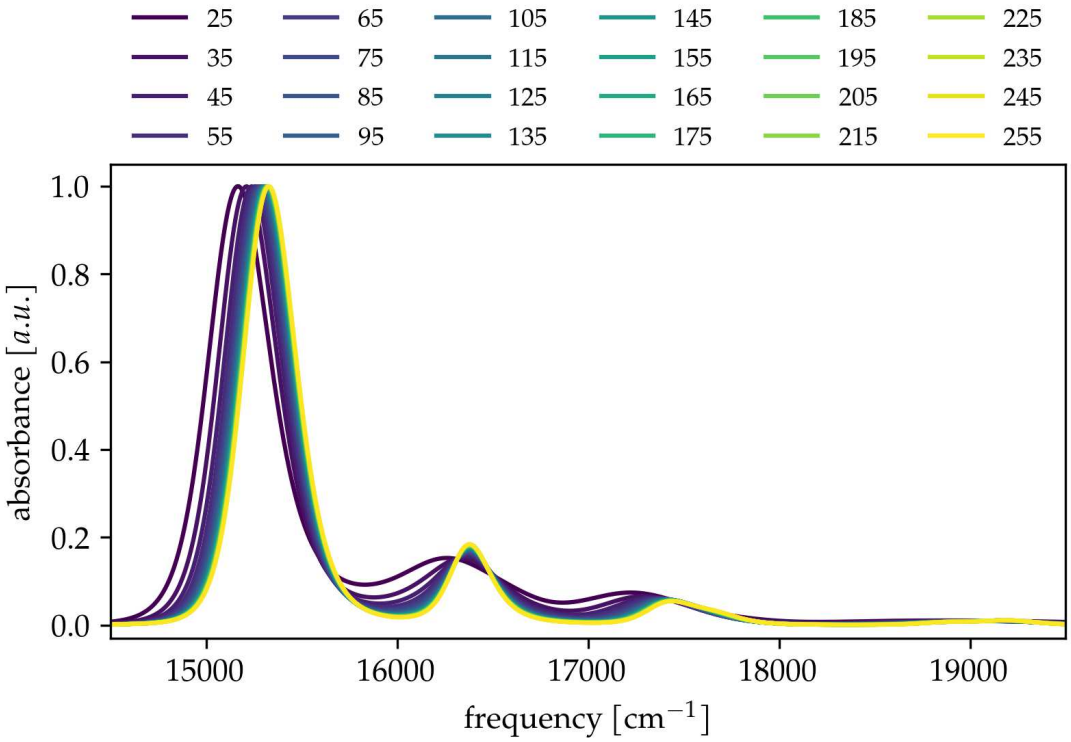


**Figure A.1:** Simulated linear absorption spectra of a spectroscopic model of Chl*a* molecule soluted in diethyl ether, with a single explicit vibrational mode ($N_V = 1$), for different values of the targeted relaxation time $\tau_{T,1}$. No optimisations were performed in this case and this figure's purpose is to only illustrate the overall effect of the parameter in question.

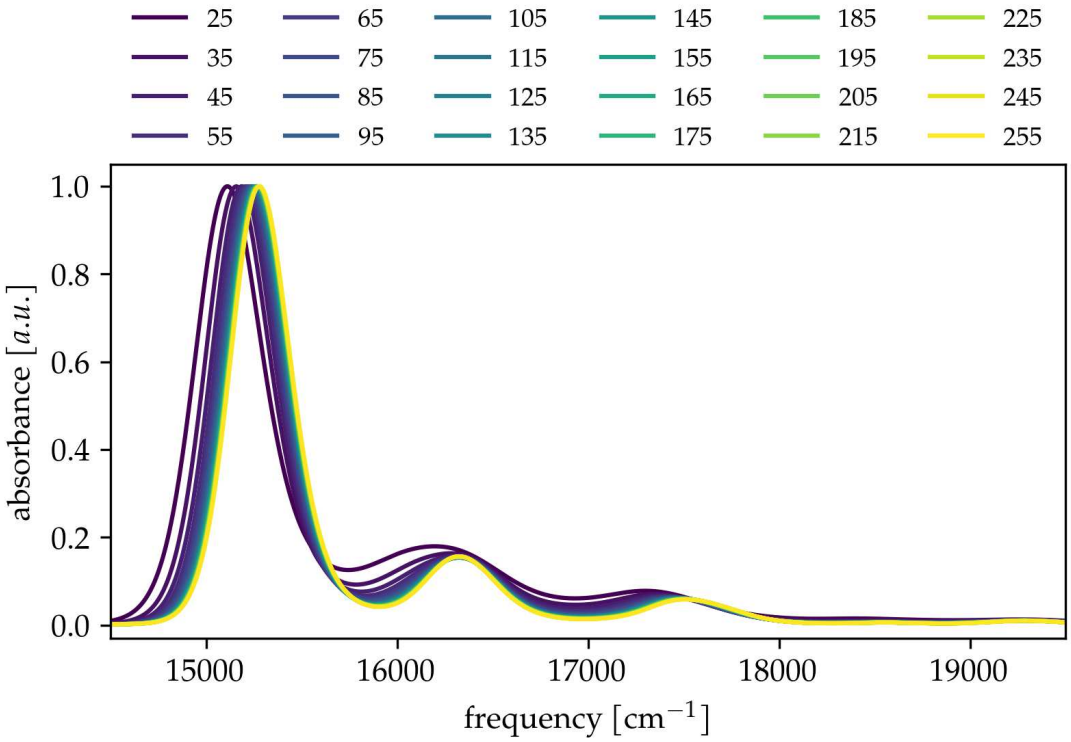


**Figure A.2:** Simulated linear absorption spectra of a spectroscopic model of Chl*a* molecule soluted in diethyl ether, with two explicit vibrational modes ($N_V = 2$), for different values of the targeted relaxation time $\tau_{T,11}$. No optimisations were performed in this case and this figure's purpose is to only illustrate the overall effect of the parameter in question.

# B. Mathematical methods

## B.1 System truncation

### B.1.1 Motivation

The computational resources required for simulating the dynamics of an open quantum system are tightly dependent on the system size. That is, on the dimension of the system Hamiltonian. The Hamilton matrices that are being discussed in this thesis have two main components: electronic and vibrational. In the context of chlorophyll molecules, the electronic energies that enter the effective Hamiltonian are well-defined and energetically well-separated. Hence, the electronic energy levels form the backbone of the Hamiltonian. In contrast, the vibrational modes included in the Hamiltonian and assigned to each of the electronic levels are only approximations of the real vibrational modes. Real vibrational modes may have convoluted potential energy surfaces that would be rather difficult to work with in the calculations. Hence, the potential surfaces are approximated around their minima by a quadratic potential, resulting in everyone's favourite linear quantum harmonic oscillator. The drawback of this harmonic approximation is the lack of an upper boundary for the vibrational Hamilton operator.

One of this thesis aims is to simulate the absorption spectra of Chl*a* molecule, particularly the Q-band region of the spectra, which plays a major role in photosynthetic light harvesting. Even though only two electronic transitions lay in this spectral region, many vibrational modes are appended to those transitions. Each one with a potentially infinite number of vibrational states that might be further coupled.

### B.1.2 Theory

The idea behind the approximation is to omit all states of the system that aren't directly contributing to the simulated absorption spectra. The goal is to truncate the system Hamiltonian (along with other system operators) according to its spectrum, i.e. the eigenenergies, in such a way that the Hermitian property of the truncated Hamiltonian is preserved, as well as the remaining eigenenergies. This task thus represents a *Hermitian inverse eigenvalue problem*: finding a Hermitian matrix $H_f$ and a unitary matrix $U_f$ for a given set of eigenvalues $\lambda$ that satisfies:

$$\mathbb{1}\lambda = U_f^\dagger H_f U_f \,. \tag{B.1}$$

The approach I adopted is based on the work of Padilla et al. (2017), who presented an algorithm that searches specifically for the closest Hermitian matrix, in terms of a Euclidean norm, to a given ansatz matrix $H_{ansatz}$. Only the algorithm is described here; the mathematical proofs and the derivation of the method can be found in the referenced paper.

Consider a complex Hermitian matrix $H$ of $n \times n$ dimension: $H \in \mathbb{C}^{n\times n}$ : $H^\dagger = H$, where † denotes Hermitian conjugate. The truncation algorithm consists of these steps:

1. Find the eigenenergies $\lambda$ and the unitary matrix $S$ that diagonalizes $H$: $S^\dagger H S = \lambda\mathbb{1} := h$.

2. Sort the values of $\lambda$ in increasing order and reorder the rows of matrix $S$ correspondingly.[1]

3. Based on the values of $\lambda$, determine the eigenvalues you want to get rid of and remove the rows and columns of the corresponding indices from the Hamiltonian $H$ and from the diagonal matrix $h$. If we denote objects of truncated dimensions (i.e. $m \times m$) by a tilde, we obtain $\widetilde{H}$ and $\tilde{h}$.

4. Find the unitary matrix $Q$ that diagonalizes $\widetilde{H}$: $Q^\dagger \widetilde{H} Q = \Lambda \mathbb{1}$.

5. Sort the values of $\Lambda$ in increasing order and reorder the rows of matrix $Q$ correspondingly.[1]

6. The result is obtained by transformation: $\widetilde{H}_f = Q\tilde{h}Q^\dagger$.

If the system truncation performed in step 3 is denoted by an action of an operator $T_{m\leftarrow n}$ such that $T_{m\leftarrow n} : \mathbb{C}^{n\times n} \longrightarrow \mathbb{C}^{m\times m}, m \leq n, A \in \mathbb{C}^{n\times n} : T_{m\leftarrow n}A = \widetilde{A} \in \mathbb{C}^{m\times m}$, the whole truncation algorithm can be expressed as:

$$\widetilde{H}_f = Q\Big(T_{m\leftarrow n}\big(S^{-1}HS\big)\Big)Q^{-1}. \tag{B.2}$$

After the truncation of the system Hamiltonian is performed, the other system operators have to be truncated as well. A general system operator $O \in \mathbb{C}^{n\times n}$ would be transformed as:

$$\widetilde{O}_f = Q\Big(T_{m\leftarrow n}\big(S^{-1}OS\big)\Big)Q^{-1}\,. \tag{B.3}$$

[1] This step is done by default in the previous step if the function `eigh` from the Python library Numpy (Harris et al., 2020) is used for solving the eigenvalue problem.